A BIO-INSPIRED METHODOLOGY OF AUTOMATIC PERCHING FOR UNMANNED AERIAL VEHICLES

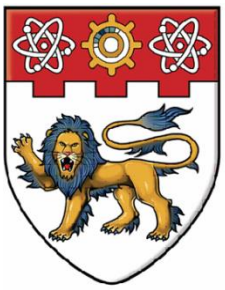

NANYANG TECHNOLOGICAL UNIVERSITY

A BIO-INSPIRED METHODOLOGY OF AUTOMATIC PERCHING FOR UNMANNED AERIAL VEHICLES

CHI WANCHAO

CHI WANCHAO

SCHOOL OF MECHANICAL AND AEROSPACE ENGINEERING

2016

2016

A BIO-INSPIRED METHODOLOGY OF AUTOMATIC PERCHING FOR UNMANNED AERIAL VEHICLES

CHI WANCHAO

SCHOOL OF MECHANICAL AND AEROSPACE ENGINEERING

A thesis submitted to the Nanyang Technological University
in partial fulfillment of the requirement for the degree of
Doctor of Philosophy

2016

Abstract

Current unmanned aerial vehicles (UAVs) have to stay airborne during surveillance missions, decreasing their energy efficiency dramatically and therefore limiting their endurance significantly. On the other hand, birds perch to conserve energy while maintaining surveillance over their domain. A biomimetic methodology of automatic perching for UAVs is thus a promising solution to their endurance problem.

Firstly, an experimental study of parrots' perching is conducted to obtain bio-inspirations of perching principles, and the perching procedure is generalized into three stages following which the perching methodology is addressed. Secondly, varying tau-dot, as observed from the approaching flight of parrots, is proposed with a fuzzy logic for perching flight guidance of UAVs and it outperforms the conventional assumption of constant tau-dot in terms of flight time. Thirdly, a scale-dependent expansion model (SEM) is derived for visual perception of tau-dot, and three visual identification algorithms are evaluated for best perception performance. Experiment results verify the effectiveness of the SEM, making onboard autonomous guidance possible. However, improvement on perception accuracy and reliability is still needed. Fourthly, a two-dimensional perching model of quadrotors covering dynamic interaction with perch is established based on analysis of the balancing procedure of parrots after touchdown. Simulation validates the applicability of the model to biomimetic perching. Finally, a gripping perching mechanism featuring force amplification and sensing is designed, and a fuzzy control law is proposed for automatic gripping. Experiments of indoor and outdoor remotely controlled perching, indoor automatic perching, and dynamic automatic gripping are performed, and results show that the perching mechanism is capable of fulfilling reliable and automatic attachment to perch.

The proposed methodology of automatic perching for UAVs covers the complete perching procedure, although its effectiveness has only been verified for each perching stage individually. Future work on enhancement of each component of the methodology and their integration can be done to validate overall effectiveness.

Acknowledgements

First of all, I would like to express my sincere gratitude toward Prof. Low Kin Huat, my supervisor, and Prof. Hoon Kay Hiang, my co-supervisor, for their responsible guidance all the way along my PhD study. Prof. Low has demonstrated great enthusiasm into research, and I have enjoyed many enlightening discussions with him in the past four years. His spirit of diligence in work also encourages me a lot to devote myself into research. Prof. Hoon has also been caring about my research progress all the time and given me many valuable comments. Their supervision is greatly appreciated.

I would also like to thank Dr. Zhao Weihua and Dr. Chiew Soon Hooi for the reliable indoor quadrotor testing system that they build up. Some of the experiments presented in this thesis were conducted collaboratively with them. Their insightful feedbacks have facilitated the development of the perching mechanism and its control law significantly. Senior PhD students from our group, Dr. Zhou Chunlin, Dr. Wang Ping, Mr. Li Lei and Dr. Luu Trieu Phat, are acknowledged for their helps and comments to my research. Supports from Mr. Lim Eng Cheng, Ms. Agnes Tan and Mr. You Kim San, technicians in Robotics Research Center, NTU, on many technical problems and documentary work of the project are greatly appreciated. Contributions from Final-Year-Project and URECA undergraduate students are acknowledged as well.

Moreover, I want to attribute my current achievement to the firm supports of my families. Their love and understanding have encouraged me to this far, and will continue to encourage me further in the future.

Last but not least, the sponsorship of DSO, Singapore to this project is acknowledged.

Table of Contents

List of Figures

List of Tables

Chapter 1 Introduction

This thesis presents the investigations done by the author on the bio-inspired methodology of intelligent perching with Unmanned Aerial Vehicles (UAVs). Three aspects of the topic are mainly studied, namely bio-inspirations from perching birds in nature, perching mechanism development and control strategies for autonomous perching of UAVs. In this chapter the background, motivation, objectives, scope and the outline of the thesis are introduced.

1.1 Background and Motivation

Unmanned Aerial Vehicles are defined as powered aircrafts that don't involve any onboard pilot and can either be remotely operated or fly autonomously with pre-programmed automation systems [1][2][3]. This term came into use in early 1990s, while the first UAV, "Aerial Torpedo", was developed by the US Navy as a long-range bombing weapon in 1917. Due to limitations in electronic components and control techniques, the UAVs developed at early stage were usually bulky and inaccurate in terms of autonomous flight. Moreover, military applications such as bombing and reconnaissance had always been playing an important role in the development of UAVs from then on, as World War II and Cold War followed consecutively. Micro-processers based on integrated circuits were developed significantly in 1980s, which further prospered the UAV industry greatly in 1990s. It was then that UAVs of small scale were developed rapidly. UAVs for civilian applications, on the other hand, had never reached fruition as it deserves by the end of 1990s, primarily because of airworthiness authorities [2]. The situation has changed significantly when it comes to the 21st century. With the remarkable advances in electronics, micro-processers and sensors like gyroscopes, accelerometers and magnetometers are produced with higher performance, smaller scale factor and lower cost, which makes the vast applications of UAVs possible. Moreover, civil aviation market has been growing big and mature, and therefore civil applications of UAVs start to bloom. For example, Phantom series and Inspire series produced by DJI [4] have been prevailing in the field of aerial photography. They have been applied to many scenarios such as aerial filming and traffic monitoring.

As one can see, the scale, operation range and configuration of the UAVs vary widely, be it for military or civil applications. UAVs have been generally classified into seven categories according to their scale and/or operation range: high-altitude long-endurance (HALE), medium-altitude long-endurance (MALE), medium-range or tactical UAV (TUAV), close-range UAV, mini UAV (MUAV), micro UAV (MAV), nano air vehicles (NAV) and remotely piloted helicopter (RPH) [2]. Some main configurations of UAVs include fixed-wing, rotary wing and flapping-wing. Fixed-wing UAVs have the advantage of high flight speed and long endurance, while UAVs with rotary wings are characterized by the capability of vertical take-off and landing and hovering, and also the high maneuverability [2]. Flapping-wing UAVs are able to fly as birds or insects, but their aerodynamic efficiency and payload capacity need to be improved. As HALE, MALE, TUAV and close-range UAVs all have operation range larger than 100 km, most of them unsurprisingly employ large scale fixed-wing configuration and consume aircraft fuel for long endurance, such as Global Hawk, Predator, Reaper and Pioneer. For MUAVs and MAVs, however, they aim for operations within range of 30 km, and usually weigh in the order of less than 20 kg [2]. Due to this targeted range and limitations of size and payload, batteries are mostly utilized as power source. Also, agility is one of the desired features for these UAVs, which makes rotary wing UAVs rather prevalent in these two categories. Quadrotor which has four rotors for thrust and cancels gyroscopic effects intrinsically is a typical UAV platform among these UAVs with rotary wings. Consequently, limited endurance of aerial operation becomes a big problem for them. As MUAVs and MAV are now being paid more and more attention to for both military and civilian surveillance applications, such as monitoring the battlefield in urban environments, search and rescue, mapping, traffic monitoring, and even parcel delivery, short endurance has become the bottleneck for their applications. Currently these UAVs have to keep flying during the surveillance missions, decreasing the efficiency of energy consumption dramatically. Although one way to solve this problem is increasing the energy density of the batteries, it’s still far beyond applicable in near future. This is where the concept of perching applies.

The concept of perching is apparently derived from the master of flight in nature--birds. Unlike current UAVs, birds perch now and then in some strategic locations where they can continue the surveillance on their domain for predator and prey while conserving energy for more critical needs [5]. Consequently, birds can achieve long endurance for surveillance tasks with high energy efficiency. A mini UAV or micro UAV would also be able to keep conducting the surveillance missions for a long time if it can perch to some vantage positions, such as roofs, branches, lampposts and power lines. Therefore, the bio-inspired perching methodology is evidently a promising solution to the endurance issue of UAVs, and it has become an emerging research topic in applications of surveillance with UAVs. However, most of previous investigations focused only on either one of the two aspects, namely the flight control of the perching UAVs and the perching mechanism design for a certain type of UAVs. As a result, the existing perching flight control research took into account only simple concepts of perching mechanism [6][7] or even none [8][9][10]; on the other hand, the existing perching mechanisms were designed with barely a little or none flight control addressed [11][12][13][14][15][16][17]. Moreover, existing research paid little attention to bionic engineering. Researchers in the fields of biology, ornithology and even psychology have carried out some interesting studies on birds' perching, and some inspiring conclusions have been drawn. Unfortunately, only a few works on UAV perching partially cover these bio-inspirations. Dynamics modeling of birds' perching for application with UAVs is even more lacking. Furthermore, the position and velocity feedbacks of the existing flight control were achieved mostly via external motion capture systems, for instance, VICON system [6][7][18]. Thus, topics on automatic perching of UAVs with onboard capabilities of target identification and distance perception are of great interest and necessity. Research on similar topics can be found in the fields of simultaneous localization and mapping (SLAM) and computer vision, but they are not addressed from the perspective of perching.

In summary, a comprehensive biomimetic methodology on automatic perching of UAVs is significantly lacking in existing research. It motivates systematic

investigations on the whole perching procedure of UAVs to provide a complete and effective solution to the automatic perching of UAVs.

1.2 Objectives and Scope

In this thesis, the author aims to develop a systematic methodology of automatic perching for quadrotors that belong to categories of mini or micro UAV so as to increase their task endurance. The reason for focusing on UAVs of such categories is that they have experienced rapid growth in research and development, for both military and civilian applications during last decade [18][19]. They have very extensive potentials in future UAV market, but their short endurance remains a big problem, especially for multirotor UAVs. Quadrotors are the most typical configuration among multirotor UAVs, and they possess outstanding aerial maneuverability and relatively large payload capacity, which makes them an ideal platform for surveillance applications, especially in clustered environments like urban regions. The UAVs utilized in this research are quadrotors with 10-inch propellers that belong to micro UAV category. For simplicity UAV means only the targeted UAV categories hereafter, unless otherwise stated. Such a methodology will be based on bio-inspirations from perching birds to guarantee its effectiveness intrinsically. It is supposed to address the problems arising from the complete perching procedure of UAVs, and provide a solid guideline for UAVs to automatically achieve reliable perching. The target perches taken into account include branches, lampposts, walls, ground, and roofs which birds usually perch to. Such a broad range of perching circumstances is to generalize the applicability of the methodology. To accomplish the objective, problems that will be tackled include:

1. Experimental study on birds' perching procedure. As a biomimetic research topic, UAV perching requires bio-inspirations as substantial references. Firstly, the whole perching procedure needs to be generalized into a standard sequence for UAVs to follow. Secondly, thorough quantitative analysis of the locomotion and maneuvers of birds along the perching procedure will be conducted according to the generalization. Eventually the perching maneuvers of birds are supposed to be better understood.

2. Navigation method of approaching flight for perching. The approaching flight data of birds from the experimental study will be evaluated from the perspective of *Tau Theory*, a theory of visual perception of approaching motions in humans, birds and insects. The applicability of the theory to the perching flight of UAVs will be examined and a novel navigation method based on *Tau Theory* is supposed to be developed for UAVs. The corresponding navigation controller will further be implemented and evaluated through experiments with UAVs.

3. Visual Identification of perch and visual perception of tau information. The tau-based navigation method to be developed is most likely to require feedback of tau information. On the other hand, in humans, birds and insects tau information almost totally relies on visual perception. Therefore, it is rather necessary to explore the relation between visual cues, for instance, scale of the objects, and tau information. To obtain the visual cues, visual identification of perch is the primary prerequisite. With these two aspects addressed, experiments with UAVs will be performed for validation.

4. Dynamics modeling of the balancing process of perching UAVs after touchdown. The modeling will be based on the locomotion response of birds after touchdown from previous experimental study, and the control dynamics of UAVs are supposed to be incorporated into it. Analytical derivation of the equation of motion of perching UAVs will be performed to reveal the dynamic process. Validation of the model with data from the experimental study will be carried out. With the dynamics model established, the balance of UAVs can be achieved readily.

5. Perching mechanism featuring reliable attachment to perch. The last piece towards a complete perching methodology for UAVs is reliable attachment to perch which is accomplished with a perching mechanism. Taking into account the required conditions derived from the perching dynamics model, sufficient

force for securing the attachment with perch will be emphasized during mechanical design and kinematic optimization of the perching mechanism. The corresponding controller of the perching mechanism based on force feedback will be developed for reliable operation. Finally the perching mechanism and its controller will be examined through a series of experiments with UAVs.

With the aspects above thoroughly addressed, the perching methodology derived should be capable of perching multirotor UAVs reliably in a number of circumstances. It should be noted that it wouldn't compromise the generality of the perching methodology significantly even if quite a portion of the development will be made and evaluated in indoor lab environments. Extending the applicability of the proposed perching methodology in outdoor environments will be discussed in the section of future works.

1.3 Outline

This thesis consists of 7 chapters. A systematic review of research on perching in fields of ornithology, biology, navigation and control of UAVs and kinematics is conducted in Chapter 2. Firstly, studies in anatomy structures of birds involved in perching are comprehensively introduced. Secondly, literatures on distance perception and flight navigation strategy of birds during perching and their applications to robots and UAVs are reviewed. Lastly, existing perching mechanism designs for various UAV platforms are presented with comparison on their advantages and disadvantages.

An experimental study on characterization of parrot's perching maneuvers is conducted and introduced in Chapter 3. Firstly, the procedure of parrot's perching is generalized based on observations from the experiment. Secondly, the approaching flight data are evaluated with *Tau Theory* to identify the tau-dot patterns of the parrots. Lastly, the balancing maneuvers after touchdown involving the trajectory of the center of mass and the body angle of the birds are investigated for the purpose of dynamic modeling.

Chapter 4 addresses the autopilot controller for approaching flight to the perch based on modified *Tau Theory* and fuzzy logic. Advantages of varying tau-dot compared with conventional constant tau-dot are analyzed based on experiment data. The fuzzy controller for navigation is then designed and implemented with our indoor testing system. Perching flight experiments are finally performed using the constant tau-dot strategy and varying tau-dot strategy respectively to validate the effectiveness of the proposed fuzzy controller.

Vision-based perch identification and tau information estimation are studied in Chapter 5 to provide visual feedback for the navigation controller developed for approaching flights. Three identification methods based on LabVIEW are proposed and examined systematically in three scenarios. A scale-based tau estimation model named SEM is further derived and validated via experiments of approaching flights with visual identification. With tau estimation integrated into the navigation controller, the control loop of the visual navigation of perching flight is completed.

With the navigation of approaching flight addressed, the dynamic balancing procedure after touchdown is dealt with in Chapter 6. Firstly, a dynamics perching model covering the response of UAVs after touchdown is established. The UAV dynamics is taken into account as well. Validation is made using data from the parrots' perching experiments. Secondly, a perching mechanism mimicking birds' feet is designed for reliable attachment to the potential perch. Kinematic optimization is carried out to maximize the gripping force. Thirdly, control laws for the perching mechanism designed are presented. Fuzzy logic is utilized to tackle the non-linearity and the indeterminacy problems. Effectiveness of the perching mechanism is verified through a series of gripping and perching experiments with UAVs.

A summary of the work that has been done in this thesis is presented in Chapter 7, followed with discussions on the several promising topics for future investigations. Extending the perching methodology for outdoor environments is covered. Supplementary materials for previous contents of the thesis are further appended.

Chapter 2 Literature Review

Research on perching of birds emerged in the field of ornithology. With the fast development and vast applications of UAVs in the last decade, perching with a UAV has become a booming topic. Nowadays many disciplines are involved in the field of biomimetic perching with UAVs, such as biology, navigation and control, and mechanism design. In this chapter, literatures on perching-related topics are reviewed, with focus on biomimetic perching methodology for UAVs.

2.1 Biomechanics of Birds' Perching

Research specifically on birds' perching was first conducted in the field of ornithology back in late 19th century when researchers concentrated on the anatomy mechanisms of birds involved in perching [20][21][22][23]. Such topic is still the focus of ornithological research on perching in recent decades [24][25][26]. It's not until middle 20th century that were sophisticated transducers applied to investigate the perching dynamics of birds [29][30]. The traditional topic is from a perspective of birds' internal structures, while the latter one examines the interactions between birds and environments. Essentially both of these two topics explore the biomechanics behind birds' perching behavior which is rather significant for modeling birds' perching.

2.1.1 Automatic Perching Mechanism in Birds

Anatomy studies on perching birds have been addressed mainly on the automatic perching mechanism (APM). Most biologists were in favor of the conclusion that most birds utilize an automatic perching mechanism (APM) to secure themselves to the perch, even during sleep [26]. Galton and Shepherd have done very comprehensive literature review on the APM in birds in [26]. The sources that they have cited date as early as 1685, and include more than 40 papers and books on ornithology. Moreover, most of their references are either too old to be accessed by the author, or in other languages instead of English. Thus, this section is mainly based on their review.

The APM, as generally accepted, consists of an automatic digital flexor mechanism (ADFM) and a digital tendon-locking mechanism (DTLM). The ADFM takes effect when the bird perches and bends knees and ankles under body weight. The tendons that run along the leg through the knee and the ankle to the digits are stretched, pulling the digits to flex and grasp the perch [27][28] (see Figure 2.1). After the grasp is formed, the DTLM under the digit bone latches the tendons to maintain the grasping force by meshing the tiny projections on the tendons into hard ribs on the inside surface of the tendon sheath [24][25] (see Figure 2.2). Such a combination of ADFM and DTLM is deemed to enable birds to perch with little muscular effort.

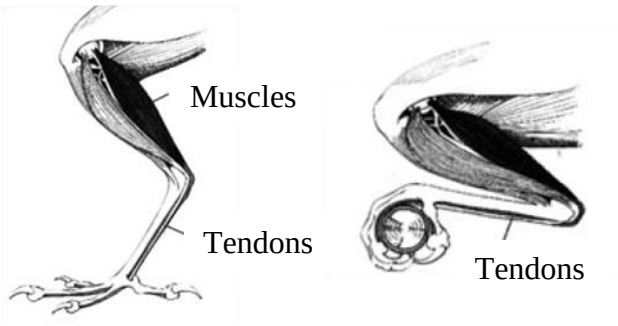

Figure 2.1 The automatic digital flexor mechanism of birds [31] (Left: the leg is extended and the digits are straight. Right: the leg is bent and the digits are flexed.)

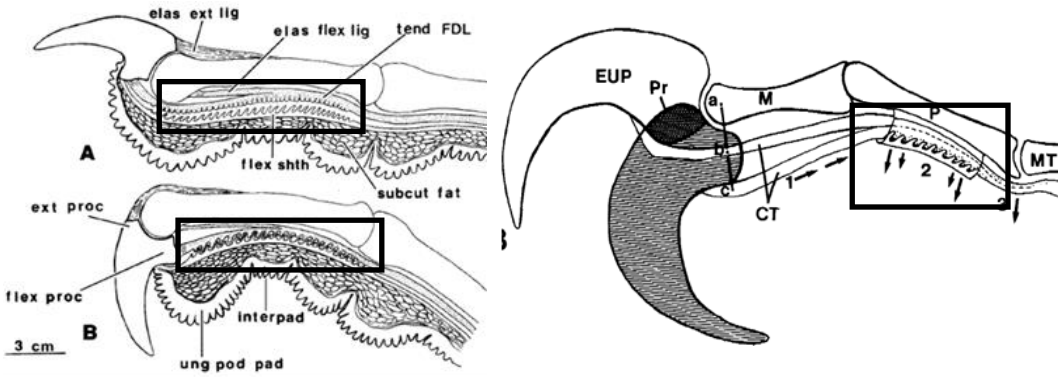

Figure 2.2 Digital tendon locking mechanism (Left: structures involved in tendon-locking mechanism [24]. Right: biomechanics vectors causing engagement of the tendon-locking mechanism [25]. The rectangular areas represent the tendon-locking mechanisms.)

The APM concept was first presented by Borelli, and further developed by Owen. Chamberlain, based on this APM concept, claimed that the medial thigh muscle is the perching muscle that flexes the digits. However, this conclusion was doubted by

Watson and Cracraft. Moreover, Watson suggested an alternative APM which is the current ADFM concept. Further, Schaffer complemented the ADFM with the DTLM based on the research of Renaut and Ranvier. Then Bock, for the first time, examined the ADFM with preliminary experiments on two species of birds, showing conflicting results with the ADFM concept. Later, Shepherd verified the existence of a DTLM by using light microscopy, and Quinn and Baumel confirmed such presence of a DTLM in a variety of different birds with the help of the scanning electron microscope. The latter two authors also revealed the biomechanics of the DTLM, and summarized the species of the DTLM, combining results from Shepherd and their own.

By analyzing the observations made in 1970s, Galton and Shepherd themselves concluded in [26] that there is no ADFM in birds and the DTLM only acts in perching with active contraction of the digital flexor muscles. Although their conclusion may not be applicable to all birds that perch since only the European Starlings were observed and studied, it at least reveals that active actuation of muscles is required for digital flexion during perching in certain birds. Their conclusion is therefore agreed with only in the sense that certain mechanisms, such as active actuation and grasp locking, are necessary for reliable perching. It can be seen that further investigations on anatomy mechanisms of perching birds are still needed to explain explicitly the principles behind birds' perching.

2.1.2 Digit Arrangement

Another important feature of a perching bird is its digit arrangement. As shown in Figure 2.3, there are five types of digit arrangement, namely anisodactyl, zygodactyl, heterodactyl, syndactyl and pamprodactyl [32]. For anisodactyl, the hallux points backward while the rest three digits forward. The zygodactyl and heterodactyl are basically rather close to each other, both with two digits forward and two backward. The difference is that for zygodactyl it's the second and the third digits that are in front while for heterodactyl it's the third and the fourth ones. Moreover, the heterodactyl is only found in trogons, which means zygodactyl, compared with heterodactyl, is more commonly seen in birds. For syndactyl two of the forward

digits are joined into one for most of their length, and for pamprodactyl all the four digits point forward, with the first and the fourth digits capable of being rotated backward. It can be seen that in all arrangements at least one digit can be arranged opposite to the rest, which functions similarly to human hands and can form an envelope grasp to perch birds firmly.

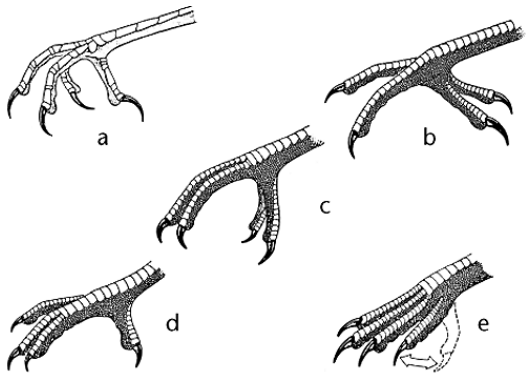

Figure 2.3 Arrangements of bird digits: (a) anisodactyl, (b) zygodactyl, (c) heterodactyl, (d) syndactyl and (e) pamprodactyl [32].

2.1.3 Claw Morphology

As shown in Figure 2.2, the claw retracts while the tendon stretches, which generates additional grasping force by 'digging' into the perch surface with the claw. Also, it enables birds to perch to a branch which the digits may even not be long enough to wrap around. In extreme cases, the claws can even function as purchases to balance the bird on rough or vertical surfaces [33], as depicted in Figure 2.4. The claw morphology related to such features has been studied. Pike and Maitland investigated the relationships between the claw geometries of a variety of birds, namely claw radius and claw angle as defined in Figure 2.5, and their body mass [34]. As concluded by the authors, for perching birds claw radius is proportional to (body mass)$^{0.34}$ while no significant relationship exists between claw angle and body mass. Fowler, Freedman and Scannella utilized similar methodology to investigate the claw morphology in raptors, which not only prey but also perch by grasping [35]. They found that the claw morphology varies among raptor species correlatively with their prey capture and restraint strategy. It suggests that the circumstances under which the claw functions play an important role in influencing its morphology, which is essentially consistent with Pike and Maitland's finding.

Figure 2.4 A gesture of a tree creeper when climbing along a trunk [33]. Its claws dig into the trunk and serve as purchases together with the tail to secure body balance.

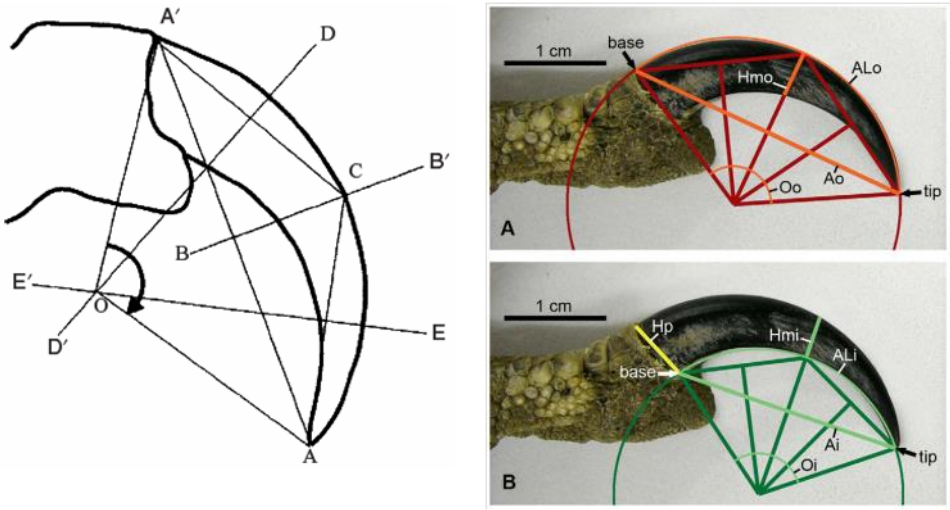

Figure 2.5 Claw geometries for quantification evaluation (Left: the outer curve of the claw is used to identify its arc center O. The claw radius is given by OA and OA', and the claw angle is defined as the angle between OA and OA' [34]. Right: Similar method was applied to study the predatory functional morphology in [35])

2.1.4 Interaction Dynamics of Birds with Perch

Fisher in 1956 first investigated the interaction dynamics between perching pigeons and the perch by utilizing a mechanical force plate to measure the landing and taking off forces applied by pigeons' legs [29][30]. His research provided a new perspective toward the biomechanics behind birds' perching behaviors, which is rather valuable. Heppner and Anderson further designed a perch integrated with simple force-sensing elements to gauge the taking off thrust exerted by pigeons' legs in [36]. The landing forces and force directions, however, were not able to be measured due to their

design limitations. With strain gauges Bonser and Rayner implemented a novel force-transducing perch capable of measuring both magnitude and direction of forces in [37]. The thrusts exerted by legs in time domain was measured and studied, and the force angles were further taken into account. Their relations with mass of the birds were analyzed, leading to the conclusion that peak forces are mass-dependent while the angles are not. Similar methodology was also adopted by Green and Cheng in [38] where they specifically looked into the factor of kinetic energy of birds during perching. Both kinematic and dynamic variables, such as approaching trajectory, speed and force, were recorded simultaneously for analysis. They drew conclusions that kinetic energy is not dissipated by aerodynamic means during perching but by the perch and the bird's legs and lower body, indicating the critical necessity of anatomy research on birds' legs, and that familiarity with perch tends to determine the preference of perching ways between high-kinetic-energy and low-kinetic-energy. The authors' perspective from kinetic energy broadens the parameter scope involved in birds' perching, and they also proposed some more parameters for future investigations.

2.1.5 Bio-inspirations

From the review above, four bio-inspirations can be derived for the development of a biomimetic perching mechanism. Firstly, it is obvious that passive actuation with ADFM is not sufficient for reliable perching. Therefore,

Bio-inspiration 1: *Active actuation is compulsory for a perching mechanism while passive actuation could be integrated complementarily to benefit the perching performance, and*

Bio-inspiration 2: *A ratchet mechanism serving as the DTLM is greatly desired to maintain the grasp without consuming any energy.*

For a biomimetic perching mechanism, its effectiveness and efficiency definitely come first, which is determined by its potential applications to various UAV

platforms. Following these two conclusions will guarantee the effectiveness and preserve the efficiency of the perching mechanism, as in the case of birds.

Secondly, based on the most common digit arrangement, it can be seen that

Bio-inspiration 3: *Envelope grasp is the most applicable means of perching a UAV to various targets, especially for outdoor applications, and perching mechanisms featuring envelope grasp are therefore preferred.*

Last but not least, the claw morphology shows certain dependence upon perching circumstances, indicating its involvement in perching. Thus,

Bio-inspiration 4: *Claws, with their geometries optimized under the very circumstances of applications such as mass and size of the UAV, and dimensions and shape of the perch, could be integrated into the perching mechanism to enhance its perching performance. However, it's not a necessity.*

The research reviewed above made the first exploration into the biomechanics of birds' perching. However, none of these researchers aimed at establishing a dynamic perching model of birds. As indicated by the results they have obtained, the dynamic interaction between birds and perch should be addressed so that a dynamic model deciphering birds' perching behaviors can be accomplished.

2.2 Navigation and Control of UAVs for Perching Flight

2.2.1 Tau Theory

Tau Theory originated from research in perceptual psychology and was first proposed by David Lee based on his study on human's visual perception of time-to-collision when braking a car [39]. The term of time-to-collision (TTC) sometimes is also referred to as time-to-contact [40]. Tau is a main concept of TTC, defined as

$$\tau = \frac{\chi}{\dot{\chi}} \tag{1}$$

where χ is the motion gap and $\dot{\chi}$ is the closing velocity of the motion gap. It was stated that information about tau could be used for braking control to avoid collision [39]. Lee further explored *Tau Theory* by studying the visual control of braking of landing pigeons, and enriched it with the conclusion that controlled braking can be achieved by keeping tau-dot ($\dot{\tau}$), time derivative of tau, constant [41]. In [42] He further generalized the concepts of motion gap and tau to various movements of animals, and presented the concept of tau coupling for synchronizing these movements. It finally leads to a comprehensive general *Tau Theory* [44]. Hecht and Savelsbergh have done great work of systematically exploring and discussing the concept of TTC [40], which covers the fundamentals of *Tau Theory*. Other researchers also tested the *Tau Theory* by studying human's braking control of reaching movements [45][47], stopping a vehicle [48][49] or landing an airplane [50]. Although conflicting results were gained from these works, they did facilitate the development of *Tau Theory*. It is noticed that *Tau Theory* has been mainly studied and developed in the field of perceptual psychology since it was proposed.

While investigations on *Tau Theory* have been carried out enthusiastically and consistently in perceptual psychology, only few applications of TTC to ground robots were published [51][53], and none application of *Tau Theory*, or even TTC, to unmanned aerial vehicles (UAVs) was found until 2012 [54]. Kendoul and Ahmed, for the first time, developed a *Tau Theory* based pilot controller, TauPilot, for unmanned aircraft systems (UASs) [54]. As shown in Figure 2.6(a), the TauPilot consists of a tau-navigation system which computes tau for the identified motion gap with online sensor data, a tau-guidance system which predicts future movements based on the prospective guidance laws of *Tau Theory*, and a tau-control system which integrates the tau-guidance laws to regulate the movement of the UASs. Their work is rather comprehensive and sound, providing a systematic control strategy of braking or landing for UASs. Research in navigation and/or guidance of UAVs using *Tau Theory* then started to grow. Zhang, Xie and Ma have published several papers on trajectory generation and guidance for UAV landing and perching [55][56][57][58]. Similar strategies of constant tau-dot, tau coupling and intrinsic tau-dot to [54] were addressed and utilized for control. See Figure 2.6(b). No UAV

platform has been developed to verify their control strategy, but their analysis was sound and simulation results made good sense for validation. Kendoul recently updated their TauPilot in [59]. Among existing guidance approaches for UAV perching, it can be seen that the constant tau-dot strategy is applied. The analysis has shown that for a constant tau-dot between 0 and 0.5 the motion gap, velocity and braking deceleration will be reduced to zero simultaneously, which means a safe landing or reaching without any collision or impact [41][54][55]. *Tau Theory* based autopilot provides a promising navigation solution for automatic perching of UAVs, which makes it of great interest.

(a)

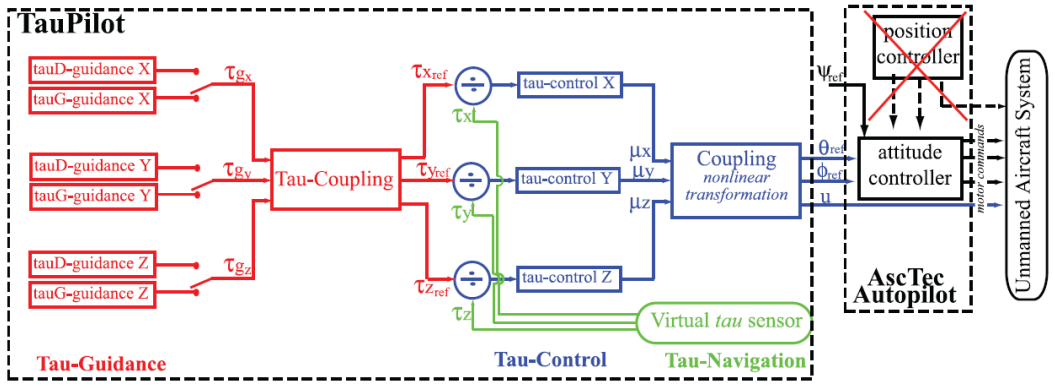

(b)

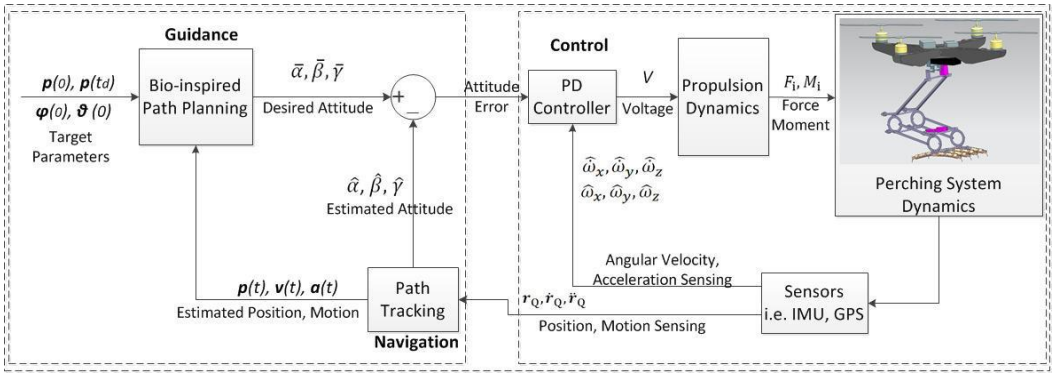

Figure 2.6 Tau theory based control strategies for perching with UAVs. (a): 4D TauPilot [59]. (b): Bio-inspired GNC system [55].

2.2.2 Flight Control of UAVs for Perching

It takes a series of aerodynamic maneuvers for birds to perch successfully. Therefore, the aerodynamics and control of various UAV platforms is another hot spot in the field of perching. Although only quadrotors are considered for investigations in this

thesis, the review here also includes fixed-wing UAVs to help draw a complete picture. Note that these methods will not be applied in this thesis so they are reviewed in a brief manner.

Wickenheiser and Garcia studied the longitudinal dynamics of a morphing aircraft concept to achieve the capability of perching [8], as shown in Figure 2.7(a). Both analytical and empirical aerodynamic analyses were performed, and some basic aerodynamic configurations and maneuvers for a fixed-wing aircraft to perch were investigated. The authors further researched the development and optimization of trajectories for perching [9]. The vehicle shape reconfiguration, or vehicle morphing, was also involved and discussed. Main efforts were made on aerodynamic analysis and its control strategy. Cory and Tedrake from MIT published their research on aerodynamic control design for maneuvers at high angles-of-attack [6], as illustrated in Figure 2.7(b). They developed a particular procedure to perch a small fixed-wing glider with an aggressive high angle-of-attack. In their investigations the motion capture system was utilized to obtain the feedback data for autonomous control, and finally a simulated perching trajectory which was utilized by Wickenheiser and Garcia in [9] was gained. Roberts and the two authors further studied the controllability of fixed-wing perching with a simplified closed-form model [10]. The optimized perching trajectory obtained previously was employed as the target trajectory to follow, and their results showed that additional actuations can facilitate perching with less control effort.

Mellinger, Shomin and Kumar from University of Pennsylvania for the first time applied quadrotors as UAV platforms for robust perching and landing [7], as depicted in Figure 2.7(c). They mainly investigated the dynamic model of the quadrotor system and its different controllers for different functions. A gripper was also designed and evaluated briefly for its payload capability with different target surfaces. However, the evaluation protocols were not introduced explicitly and the gripper was not applied to robust perching experiments as the authors focused more on the control of the quadrotor maneuvers during perching and landing. Mellinger, Michael and Kumar further investigated trajectory generation and control for precise

aggressive maneuvers with quadrotors later in [18]. They developed a similar procedure of controller design and refinement as in [6], and successfully manipulated the quadrotor to follow the desired aggressive trajectories. Still, perching is one of the potential maneuvers that they are aiming at, just as their studies in [7].

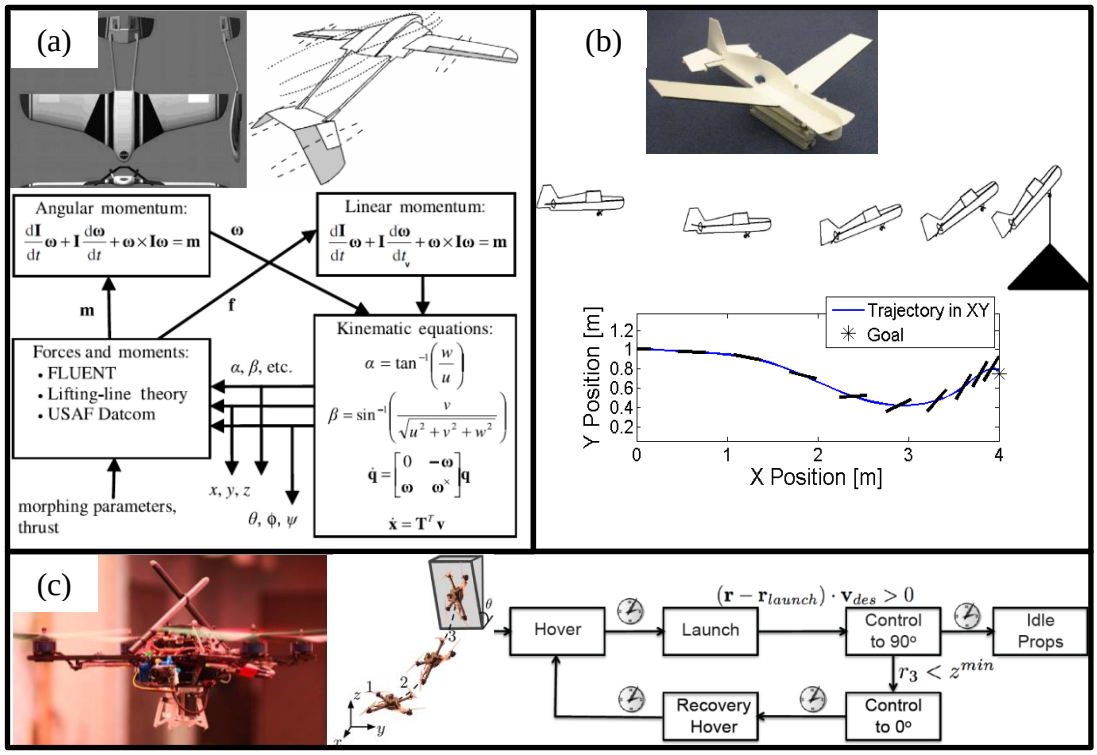

Figure 2.7 The flight dynamics control laws for perching with various UAVs. (a): Morphing UAVs [8][9]. (b): Fixed-wing UAVs [6]. (c): Quadrotors [7].

As seen from the review above, current researches on perching-related aerodynamic control are all UAV-oriented. Basically no bio-inspiration from birds for perching maneuvers is covered. Although effective control schemes have already been achieved for UAV manipulation in perching and de-perching, a systematic control strategy integrating all the sub-systems of the perching platform, such as target identifier, UAV platform and perching mechanism still should be addressed. Therefore, biomimetic modeling of birds' perching strategies and maneuvers are worth of further investigations.

2.3 Perching Mechanisms Designed for Different UAVs

Beside the ornithological research on birds' perching, researchers have also made effort to develop practical perching mechanisms to perch different UAV platforms, including gliders, fixed-wing drones and multi-rotors, under various circumstances, such as vertical surfaces and horizontal poles. Although some prototypes are not biomimetic, they do show the diversity of feasible solutions to perching with UAVs.

Anderson et al. proposed various ideas for perching, such as perching with adhesives and weighted tail line [11], and they investigated the concept of sticky pads using rat glue more specifically, as shown in Figure 2.8(a). The concept is innovative, but the perching duration is limited to the effective duration of the rat glue and the repeatable perching times are constrained by the number of sticky pads. Kovač et al. designed a simple and practical perching mechanism for a glider based on the concept of penetration of the target surface using needles [12]. Similarly, it's also a nose-first way of perching to vertical surfaces, as depicted in Figure 2.8(b). The mechanism will not work properly if the wall material is too stiff, such as metal and glass. It would also be a big challenge for the mechanism to perch a heavier UAV since the needles may not secure the perching status. While gliders as the platform for perching are intrinsically limited due to the non-power way of flight, powered UAVs are more suitable and valuable as perching platforms. Desbiens et al. developed a micro-spine mechanism, as shown in Figure 2.8(c), that enables a powered fixed-wing UAV to perch on a vertical wall [13][14]. This design is quite innovative as it's biomimetic to insects' claws. However, it encounters the same problems as Mirko's mechanism does because it uses spines to hook on the surface of the wall which is basically similar to penetrating with needles. As bio-inspirations got more and more involved into perching mechanism design for UAVs, Doyle et al., for the first time, designed a bionic gripping mechanism which follows the configuration of birds' feet for perching with multi-rotors[15][16]. Compliant material is applied to vary the stiffness along the digit so as to achieve full envelop grasp over various irregular shape targets, and the leg mechanism can actuate passively under the body weight of the UAV for perching and releasing, as shown in Figure 2.8(d). Such passive actuation is consistent with the automatic digital flexor

mechanism, as reviewed in Section 2.1.1. However, it is not necessarily desirable from engineering perspectives, because certain disturbances, say, a gust, may overcome the gravity of the UAV and therefore disengage the perching mechanism. As indicated in [26], active actuation is always compulsory for reliable perching. Moreover, it's obvious that the leg mechanism is too bulky to avoid compromise of aerodynamic characteristics of the UAV. Nagendran et al. proposed a biomimetic leg concept and the corresponding control strategies for UAV perching, enriching the bio-inspired exploration into perching [17]. The leg mechanism is inspired directly from the typical anatomy of a bird's leg, as shown in Figure 2.8(e), and it is capable of retraction to diminish its influence on aerodynamics of the UAV. However, no kinematic or dynamic analysis was performed, and therefore no prototype has been developed and evaluated.

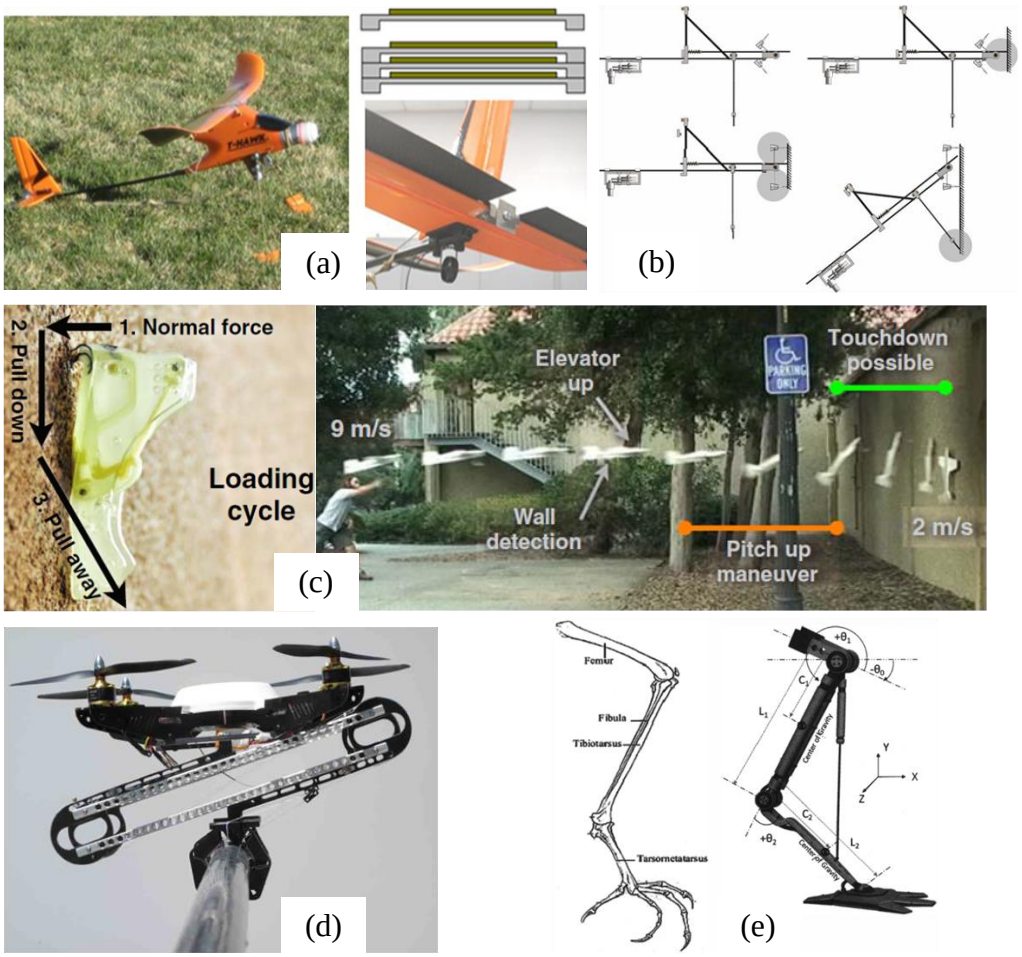

Figure 2.8 Existing perching mechanism designs for different UAVs. (a): Sticky pads. (b): Penetrating needles. (c): Micro-spines. (d): Bionic gripper. (e) Biomimetic leg.

Based on the above review, a table listing the advantages and disadvantages of these perching mechanisms is presented in Table 2.1. Several conclusions can be drawn that current perching mechanisms are mostly simple and light, which is prescribed by the peculiarity of UAVs, that they are basically designed for only a certain perching circumstance, for example, vertical surfaces, and only a certain type of UAVs, for instance, gliders, which limits their potential applications, and that passive engagement methods instead of active ones are employed, compromising the reliability of the perching mechanisms.

Table 2.1 Advantages and disadvantages of existing perching mechanisms

Sticky Pads	Pros	1) **Simple** 2) Able to attach to **vertical surfaces** 3) **Straightforward** perching maneuver
	Cons	1) **Limited times and endurance** of perching 2) P**assive** engagement system 3) Not suitable for **poor surface conditions**
Penetrating Needles	Pros	1) **Simple** and **light** 2) Able to attach to **vertical surfaces** 3) **Straightforward** perching maneuver
	Cons	1) **Intrusive** attachment 2) **Passive** engagement system 3) **Insufficient holding force** for larger scale UAVs
Micro-spines	Pros	1) **Light** 2) Able to attach to **vertical surfaces** 3) **Effective damping** design
	Cons	1) **Complex stall** maneuver and **control** 2) **Passive** engagement system 3) Only applicable to **surfaces of certain roughness** 4) **Insufficient payload capacity** for larger UAVs
Bionic Gripper	Pros	1) **Unlimited times** of repeated perching 2) Suitable for **various perching circumstances** 3) **Effective damping** design

	Cons	1) **Bulky** 2) **Passive** engagement system 3) Only suitable for UAVs capable of **vertical take-off and landing**

2.4 Summary

In this chapter literatures on perching are mainly cataloged into four topics, namely ornithological studies of perching birds, trajectory control strategy of perching birds, perching mechanisms designed for UAVs and aerodynamic control of different UAV platforms, and are systematically reviewed respectively. Besides, the flapping ornithopters which could be the UAV platform for future research on perching are also briefly reviewed. It is evident that the combination of ornithological inspirations and engineering implementation is significantly lacking in previous research of perching methodology. Therefore, bio-inspirations from birds should be investigated more systematically and be referred to more closely in theoretical modeling and engineering implementation, so that a plausible methodology can be finally derived.

Chapter 3 Experimental Study on Birds' Perching

To develop a bio-mimetic perching methodology for UAVs, it's definitely necessary to learn from nature—perching birds. Existing bio-experimental researches on birds' perching either focused on the approaching flight or only addressed the leg actuation, suggesting a default breakdown of the perching procedure of birds. Apparently such a breakdown makes sense intuitively. On the other hand, it indicates the necessity of systematization of the complete perching procedure of birds. In this chapter, an experimental study on the perching methodology of birds is carried out. Firstly, the complete perching procedure of birds is quantitatively studied and systematization is achieved on the basis of quantitative analysis and observations. Secondly, the kinematics and dynamics of birds' perching maneuvers are researched according to the systematization of the perching procedure. The prevailing *Tau Theory* of approaching strategy is evaluated, and the dynamic characteristics of the balancing maneuvers are revealed.

3.1 Experimental Method

The primary problem for perching birds should be how to obtain body balance while transiting from airborne status to on perch status. Previous investigations on the interaction force between birds' legs and the perch during landing and/or take-off, took into account some kinematic parameters such as perching trajectory, speed, kinetic and potential energy [29][30][36][37][38]. Besides, literatures also covered other topics related to birds' perching behavior. One topic is the visually guided landing of birds [60][61][62]. The primary parameters that are of interest in such topic include approaching velocity and head orientation. Similar investigations can also be found in the field of insects' landing [63][64][65]. Another topic is birds' flapping flight when perching [66][67][68][69]. Kinematic parameters involved include wingbeat frequency, flight velocity, body angle, stroke plane angle, wing angle, tail angle and so on. It can be seen that flight trajectory/velocity and body angle of birds were generally paid more attention to in the literatures. It is believed that these parameters, especially as a combination, can reflect birds' locomotion and

balancing maneuvers more effectively. Therefore, experiments in this chapter are designed and conducted to gain data of these parameters and to further promote the modeling.

The experimental setup is illustrated in Figure 3.1. Two cylindrical wooden poles attached to tripods are used as the start perch and the target perch, respectively. The distance between them is made large enough for bird subjects to establish natural perching trajectories. The poles are kept horizontal to diminish the lateral maneuvers of bird subjects during perching, as only kinematics and dynamics in the sagittal plane of birds are investigated. A high speed camera (Mikrotron EoSens mini2) is placed perpendicular to the sagittal plane to record subjects' locomotion at 500 fps. A backdrop of white cloth is utilized to enhance the view quality for the high speed camera.

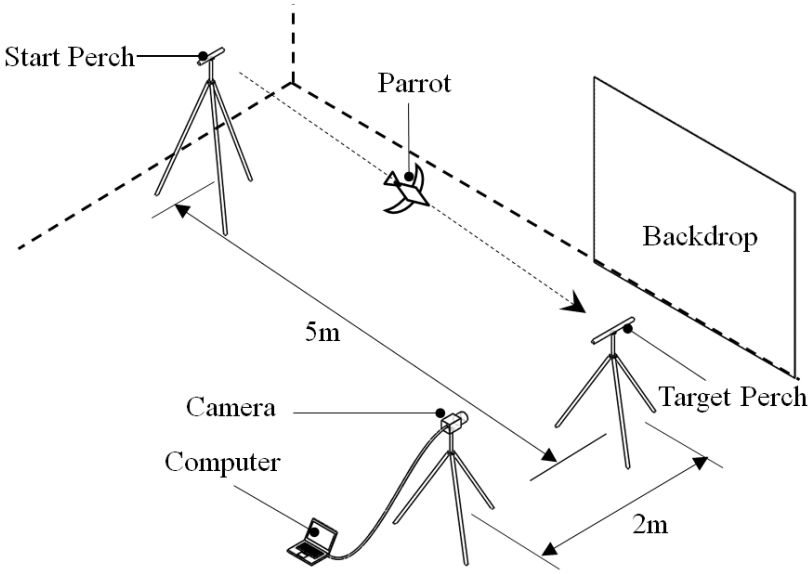

Figure 3.1 Isometric view of the experimental setup

Three parrots of similar size and well trained for perching are taken as the subjects. The weights of subject 1, 2 and 3 are 59g, 65g and 63g, respectively. Two instances of approaching flight, namely descending flight and ascending flight are taken into account. The height of the targeted perch is fixed at 1.15m, while the height of the start perch is adjusted to 1.65m and 0.65m for descending and ascending flights, respectively, as shown in Figure 3.2. Each subject perches 3 times for descending and ascending flights respectively.

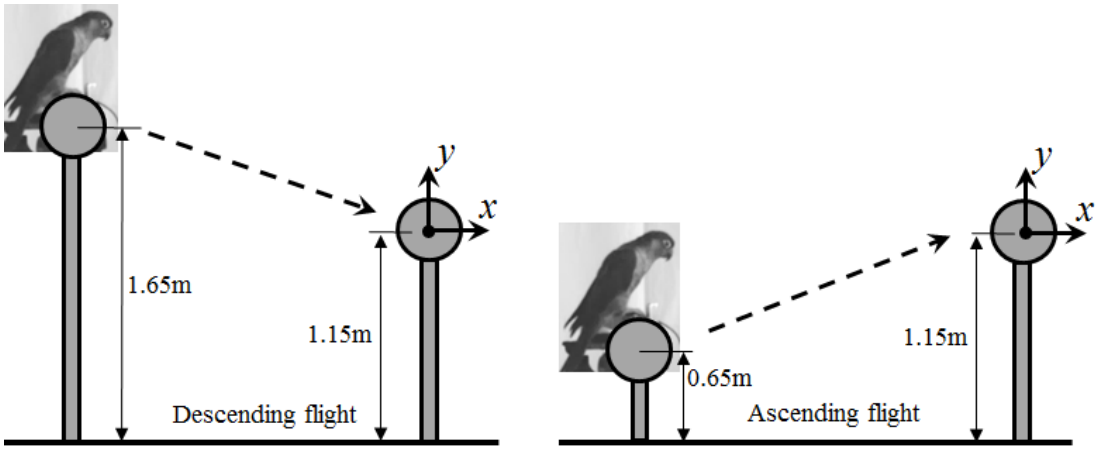

Figure 3.2 Two instances of perching experiments. Left: Descending flight; Right: Ascending flight. Note that the origin of the planar coordinate system is located at the center of the target perch.

Tracker, an open source program [70], is used to extract kinematic data from the videos. Two parameters directly extracted are the position of the center of mass (CM) of the subjects (x_{CM}, y_{CM}) and their body angle β, as defined in [68], [71] and [72], and demonstrated in Figure 3.3. For the convenience of data extraction, the line from the wing root to the rump defining the body angle (BA) is approximated with the line connecting the two marker points on the edge of birds' body figure. Furthermore, the position of CM is approximated based on an isosceles right triangle formed with these marker points, as shown in Figure 3.3. The approximation of CM position is to facilitate data extraction, and its error should be insignificant because of the small size of the parrots and the relative long flight distance. The origin of the global reference frame is located at the target perch, with *x* axis in the flight direction and *y* axis in the vertical direction. The formulae are as follows:

$$\beta = tan^{-1}\left(\frac{y_u - y_l}{x_u - x_l}\right) \tag{3.1}$$

$$x_{CM} = x_l + \sqrt{2}s \cdot \sin\left(\frac{\pi}{4} - \beta\right) \tag{3.2}$$

$$y_{CM} = y_l + \sqrt{2}s \cdot \cos\left(\frac{\pi}{4} - \beta\right) \tag{3.3}$$

where $s = \frac{1}{2}\sqrt{(x_u - x_l)^2 + (y_u - y_l)^2}$. Note that (x_u, y_u) and (x_l, y_l) are the coordinates of the upper and lower marker points, respectively.

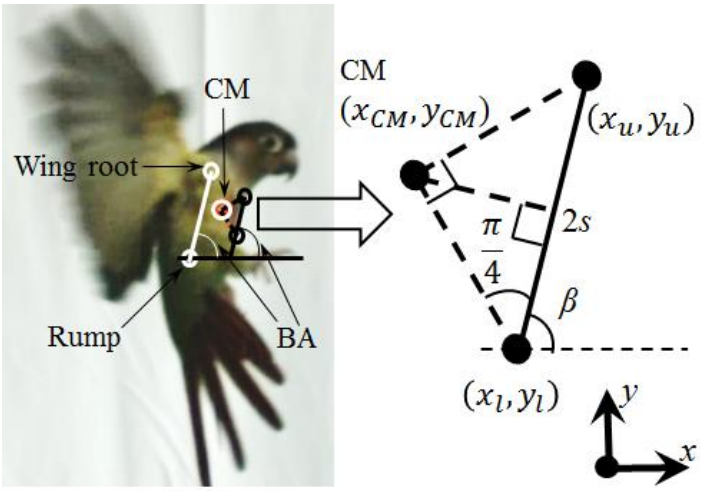

Figure 3.3 Definitions of the CM and BA of the parrot. The white circles and line denote the definitions in [63] and [68], while the black ones represent the approximation used for convenience of data extraction. The upper black point is located at the neck root, and the lower one is at the belly. The CM is estimated as the vertex of the isosceles right triangle formed together with the two approximation points. The BA is represented by β.

A series of footages from one perching trial with extracted information is integrated and shown in Figure 3.4. Footages A to E demonstrate the approaching flight before touchdown, while footages F and G depict the balancing procedure of the parrot after touchdown. The light blue and red circles represent the two marker points for positioning. The pink lines denote the coordinate axes, and the dark blue line at the bottom right corner is the calibration stick for the distance in the scene.

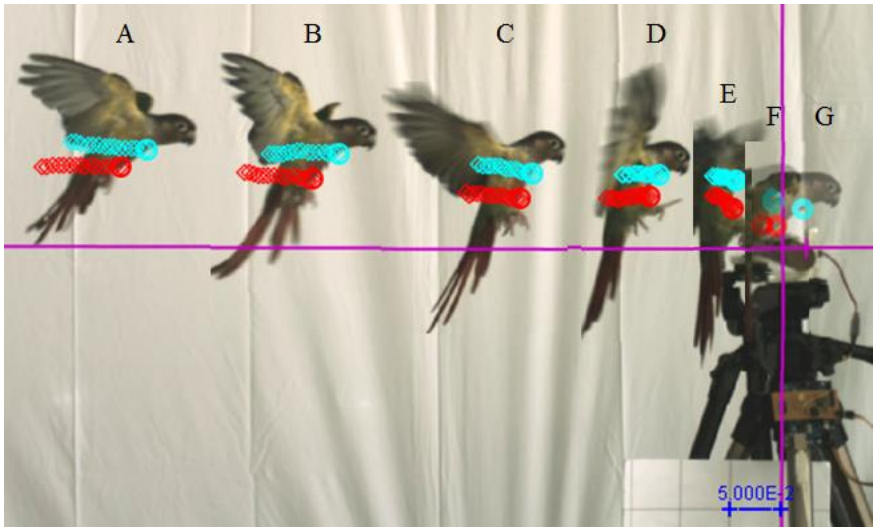

Figure 3.4 Footages of the perching procedure of a parrot

3.2 Generalization of the Perching Procedure of Birds

Birds that fly and perch have two kinds of locomotors, wings and legs. Perching or landing can be considered as a transition procedure from winged locomotion to legged locomotion, while taking off the other way [73][74][75][76]. Thus, it makes sense that generalization of the whole perching procedure from the perspective of locomotors can definitely facilitate the exploration into the perching principles of birds. Although systematic observations on the perching behaviors of birds can be found in literatures [60][63][68], the generalization of the perching procedure has never been addressed. Based on the data obtained from the experiments with the parrots, the perching procedure is generalized in this section.

3.2.1 Locomotion Analysis of Perching Parrots

A typical set of perching trajectory data of a parrot from our experiment is shown in Figure 3.5. The circles denote the CM position of the parrot extracted from consecutive flapping cycles during perching. Gaps exist between the clusters of the circles, because the marker points on the parrot's body are blocked by the flapping wing for approximately half of the flapping cycle. To depict the trend of the trajectory more explicitly, a solid line representing the fitted trajectory is also drawn. The CM position at the moment of touchdown is marked with a solid circle, and the origin is located at the perch.

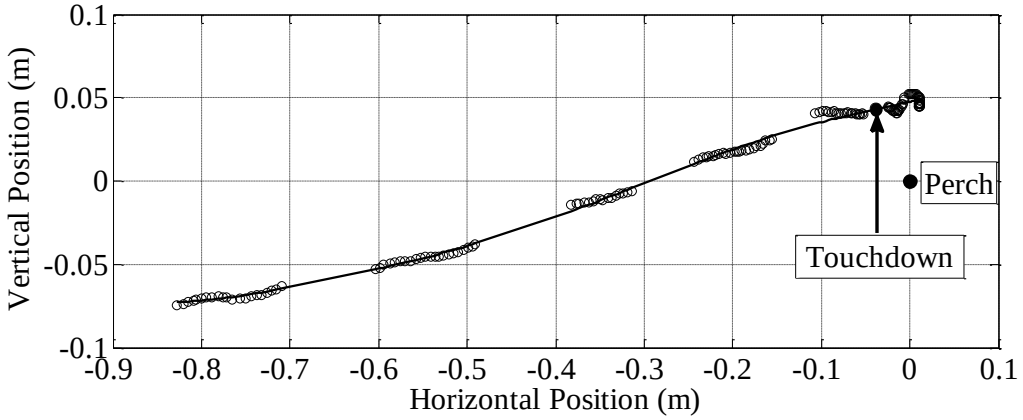

Figure 3.5 CM trajectory of the parrot during perching. The circles denote the position of the CM extracted from the video, and the solid line represents the fitted trajectory. The solid circle on the trajectory is the estimated position of the CM at touchdown. The origin is located at the perch.

It can be seen that during the final approaching stage the parrot ascended toward the target perch, although it was actually the descending flight scenario. It is generally accepted that such a trajectory will help birds brake before touchdown. The trajectory during each flapping cycle is relatively smooth, with small fluctuation probably resulting from the up- and down-strokes. The parrot even approached the perch almost horizontally during the flapping cycle immediately before touchdown, which means the vertical approaching speed is close to zero. Generally, the parrots also start to stretch their legs in this period, getting ready for the touchdown. On the other hand, the obvious modulation of the trajectory after touchdown indicates the effort the parrot makes to regulate the interaction with the perch. The CM at first goes downward, suggesting that the parrot was damping the approaching speed by flexing its legs. Finally the CM is lifted to the stable region directly above the perch by actively stretching its legs, and balance is obtained. During this process its wings also assist in obtaining the balance by generating desired lift. With the CM eventually balanced, the transition from winged locomotion to legged locomotion is successfully accomplished. Apparently, discrepancy exists in the maneuvers before and after touchdown. To further evaluate this maneuver difference from the perspective of body posture, the body angle of the parrot during the whole perching procedure is analyzed.

Figure 3.6 demonstrates the body angle of the parrot during perching. The circles denote the body angles at the specific time, with the moment of touchdown defined as T=0. Similarly, only data from the portion of the flapping cycle that the parrot body is not blocked by the wings are plotted. It shows that the body angle almost proportionally increases to around 90 degrees before touchdown, which is consistent with previous research [61][68]. Also, the fluctuation of the body angle in each flapping cycle is even more obvious than that of the CM trajectory. The body angle of the parrot tends to increase during the upstroke (backstroke) and decrease during the downstroke (forthstroke). This implies that the resultant forces on the wings generate a counterclockwise moment in upstroke and a clockwise moment in downstroke at the wing roots in each flapping cycle. Another potential contribution may come from the internal torque that is applied to rotate wings about their

spanwise axis in the flapping cycle. This information is rather valuable because it might reflect one of the potential mechanisms by which the parrot adjusts its posture with wings for perching. Compared with the characteristics before touchdown, the body angle decreases quickly to around 40 degrees and gradually converges to the neutral perching posture of about 50 degrees after touchdown. Such a difference in the characteristics of oscillation of the body angle further validates the distinguished maneuvers of the parrot before and after touchdown.

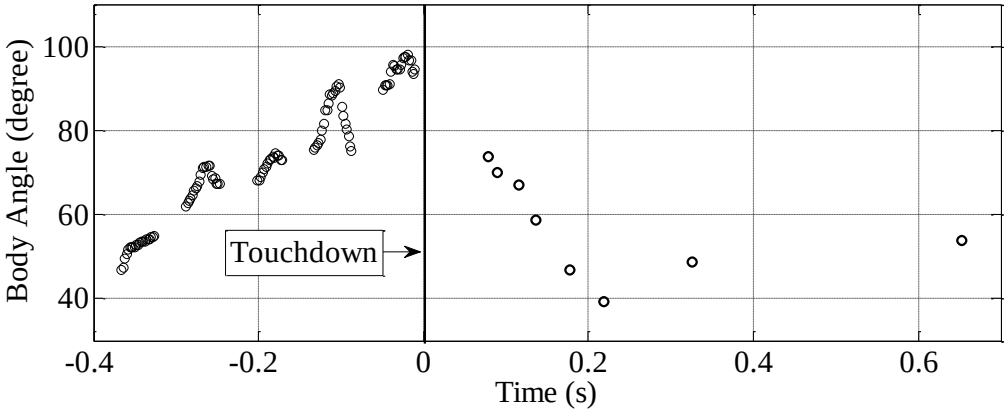

Figure 3.6 Body angle of the parrot. T=0 represents the touchdown moment.

Consequently, it can be concluded that both locomotors, i.e., wings and legs, play a significant role in damping the approaching speed and obtaining body balance during perching, and that touchdown is a marking point of the change of the primary locomotor during the perching procedure.

3.2.2 Perching Procedure Generalization

Following the locomotion analysis of perching parrots in previous section, the perching procedure can be generalized into three stages, namely pre-perching, on-perching and post-perching, as illustrated in Figure 3.7. The three stages are divided by two moments, touchdown and when the wings are folded by the bird, and they are featured by different types of the locomotors.

The key maneuvers of the whole perching procedure is further elaborated as follows. During pre-perching, birds first approach the target perch with a preferred or favorable flight trajectory along which the approaching speed is reduced by pitching up the body angle and changing the flapping direction of wings. When it comes close

to the touchdown birds will stretch their legs and expand their feet to get ready for the touchdown. On-perching starts from the moment of touchdown when the feet of birds contact the perch. As the approaching speed at this moment is not reduced to zero yet, an impact is expected. To avoid any injury, birds flex their legs and manipulate the lifting force to damp the impact. Through a series of dynamic regulating maneuvers reliable attachment to the perch is achieved and body balance is eventually secured. Once birds obtain the body balance, their wings are folded and successful perching is accomplished. Maneuvers thereafter, such as sitting, walking and hopping, generally merely involve legs. This stage is therefore classified as post-perching. Note that take-off can also be included in the post-perching stage, as a maneuver that involves both legs and wings.

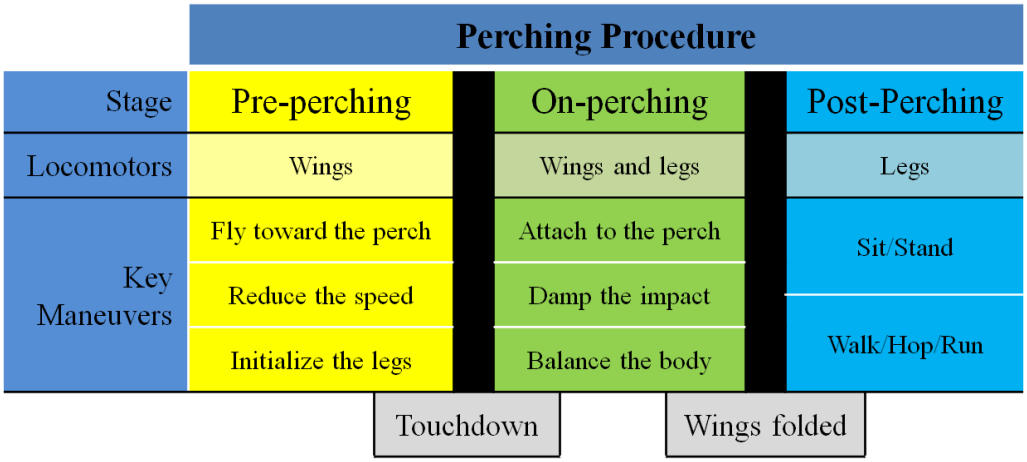

Figure 3.7 Generalized perching procedure of birds

Apart from facilitating classified research on the perching principles of birds, another main benefit of the generalization of the perching procedure is providing a scientific guideline for the development of the automatic perching methodology for UAVs which is exactly the topic of this thesis. As a result, the investigations in this thesis are organized following the manner of such a generalization.

3.3 Pre-perching--Approaching Flight before Touchdown

As wings are the only locomotors of birds before touchdown, the key points should be the approaching flight and its navigation method. The trajectory of the approaching flight can reveal the perching preference of birds under different perching circumstances and therefore can give some reflections on the navigation

method for UAV perching. *Tau Theory* has been found also applicable to birds' landing, so it will be the focus of the navigation study in this thesis.

3.3.1 Trajectories and body angles of approaching flights

The trajectories of the CM of the parrots before touchdown are extracted and plotted in Figure 3.8. It should be noted that since the body of the parrot is generally blocked by one wing for a certain period in each flapping cycle, the positions of the two marker points in this period are estimated for extraction and smoothened in post-processing. Generally, all the perching trials show the preference of the parrots to approach the perch with an ascending trajectory, no matter whether it is the descending or ascending perching scenario. The only exception exists in the case of descending perching of bird 2, one time of which the bird approached the perch with a slightly descending trajectory (the green curve in the middle subplot of the left column of Figure 3.8). Such a preference makes sense in multiple aspects. Firstly, consider the locomotion in vertical direction. An ascending trajectory in descending perching scenario means birds dive at first and then pitch up later. From the perspective of force manipulation, such a trajectory can turn the gravity force in birds' favor, because the gravity force will decrease the vertical velocity of birds, instead of increasing it in the case of a descending trajectory. Consequently birds can save some effort of wings' flapping for braking in the vertical direction and thus the risk of injuring birds' legs or feet can also be reduced. Besides, for the ascending perching scenario, a descending trajectory means that extra energy needs to be consumed to lift the bird to a higher height along the flight, which is not desirable. This could probably be the reason why no descending trajectory is observed for the ascending perching scenario. Secondly, for the horizontal locomotion, birds in the descending perching scenario can gain velocity with less effort during the beginning stage of the flight because the increased vertical velocity from the diving maneuver can help generate the aerodynamic lift that can be manipulated to accelerate the bird in horizontal direction. Despite the overall ascending trend of the trajectory, an interesting phenomenon should be noted that the trajectories tend to exactly reach or slightly go over the peak at touchdown. It verifies the necessity of generating appropriate engagement angle and close-to-zero vertical contact velocity for birds.

However, such kind of ascending trajectories is more applicable to fixed wing UAVs whose lift is mainly generated by wings, just like birds. For UAVs like quadrotors, the lift is all generated by the propellers, and therefore it is not necessarily the optimal trajectory for quadrotors.

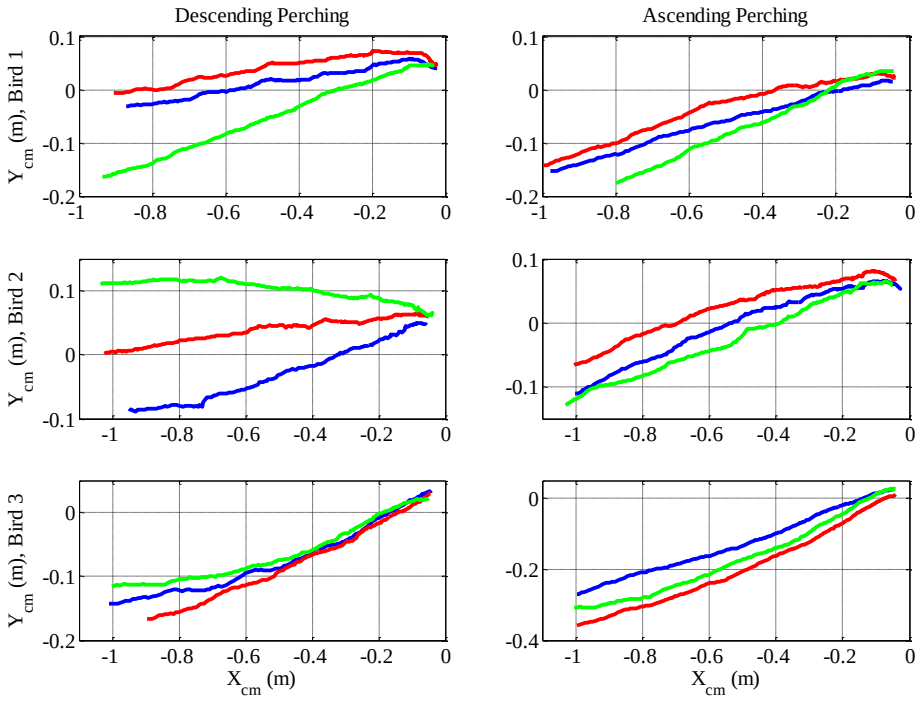

Figure 3.8 Trajectories of the CM of the parrots before touchdown. The three rows show the data from parrot 1, 2 and 3, respectively, while the left and right columns represent descending and ascending perching, respectively. Different colors denote multiple perching trials.

The time series of the body angles of the parrots before touchdown are illustrated in Figure 3.9, with the moment of touchdown defined as T=0. It can be found that in common birds tend to pitch up their body angle from 40~60 degrees at the beginning of the recorded data to 80~100 degrees at touchdown. This is consistent with the analysis of the CM trajectories, as pitching up is directly related to braking. Quadrotors use similar braking method by pitching up, but they need to pitch down to generate forward lift, which is not the case for birds.

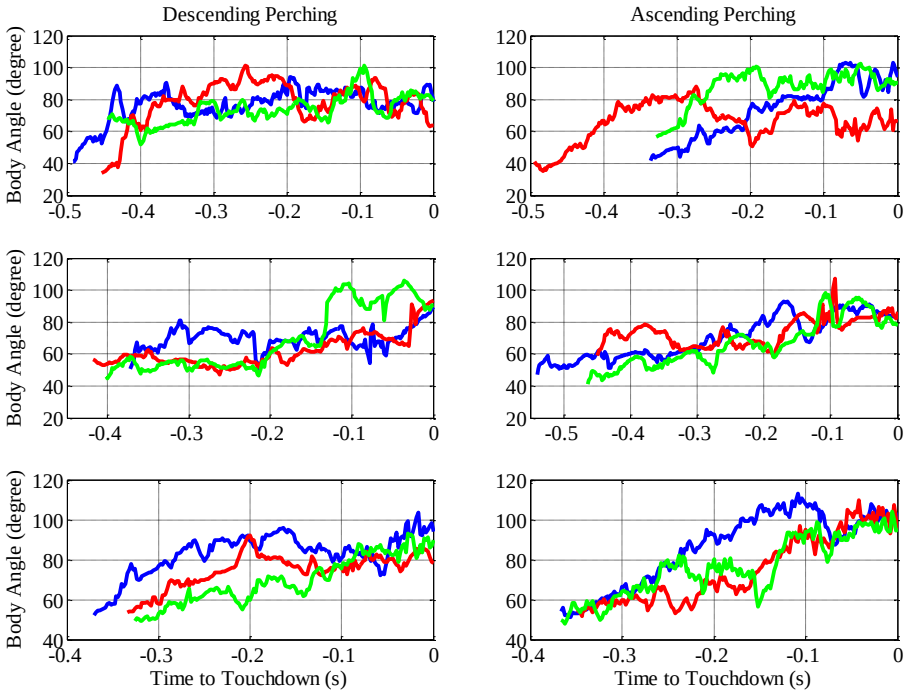

Figure 3.9 Body angles of the parrots before touchdown. The three rows show the data from parrot 1, 2 and 3, respectively, while the left and right columns represent descending and ascending perching, respectively. Different colors denote multiple perching trials.

3.3.2 Navigation Patterns of Tau-dot

With the characteristics of birds' approaching flight analyzed, the navigation method that birds use should be further addressed. According to *Tau Theory*, the position gap and the velocity of gap closure are required to calculate tau, and further tau-dot. The velocity information of the parrots is calculated based on the position information extracted. To reduce the effect of the position error resulting from manual selection of the marker points on the velocity calculation, the trajectories are first fitted with third order polynomials. The calculation of the velocities is then done based on the fitting result. It also should be noted that the origin of the world frame for trajectory extraction is set at the center of the target pole. However, the final position of the center of mass of the parrot after perching is actually above the origin. To make tau-dot accurate, the final position of the center of mass of the birds, instead of the origin, is taken as the target position. Figure 3.10 demonstrates the time-to-contact, or tau, in x (horizontal) direction during the perching flights, and Figure 3.11 shows the corresponding tau-dot. Y direction is not taken into account because the case of over-

peak of the trajectory at touchdown, as discussed in previous section, is not addressed by *Tau Theory*.

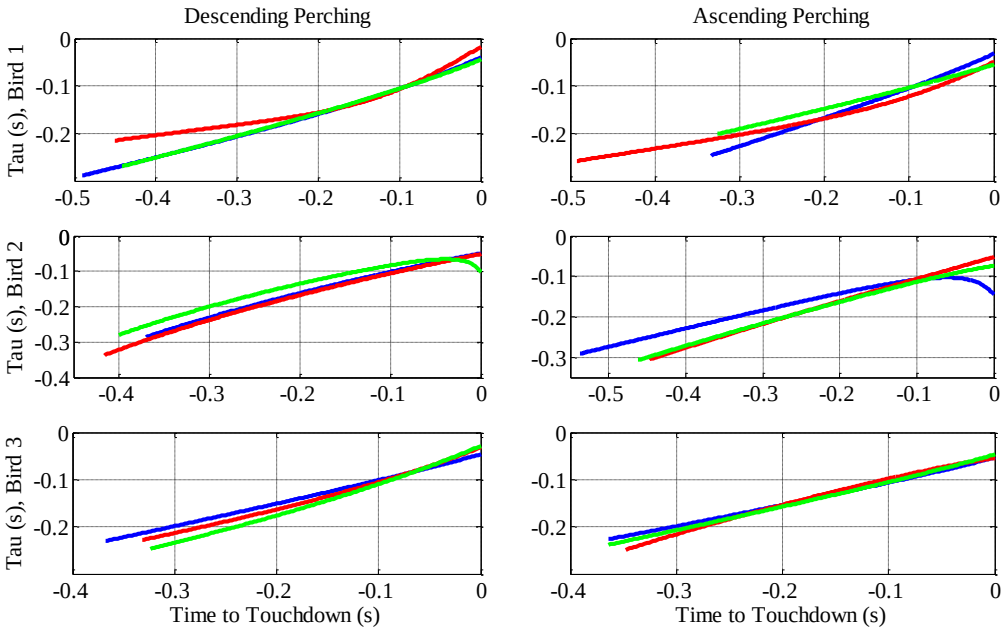

Figure 3.10 Tau vs. distance in x direction for descending (left column) and ascending flights (right column). Different colors represent different perching flights.

In Figure 3.10, the horizontal axis denotes the actual time to touchdown, with the touchdown moment defined as T=0, while the vertical axis represents tau calculated from the fitted data of distance and velocity in x direction. From the figure it can be seen that the trends of the curves of tau are rather consistent, not only within each perching scenario and each bird but also among different scenarios and birds. Tau curves of some perching trials, such as those in green for different birds and different scenarios are approximately linear, supporting the conclusion drawn by other researchers that a constant tau-dot is expected. However, variation in the slope of the tau curves is also observed for most of the trials, which leads to varying tau-dots. To further evaluate the variation of the tau-dots, the corresponding tau-dot curves are plotted in Figure 3.11.

It shows that actually tau-dot does tend to stay constant or vary little when the birds are not close to the target yet; however, it rarely stays constant through the whole perching flight. Moreover, the preferred range of tau-dot from 0 to 0.5 for birds to

achieve optimal perching, as stated in *Tau Theory*, is not observed. Basically tau-dot varies between 0 and 1. No general trend of tau-dot for all birds can be concluded, but it is obvious that for each bird a certain trend does exist. Bird 1 and 3 tend to increase the tau-dot to above 0.5 as they approach the perch, while bird 2 is likely to decrease the tau-dot to below or maintain it around 0.5. Note that tau-dot of bird 2 even becomes negative right before touchdown during two perching flights, which means the velocity is reduced quicker than the distance. To cover all typical cases of varying tau-dots, four patterns are concluded, namely the increasing pattern (red curves of bird 1 and red and blue curves of bird 3 in descending perching), the quasi-constant pattern (green curve of bird 1 in ascending perching), the negative pattern (green curve in descending perching and blue curve in ascending perching of bird 2) and the decreasing pattern (red curve of bird 3 in ascending perching).

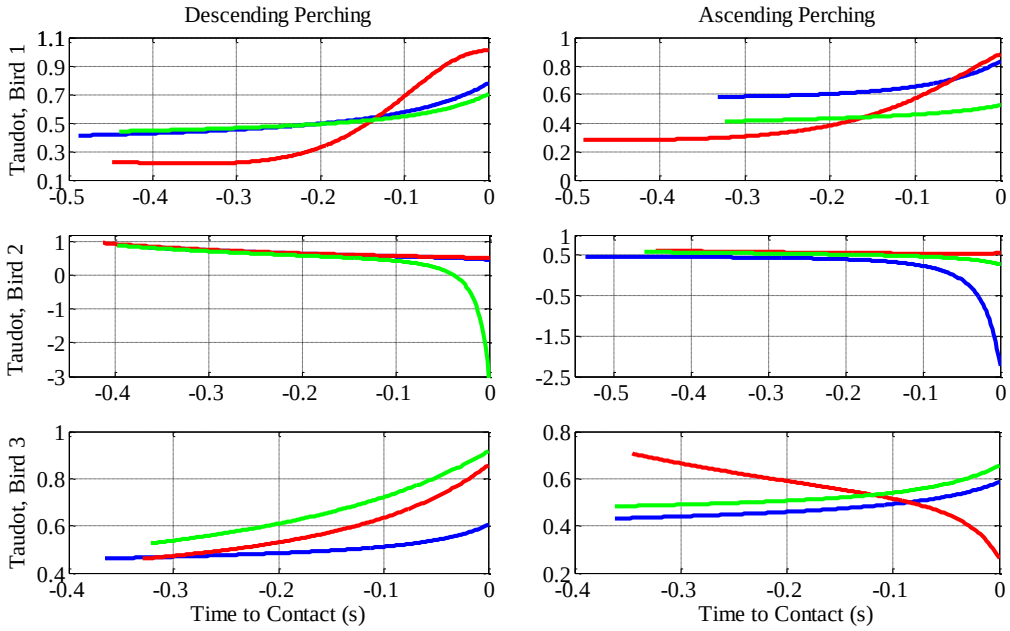

Figure 3.11 Tau-dot in x direction for descending (left column) and ascending flights (right column). Different colors represent different perching flights.

3.3.3 Discussion

Analysis of the approaching flights shows that the parrots tend to approach the perch from below with an ascending trajectory and a pitching-up body angle, no matter whether the start position of the flight is above or below the target perch. It is believed such a maneuver makes the flight control, such as braking and engaging the

perch with a desired angle, easier for the birds. The analysis of the navigation patterns of tau-dot based on *Tau Theory* demonstrates obvious varying patterns different from the constant one proposed and accepted in existing research. It further results to a conclusion of four typical varying patterns which can be potentially applied as the navigation patterns for UAVs.

3.4 On-perching Balancing Maneuvers after Touchdown

A typical on-perching sequence of bird 2 is demonstrated in Figure 3.12. The horizontal and vertical lines represent the x and y axis respectively, while the two circles denote the corresponding marker points. It can be seen from the footages that after touchdown the bird flexed its legs to damp the impact. When the legs reached flexion limit they started stretching to lift the body toward the balance position which is directly above the perch. Also, the body angle of the bird was manipulated during this procedure. Further quantitative analysis is conducted in the following section.

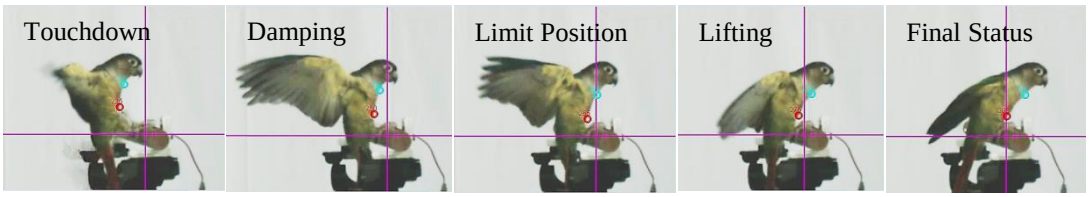

Figure 3.12 Footages of an on-perching sequence of bird 2. Touchdown: the feet contacted the perch; Damping: the legs flexed to damp the impact; Limit Position: the legs flexed to the maximum position; Lifting: the legs stretched to lift the body to above the perch; Final Status: the body's CM was directly above the perch to obtain balance.

3.4.1 Trajectory of the CM

The trajectories of the CM and the body angles of the three parrots after touchdown are first extracted. Figure 3.13 shows the CM trajectories, grouped into two columns of descending (left column) and ascending flight (right column). It can be seen that all the trajectories tend to converge to a region above the perch, which is consistent with the fact that the projection of the bird's CM needs to be located within the support polygon on the perch. This is exactly the transition process of the parrots from winged locomotion to legged locomotion. The trajectories from descending flight of bird 1 and 2 shows that even under the same perching circumstances the CM

trajectories of an individual bird may vary significantly. This is probably because the initial conditions at touchdown, for instance, the touchdown velocity, are not controlled in a consistent way by the birds. On the other hand, bird 3 has shown better consistency in both perching scenarios. Generally, the initial conditions of bird 3 at touchdown, such as instantaneous positions of the CM and touchdown angle, are closer among trials compared to those of other birds.

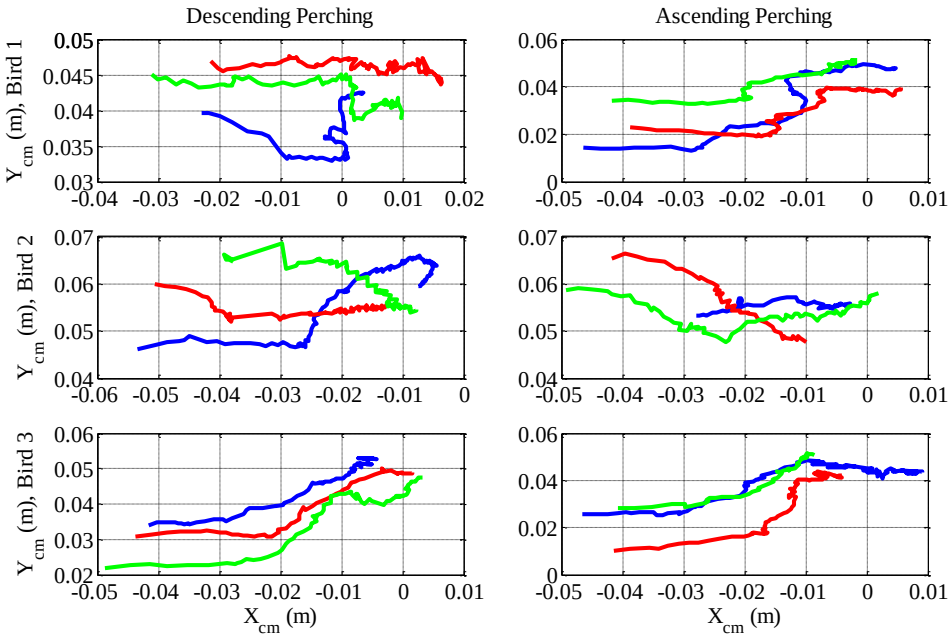

Figure 3.13 Extracted trajectories of the CM of the parrots after touchdown. The left column shows trajectories of the CM in descending perching for bird 1, 2 and 3, respectively, while the right column demonstrates those in ascending perching for birds 1, 2 and 3, respectively. Curves in different colors represent data from different trials.

It's obvious that the trajectories of the CM generally remain horizontal for a certain period after touchdown, which means the vertical touchdown velocity is almost zero, and then go up to the final balance position. These characteristics correspond to the observation that after touchdown birds generally flex their legs to decelerate first while rotating their body toward the balance region above the perch, and then stretch the legs to lift their body. Figure 3.13 also demonstrates that the perching trajectories after touchdown with descending and ascending flights are generally different (birds 1 and 2), although they can be consistent for certain birds (bird 3).

3.4.2 Body Angle, β

Despite of the discrepancy in the trajectories of the CM, it is found that the body angles between descending and ascending flights show greater consistency for every subject. Therefore mean body angles across 6 perching flights for each subject are obtained and depicted in Figure 3.14. Note that the number of data points is equal to that of the single perching trial with the least time steps among all 6 trials. The same averaging method is also used to obtain the mean values of the remaining parameters in this section.

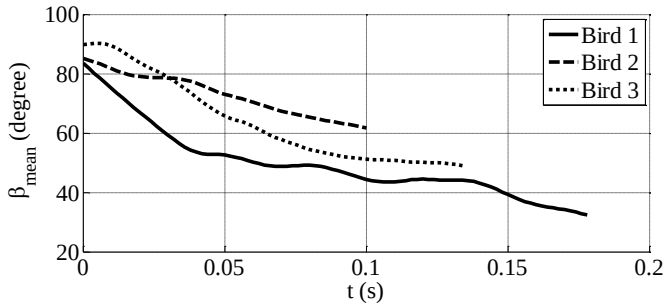

Figure 3.14 Mean body angles β_{mean} of the three birds over time after touchdown (bird 1: solid curve; bird 2: dashed curve; bird 3: dotted curve).

A manifest characteristic can be seen in Figure 3.14 that all the subjects possess a body angle of around 80 to 90 degrees at touchdown, which is consistent with previous research [61][68]. This is generally believed to be associated with the deceleration of the flight before touchdown. Figure 3.14 shows that the initial increase of the body angle to above 80 degrees is also associated to the balancing maneuvers after touchdown, since it can provide sufficient clearance for adjustment of the body angle. However, the adjustment of the body angle shows no consistent pattern. It is approximately linear for bird 2, while more complex for birds 1 and 3. This further indicates the different preferences of the perching maneuvers of different birds. From the perspective of time domain, the subjects achieve balanced perching status generally within 0.2s from touchdown. Sometimes there is no flapping of wings during this period if the approaching control is perfect (bird 3, the second descending perching and the third ascending perching), but up to one flapping cycle has been observed in most perching trials. Therefore, it can be concluded that the flapping of wings can significantly assist birds in obtaining balanced perching status.

3.4.3 Spatial Coordinates of the CM in Time Domain

As no general pattern has been found in the spatial CM trajectories of all birds, the mean coordinates under Cartesian and polar frame are further analyzed in time domain. The relationship between polar coordinates and Cartesian coordinates (x_{cm}, y_{cm}) is given by

$$r_{cm} = \sqrt{x_{cm}^2 + y_{cm}^2},\ \theta_{cm} = \cos^{-1}\frac{x_{cm}}{r_{cm}}. \tag{3.4}$$

The mean Cartesian coordinates $x_{cm-mean}$ and $y_{cm-mean}$ of the CM of the three birds are illustrated in Figure 3.15(a) and Figure 3.15(b), respectively. It shows that the *x* coordinates consistently converge to around 0, while *y* coordinates to around 0.05. The steeper slope of the *x* plots at the first 0.05 second means the horizontal velocity is mainly damped during this period. However, the *y* plots generally show large changing rate from 0.05 to 0.1 second, which corresponds to the body lifting stage of the birds. This indicates that the perching maneuvers of birds might just decouple the adjustment of the CM in *x* and *y* directions, and therefore it suggests the applicability of a decoupled 2-DOF dynamic model. The decaying trend in *x* coordinate conforms to such a model, but the dynamic attenuation in *y* coordinate shows no obvious consistent characteristic. To seek more support on the applicability of a 2-DOF dynamic model, the polar coordinates are further analyzed.

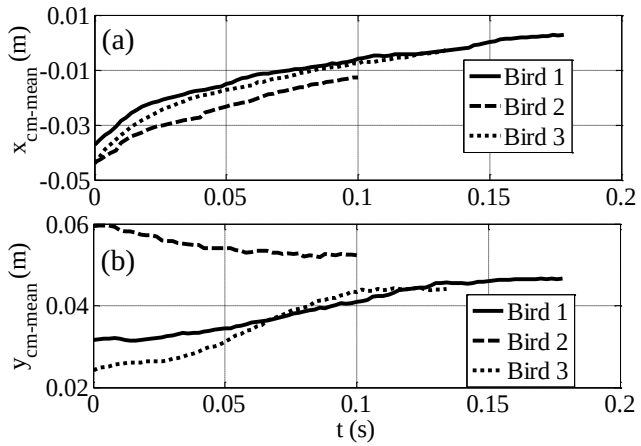

Figure 3.15 Mean Cartesian coordinates (a) $x_{cm-mean}$ and (b) $y_{cm-mean}$ of the three birds (bird 1: solid lines; bird 2: dashed lines; bird 3: dotted lines).

The mean radial coordinates $r_{cm-mean}$ and the mean angular coordinates $\theta_{cm-mean}$ of the CM of birds 1, 2 and 3 are obtained and depicted in Figure 3.16(a) and Figure

3.16(b), respectively. It can be seen that the consistency among birds still holds. More importantly, the attenuation of both radial and angular coordinates is much more obvious. Oscillation in radial coordinate agrees especially well with the behavior of a typical 2-DOF mass-spring dynamic system. The decaying of the angular coordinate is nearly linear, suggesting the possibility of simple dynamics modelling.

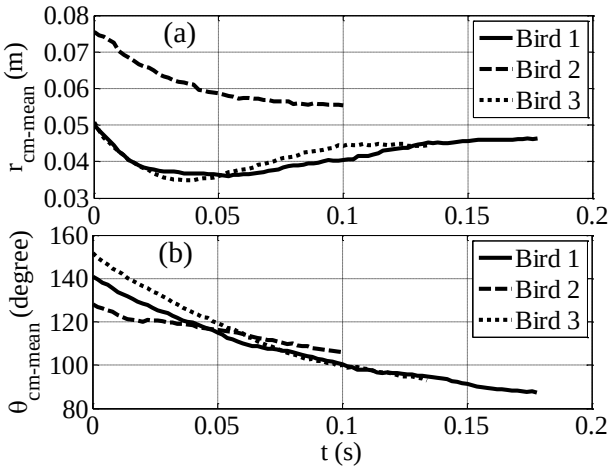

Figure 3.16 Mean polar coordinates (a) $r_{cm-mean}$ and (b) $\theta_{cm-mean}$ of the CM of the three birds (bird 1: solid lines; bird 2: dashed lines; bird 3: dotted lines).

3.4.4 Discussion

Based on the results presented above, both the position of the CM and the body angle are adjusted adaptively to achieve balanced perching. Also, both wings and legs play a significant role in damping the approaching speed and balancing the body. Moreover, the data analysis in the sagittal plane indicates that a decoupled 2-DOF mass-spring dynamic system should be applicable for modelling the perching maneuvers of birds after touchdown. The manipulation force in radial direction and torque in angular direction can be provided by wings and legs. For quadrotors, a lift force and pitch-adjusting torque can be readily generated. Therefore, a 2-DOF dynamic perching model should also be applicable to quadrotors.

Furthermore, is it the case that these maneuvers are totally achieved by work of manipulation forces and moments from wings and legs? Intuitively it would not be energy-efficient if so, as actuation of the locomotors for damping and adjusting body posture requires intense energy consumption. Moreover, it would risk the locomotors

getting injured. On the other hand, if the kinetic energy of the bird at touchdown is harvested to help manipulate the body, the extra energy needed for the locomotors could be significantly reduced, and the risk of injury of the locomotors would also be diminished greatly. That is, the approaching velocity does not necessarily need to be reduced to zero at touchdown; on the contrary, a velocity with certain magnitude and angle might benefit birds for damping and balancing with alleviated muscular effort of their locomotors. Thus, energy efficiency imposes requirement of control on the initial conditions at touchdown on perching quadrotors.

3.5 Summary

A biological study on the perching procedure of parrots is carried out in this chapter. To establish a fundamental strategy for UAV perching, the trajectories of the CM and body angles of the parrots are analyzed and the perching procedure is consequently generalized into three stages, namely pre-perching, on-perching and post-perching. According to the generalization, the perching locomotion of the parrots is divided into two parts, with touchdown as the division point, and is investigated separately. From the perspective of *Tau Theory* four navigation patterns of varying tau-dot are concluded through detailed analysis of the approaching flights before touchdown. The balancing process after touchdown involving both CM trajectory and body angle is evaluated thoroughly. The applicability of a 2-DOF dynamic model to the balancing process of a perching quadrotor is also discussed preliminarily. The whole perching procedure of birds is addressed from a biological perspective sequentially according to the generalization. Profounder exploration into the characterization and modeling of the procedure for perching with UAVs will also be conducted in a similar sequential way in the following chapters.

Chapter 4 Fuzzy Guidance of Pre-perching Flight of UAVs Based on Varying Tau-dot

Constant tau-dot has been applied as the control strategy to guide UAVs for perching. However, from experiments with parrots varying tau-dot is found. Therefore, the potentials of varying tau-dot to be applied to pre-perching flight guidance for UAVs require thorough investigations. As varying tau-dot means real-time regulation during the pre-perching flights, its comparison with constant tau-dot can reveal the principles of the regulation process and facilitate the UAV guidance strategy design.

4.1 Varying Tau-dot for Guidance of Pre-perching Flight

4.1.1 Varying Tau-dot as Discrete Constant Tau-dot

For one-dimensional motion, the formulas of distance, velocity and acceleration under constant tau-dot, as in [54][55], are as follows,

$$\begin{cases} \chi(t) = \chi_0(1 + k\dot{\chi}_0 t/\chi_0)^{\frac{1}{k}} \\ \dot{\chi}(t) = \dot{\chi}_0(1 + k\dot{\chi}_0 t/\chi_0)^{\frac{1}{k}-1} \\ \ddot{\chi}(t) = \dfrac{\dot{\chi}_0^2}{\chi_0}(1-k)\left(1 + \dfrac{k\dot{\chi}_0 t}{\chi_0}\right)^{\frac{1}{k}-2} \end{cases}. \tag{4.1}$$

Since varying tau-dot is found from experimental data, it is of interest to see whether these formulas still hold under the assumption that for each short-enough sections of the time series of varying tau-dot, constant tau-dot can be applied. To do so, tau-dot from fitted experimental data at each time step is substituted into the formulas above to estimate the distance and velocity at next time step. Note that only the initial distance and velocity from the fitted experimental data are utilized to initiate the estimation. Afterwards only estimated values are used to propagate the estimation. Finally the estimated values are compared with the raw experimental data. In order to cover all typical patterns of tau-dot, four flights are chosen for verification, namely descending flight 2 of bird 1 with the increasing pattern, ascending flight 3 of bird 1 with the quasi-constant pattern, descending flight 3 of bird 2 with the negative pattern and ascending flight 2 of bird 3 with the decreasing pattern. The results are depicted in Figure 4.1.

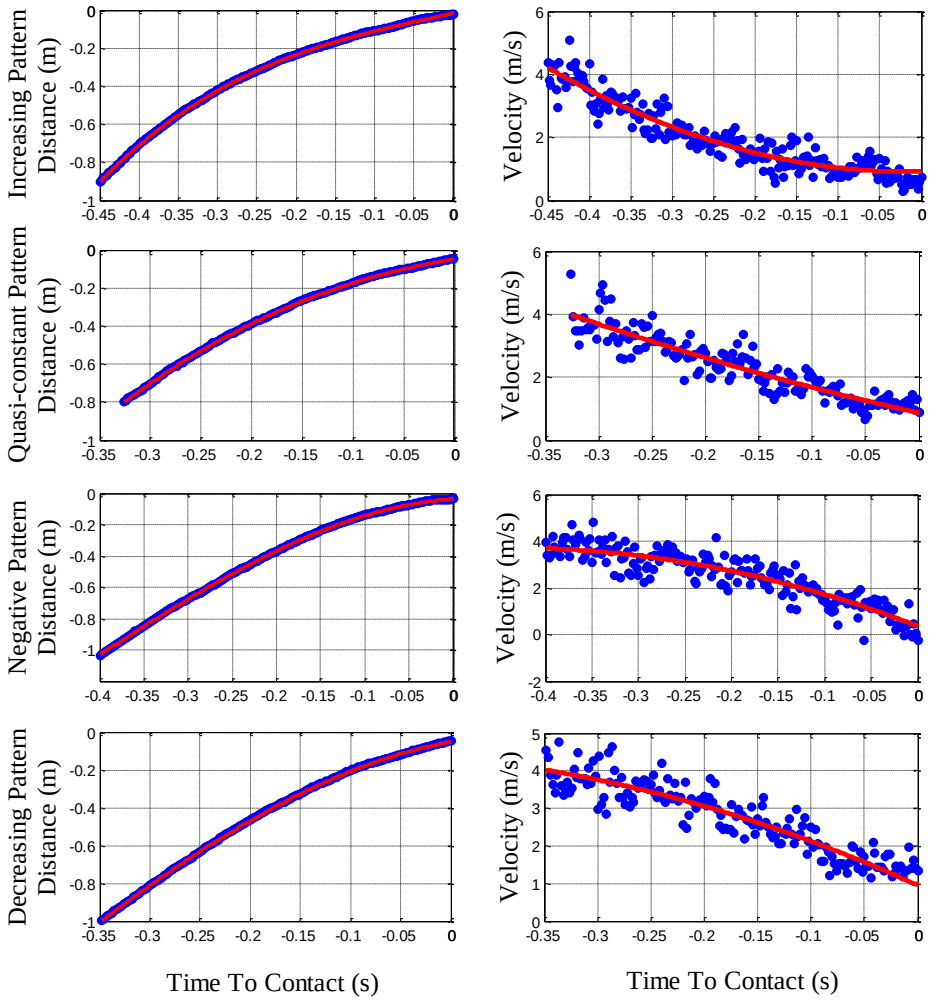

Figure 4.1 The estimated (red curves) distance (left) and velocity (right) versus experimental data (blue dots)

For all four patterns, the estimated distances are almost exactly overlapping with the experimental data, showing great agreement, and the estimated velocities also follow the trend of experimental data closely. Even better agreement can be obtained if the comparison is done with fitted experimental data. It can be concluded, therefore, that the formulas for constant tau-dot can be applied to the case of varying tau-dot in a discrete way.

4.1.2 Justification of Varying Tau-dot

As concluded in [39][54][55], a constant tau-dot between 0 and 0.5 leads to simultaneous zero-reaching for distance, velocity and acceleration, and therefore no

collision or impact will occur, making it the optimal strategy for safe landing. However, in our experiments, the parrots rarely keep the tau-dot within this optimal range. Why would they risk their landing safety in such a way? On one hand, it might be because they cannot track the tau-dot accurately. On the other hand, it could be due to the potential advantages that they would get, such as less energy consumption or shorter time. In previous section it has been verified that varying tau-dot can be interpreted as constant tau-dot in a discrete manner, but a rational justification of the varying tau-dot is still necessary. From the formulas, one can derive that, for a constant tau-dot between 0 and 0.5, the closer the distance gets to zero, the smaller the velocity becomes, and the longer relatively it takes to reach zero. For birds, this means less agility to manipulate for landing. Also, since they need to keep flapping to remain airborne with small approaching speed at the final stage of landing, the energy consumed would be larger, reducing the energy efficiency. It therefore makes sense that in order to close the distance gap more quickly, to maintain the flight agility, and to save some energy during the final stage of landing, birds vary the tau-dot beyond the optimal range accordingly along the perching flight and perch with non-zero final velocity and acceleration which are within a certain acceptable range. To validate this hypothesis, the perching time and touchdown velocity of the four patterns are compared with the values calculated with constant tau-dot of 0.3 under the same initial conditions. The results are listed in Table 4.1

Table 4.1 Comparison between varying tau-dot and constant tau-dot

	Varying $\dot{\tau}$			**$\dot{\tau} = 0.3$**		
	Time (s)	***Vel. (m/s)***	***Acc. (m/s^2)***	***Time (s)***	***Vel. (m/s)***	***Acc. (m/s^2)***
Increasing Pattern	0.450	0.90	0.5	0.716	0	0
Quasi-constant Pattern	0.348	0.85	-7.5	0.671	0	0
Negative Pattern	0.400	0.35	-15.3	0.932	0	0
Decreasing Pattern	0.326	0.94	-12.9	0.830	0	0

It is obvious that the approaching time for varying $\dot{\tau}$ is much shorter than that for $\dot{\tau} = 0.3$. Compared to varying $\dot{\tau}$, the time differences are 59.1%, 133.0%, 92.8%, and

154.6%, respectively. The cost at which the significant time differences are obtained is the less-than-1m/s final velocity and the final acceleration of up to 1.56g, where g represents the gravitational acceleration. Such a deceleration of 1.56g can be generated readily from pitching up the body and wings due to the non-zero approaching velocity, instead of from flapping the wings which costs more energy. As long as birds can physically withstand the final velocity and deceleration, the cost of those huge time differences should be rather affordable. Since perching flights with regulated varying tau-dot are quicker and thus more efficient than with constant tau-dot, varying tau-dot is justified to be utilized for perching flight guidance.

4.2 Design of Fuzzy Logic Based on Varying Tau-dot

According to the experiment data, the varying tau-dot is mostly kept between 0 and 1. When it occasionally exceeds 1, it tends to stay very close to 1. However, for the case of decreasing to below 0, no such limit has been observed. From the formulas of constant $\dot{\tau}$, one can derive that for $\dot{\tau} \leq 0$, the distance, velocity and acceleration will go to zero at infinite time, which means relatively large deceleration for current approaching velocity. For $0.5 < \dot{\tau} < 1$, the distance and velocity will get to zero at finite time but the final acceleration will tend to infinity, which means deceleration at the beginning is small and rapidly increases to infinity at the final stage. For $\dot{\tau} = 1$, the motion will be a uniform one with constant velocity and zero acceleration. It's rather likely that tau-dot are associated with the current approaching state of birds, and is interpreted in certain ways to help regulate parameters such as velocity and acceleration. Such piecewise empirical regulations make fuzzy logic quite applicable, and therefore a fuzzy guidance strategy is designed.

Tau-dot is the parameter that the fuzzy logic is supposed to tune. On the other hand, the distance gap to be closed and the time to contact, tau, are taken as the reference inputs, which is equivalent to the combination of the distance gap and the approaching velocity. However, tau can provide a more straightforward timing sense for maneuvering actions. Based on the comparison results from previous section, the decreasing pattern is chosen for modeling template because of its shortest perching time. It should be mentioned that other patterns can also be modelled to meet

different requirements for various applications. To facilitate the modelling, the distance, time to contact and tau-dot of the decreasing pattern are plotted in Figure 4.2. Each parameter is further fuzzified into three fuzzy sets, namely small (S), medium (M) and large (L). The universe of discourse for distance and tau, however, needs to be set more on a case-by-case basis, because they could be any values in different cases. Taking the specifications of our experiment setup into account, we set [-3m, 0] and [-12s, 0] for distance and tau, respectively. The universe of discourse for tau-dot can be case-independent, and is set [0.2, 0.8]. The membership functions (MFs) finally designed are shown in Figure 4.3. Note that none of the MFs is symmetrically distributed. The MFs of distance and tau are shifted toward zero while that of tau-dot toward 0.8, so as to feature the sudden decreasing of tau-dot when close to touchdown. The fuzzy inference rules are listed in Table 4.2. The large portion of L output is to keep tau-dot in the Large fuzzy set and consequently to shorten the overall perching time. Finally the surface plot of the fuzzy logic rules is illustrated in Figure 4.4

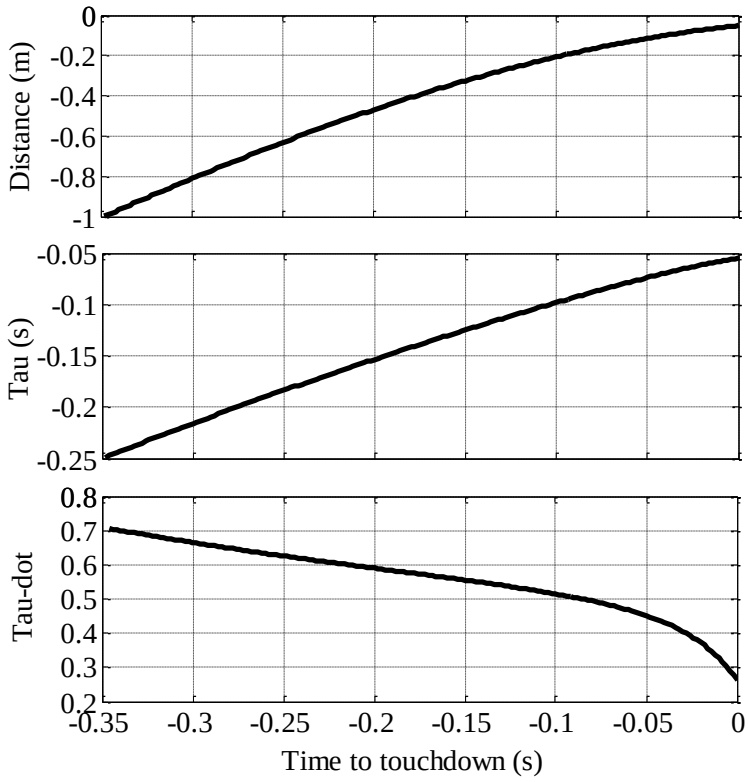

Figure 4.2 The distance, tau and tau-dot of the decreasing pattern

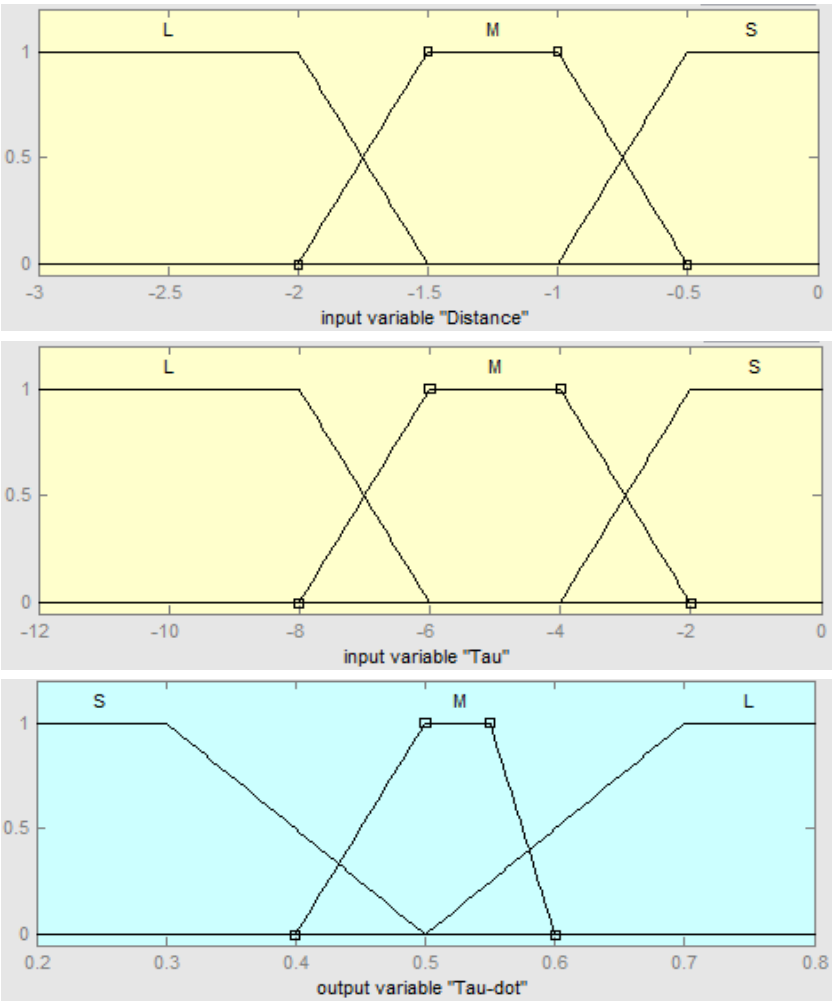

Figure 4.3 Membership functions of the input and output variables

Table 4.2 Fuzzy inference rules

		Distance		
		S	M	L
Tau	S	S	M	L
	M	M	L	L
	L	L	L	L

The fuzzy logic needs information on distance and tau to calculate the desired tau-dot. The measured values from the motion capture system are not used as feedback for the fuzzy logic, because there is another position controller on the lower level to follow the desired position and a certain delay, which would lead to undesired

velocity, exists. Instead, the estimated distance and tau based on discrete varying tau-dot are employed. Finally an estimator is designed as follows to render the estimated values.

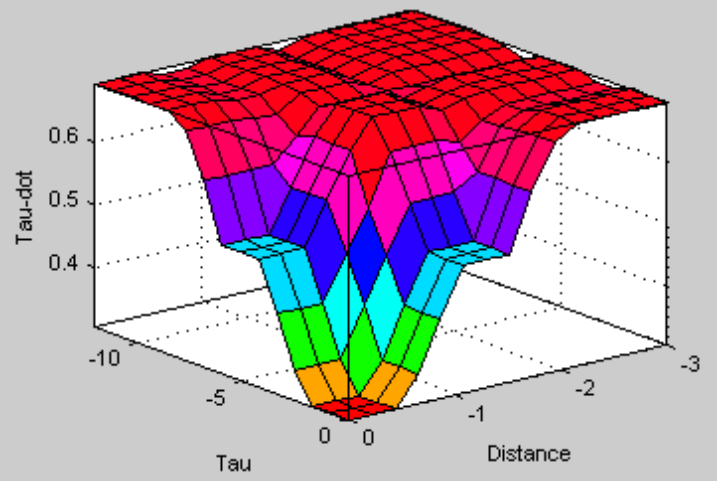

Figure 4.4 Surface plot of the fuzzy logic

Given the estimated $\chi(n)$ and $\tau(n)$ from last loop, the fuzzy logic can calculate the desired $\dot{\tau}(n)$. Then the estimated $\chi(n+1)$ and $\tau(n+1)$ can be expressed as,

$$\chi(n+1) = \chi(n)(1 + \dot{\tau}(n)dt/\tau(n))^{\frac{1}{\dot{\tau}(n)}} \quad 4.2$$

$$\tau(n+1) = \dot{\tau}(n)dt + \tau(n) \quad 4.3$$

where *dt* is the time step.

With the estimator designed, the control loop is completed and the control diagram is demonstrated in Figure 4.5.

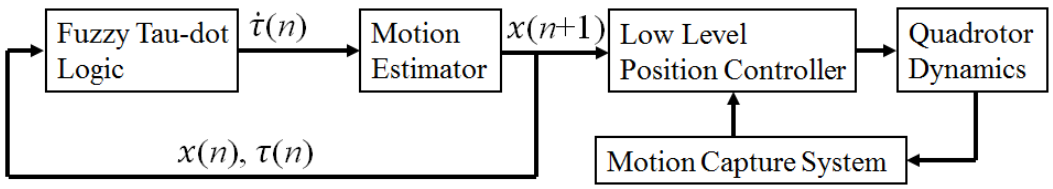

Figure 4.5 Control diagram of the UAV perching system

4.3 Experiment of 1D Pre-perching Flights with Varying Tau-dot

4.3.1 Method

A quadrotor with 10-inch propellers is used for perching flights and a VICON motion capture system is utilized to measure the position of the quadrotor. The

control algorithm is implemented in Matlab/Simulink and run on a workstation PC. The control commands are then transmitted to the quadrotor via wireless communication. The experiment setup is shown in Figure 4.6. Similar setup is also utilized in [77].

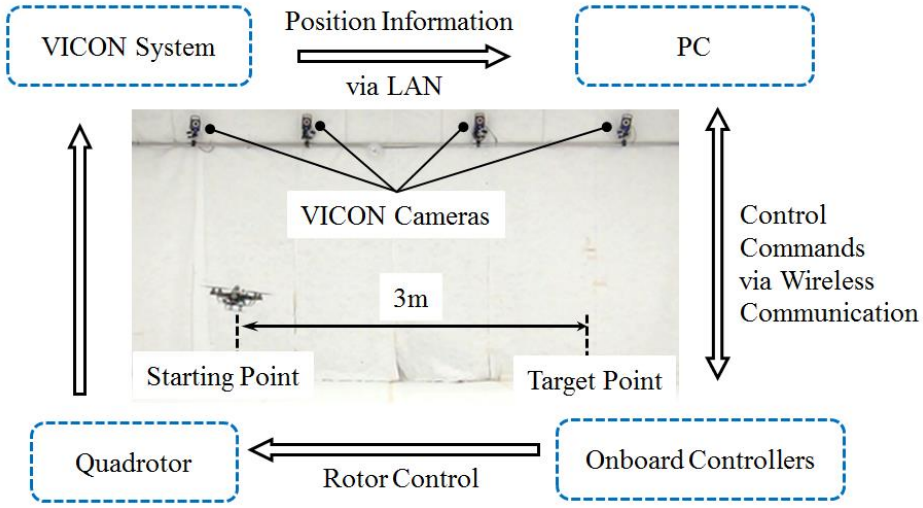

Figure 4.6 Experiment setup for perching of UAVs with the fuzzy logic

The quadrotor will take-off to 1m height at the position 0.1m away from the starting point, and then be commanded to fly toward a position 0.3m over the starting point in the horizontal flight direction to give itself a non-zero initial velocity. When the quadrotor reaches the starting point, the fuzzy logic of varying tau-dot, or a constant tau-dot (0.3) controller in the other case, will be activated and take over the control of the perching flight toward the target position. The estimated distance and tau, and the measured values from VICON are recorded for further analysis. Since only the case of one dimension is considered, the lateral and vertical positions of the quadrotor are kept constant during the perching procedure. Ten perching flights are performed for each case.

4.3.2 Results and Discussion

The estimated distance (dotted curves) and the measured distance (solid curves) of the quadrotor to the target from one flight with constant tau-dot (red curves) and varying tau-dot (blue curves) are plotted in Figure 4.7 and the corresponding varying tau-dot generated by the fuzzy logic is shown in Figure 4.8.

It is obvious from Figure 4.7 that with the same initial distance gap and initial approaching velocity, the fuzzy logic of varying tau-dot does shorten the flight time significantly. The average perching flight time is reduced from around 7.8s for constant tau-dot to about 4.8s for varying tau-dot, which is 38.5% quicker. The delay between the estimated coordinate and the measured one for both varying tau-dot and constant tau-dot is due to the quadrotor dynamics and its control algorithm. The generated varying tau-dot, although not very close to the pattern in Figure 4.2, manages to stay above 0.5 when far from the target and drop rapidly to below 0.5 when close to the target. The final velocity for varying tau-dot is 0.21 m/s, thanks to the low level position controller, while it is 0.04 m/s for constant tau-dot of 0.3. The discrepancy in the final velocities on such a scale makes no difference between a safe and a hazardous perching, and is therefore acceptable. Consequently, the experiment results show that the fuzzy logic designed with the varying tau-dot strategy for UAVs is effective and can improve the perching performance of a constant tau-dot strategy in terms of perching flight time. Moreover, it suggests that the varying tau-dot strategy has the potential to outperform the constant tau-dot strategy in many more applications.

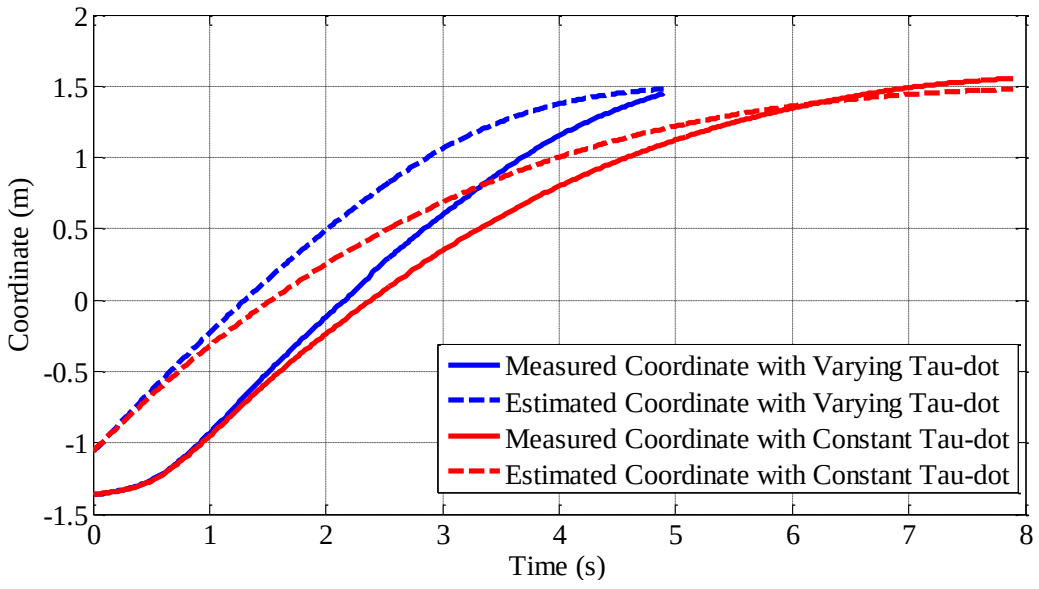

Figure 4.7 Comparisons of perching flight trajectories between constant tau-dot (red curves) and varying tau-dot (blue curves). The solid curves represent the measured coordinates via VICON system, and the dashed curves denote the estimated/desired coordinates using the different tau-dot strategies.

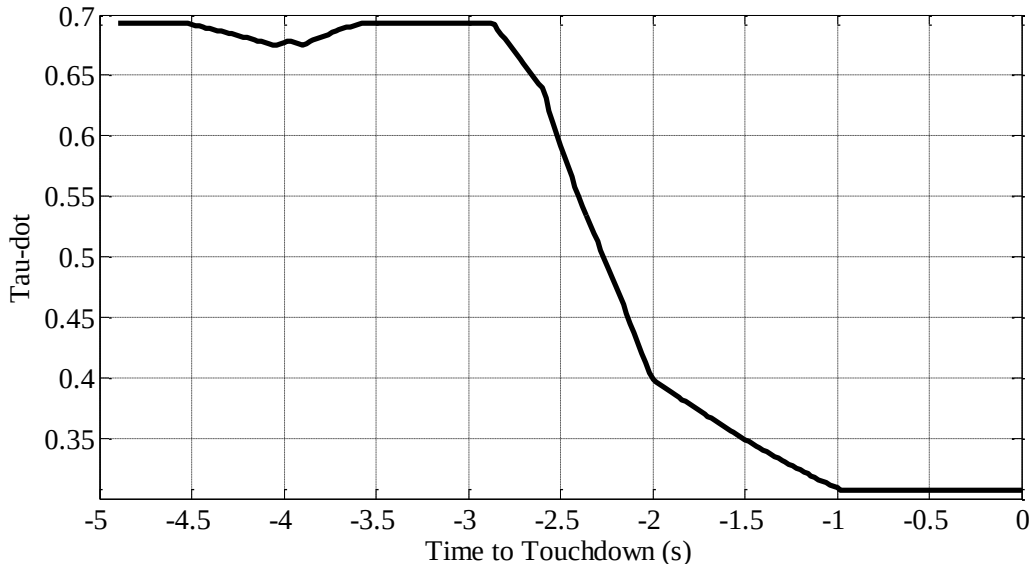

Figure 4.8 Varying tau-dot generated by the fuzzy logic

4.4 Intrinsic Tau-Coupling Guidance with Varying Coefficient

4.4.1 Tau-Coupling Strategy for Multi-Dimensional Motion

To deal with the multi-dimensional approaching motion that humans, animals and birds generally encounter, tau-coupling is believed to be the strategy to coordinate the movements among different dimensions. Its equation can be expressed as

$$\tau_y = k_{xy}\tau_x, \tag{4.4}$$

where τ_x and τ_y represent the taus of the multi-dimensional approaching motion, and k_{xy} denotes the ratio between them. As derived by D. Lee [42][46], k_{xy} needs to be a constant between 0 and 0.5 to make the multi-dimensional motion gaps, as well as the corresponding velocities and accelerations, decrease to 0 smoothly and simultaneously. Furthermore, the kinematic equations of the multi-dimensional motion are as follows,

$$\begin{cases} y(t) = C\chi^{\frac{1}{k_{xy}}} \\ \dot{y}(t) = \dfrac{C}{k_{xy}}\dot{\chi}\chi^{\frac{1}{k_{xy}}-1} \\ \ddot{y}(t) = \dfrac{C}{k_{xy}}\chi^{\frac{1}{k_{xy}}-2}[(\dfrac{1}{k_{xy}}-1)\dot{\chi}^2 + \chi\ddot{\chi}] \end{cases} \tag{4.5}$$

where C is a constant that can be defined by the initial conditions as $C = y_0/{x_0}^{\frac{1}{k_{xy}}}$.

As it has been verified that eqn. (4.1) still holds in a discrete manner for varying tau-dot, eqn. (4.5) should apparently hold in the same way. This means as long as the reference gap-closing motion is following a designated varying tau-dot pattern, the motion in other dimensions can be readily synchronized to the same pattern with a constant k_{xy} between 0 and 0.5. With the discrete tau estimator applied to motion gap χ, the discrete form of the kinematic equation of the coupled motion gap y can be written accordingly as

$$y(n+1) = C\chi(n+1)^{\frac{1}{k_{xy}}}. \tag{4.6}$$

4.4.2 Intrinsic Tau Guidance

It's very common in reality that an object starts movement from static status, especially for UAVs that are capable of hovering. The intrinsic tau guidance strategy that D. Lee proposed in [42] and [46] can handle motion like this very well because it yields an acceleration followed by a deceleration. Intrinsic tau guidance roots from tau-coupling which couples tau of one extrinsic movement to that of another. For intrinsic tau guidance, however, no extrinsic guiding motion tau is available for coupling, so the nervous system intrinsically generates a virtual tau for coupling [42]. It can be expressed as

$$\tau_x = k\tau_g \tag{4.7}$$

where τ_x is the tau of an extrinsic motion gap, τ_g is the intrinsic tau, and k is the constant coupling coefficient. D. Lee proposed a second order intrinsic tau function for τ_g, as

$$\tau_g = \frac{1}{2}\left(t - \frac{\delta^2}{t}\right) \tag{4.8}$$

where δ denotes the duration of the motion. This function was originally assumed to be the electrical charge of the neurons flowing with a constant second-order time derivative in human body [42]. Essentially it is consistent with the free fall motion, and has the identical formula of τ_g. It is therefore also called intrinsic tauG or tau gravity guidance in some literatures [54][55]. With τ_g defined, the motion gap χ, the velocity $\dot{\chi}$ and the acceleration $\ddot{\chi}$ can be derived as

$$\begin{cases} \chi(t) = \chi_0 \left(1 - \dfrac{t^2}{\delta^2}\right)^{\frac{1}{k}} \\ \dot{\chi}(t) = -\dfrac{2\chi_0 t}{k\delta^2}\left(1 - \dfrac{t^2}{\delta^2}\right)^{\frac{1}{k}-1} \\ \ddot{\chi}(t) = \dfrac{2\chi_0}{k\delta^2}\left[\left(\dfrac{2}{k} - 1\right)\dfrac{t^2}{\delta^2} - 1\right]\left(1 - \dfrac{t^2}{\delta^2}\right)^{\frac{1}{k}-2} \end{cases}. \quad 4.9$$

There are two main advantages of this second-order intrinsic tau function. One is that it can guide the movements that start from a static state, and the other is that it provides another control parameter δ that specifies the movement duration beside the coupling coefficient *k*. For UAVs like quadrotors, hovering is their most unique feature compared to fixed-wing UAVs. Thus, in many scenarios the movements of quadrotors begin from hovering. This makes the intrinsic tau guidance with second-order intrinsic function especially suitable for applications with quadrotors. Also, the extra controllability over movement duration gives more flexibility for motion planning of the quadrotor, as already presented in [54][59].

4.4.3 Varying Intrinsic Tau-Coupling Coefficient for Guidance

In literatures the coupling coefficient *k* is still assumed to be constant and the gap, velocity and acceleration reach zero at the same time only when $k \in (0,0.5]$. Also, the larger the *k* for $0 < k < 1$, the smaller the initial acceleration, but the longer the acceleration duration [42]. As the duration of the motion is fixed to δ, the advantage and disadvantage for different *k* need to be evaluated from different perspectives other than duration. Since the endurance of UAVs is the main concern of this research, the energy consumption under different *k* values is looked into.

Without losing generality, the discrete form of the energy consumed for the motion is considered. It can be expressed as

$$E = \sum_{i=1}^{n} |F_i \cdot \Delta\chi_i| = \sum_{i=1}^{n} m|\ddot{\chi}_i \cdot \Delta\chi_i| \quad 4.10$$

where F_i, $\Delta\chi_i$ and $\ddot{\chi}_i$ are the i-th values of actuation force, small displacement and acceleration, respectively, and $i = 1,2,\cdots,n$. Eqn. (4.10) can be expanded and

calculated based on the discrete form of eqn. (4.9). For simplicity, the mass of the object is assumed to be 1kg. To simulate the conditions of pre-perching flight experiments in previous section, δ is set to 8s, and sampling rate is set to 50Hz. The intrinsic coupling coefficient k varies from 0.1 to 0.9 at the interval of 0.1. The corresponding energy consumption is calculated accordingly and depicted in Figure 4.9. It is very obvious that the energy consumption decreases as the intrinsic coupling coefficient increases. Moreover, in general the smaller the k for $0 < k < 1$, the more significant the difference in energy consumption for the same offset of k. For instance, the difference of the energy consumption for k=0.2 from that for k=0.1 is up to 45.7%, while the difference for k=0.9 from k=0.8 is only 5.8%. Consequently, it can be concluded that a larger k for $0 < k < 1$ saves more energy during the motion, at the cost of relatively higher final velocity though. Since a non-zero final velocity is acceptable, even preferable sometimes, as concluded in previous section, varying intrinsic coupling coefficient is taken as the control strategy for guidance of multiple dimensional movements.

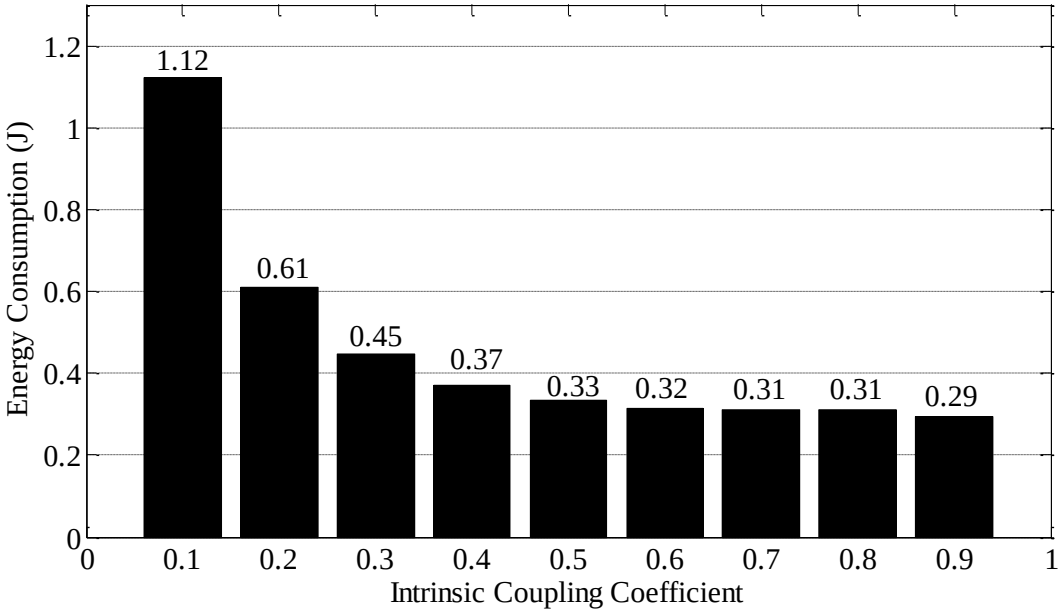

Figure 4.9 Energy consumption with different intrinsic coupling coefficients within the range of (0,1)

As the intrinsic coupling coefficient k varies between 0 and 1, the same range as that of varying tau-dot, the fuzzy logic designed for varying tau-dot is expanded for intrinsic tau-coupling guidance. Based on the motion in x direction, the fuzzy logic

will render the desired tau-dot values which are adopted as the intrinsic coupling coefficient of motion in x direction. Furthermore, the motion in y direction is coupled to that in x direction with a coupling coefficient of 1. That is, motion in x and y direction has the same tau-dot value. Such control strategy is then put into experiments for validation.

4.5 Experiment of 2D Pre-perching Flights with Varying Intrinsic Tau-Coupling Coefficient

4.5.1 Method

To evaluate the effectiveness of the proposed guidance strategy based on varying intrinsic tau-coupling coefficient, a 10-inch quadrotor is utilized to perform 10 times of 2D pre-perching flights in a horizontal plane with varying and constant intrinsic coupling coefficient, respectively. The experiment setup is the same as that in the experiment of 1D pre-perching flights with varying tau-dot. The quadrotor's movement in x direction is guided with the varying intrinsic coupling coefficients, and the motion in y direction is coupled to that in x direction with coefficient of 1. The quadrotor will take off and hover at the start point of coordinates (-1.5, 0.5, 1) meters in VICON reference frame, and then it will be commanded to fly toward the stop point at (1.5, 2, 1). The flight duration δ is set to 8s, and the constant intrinsic coupling coefficient is set to 0.3. To better differentiate the performances of the two cases, the motion estimation using eqn. (4.9) is accelerated in the algorithm. The desired trajectories yielded and the actual trajectories measured by the VICON system from two flights with varying and constant intrinsic coupling coefficient respectively are demonstrated in Figure 4.10. To examine the performance of the guidance strategy in time domain, the movements of the quadrotor from the same flights are decomposed into x and y directions in time domain and illustrated in Figure 4.11. The corresponding varying intrinsic coupling coefficients yielded by the fuzzy logic are plotted in Figure 4.12.

4.5.2 Results and Discussion

It can be seen from Figure 4.10 that the desired trajectories for varying and constant intrinsic coupling coefficients (dotted curves) are rather close, especially for the

second half of the trajectories. The small discrepancy in the first half of the trajectories mainly results from the slight difference in the initial conditions, for example, position. It is obvious that the quadrotor follows the desired trajectory more closely with the varying coefficient than with the constant coefficient. It means the varying intrinsic coupling coefficient can effectively serve as the guidance variable in terms of spatial motion. Note that the desired trajectories are basically straight lines because the coupling coefficient k_{xy} between motion in x and y directions is set to 1. However, it is not necessarily always the case.

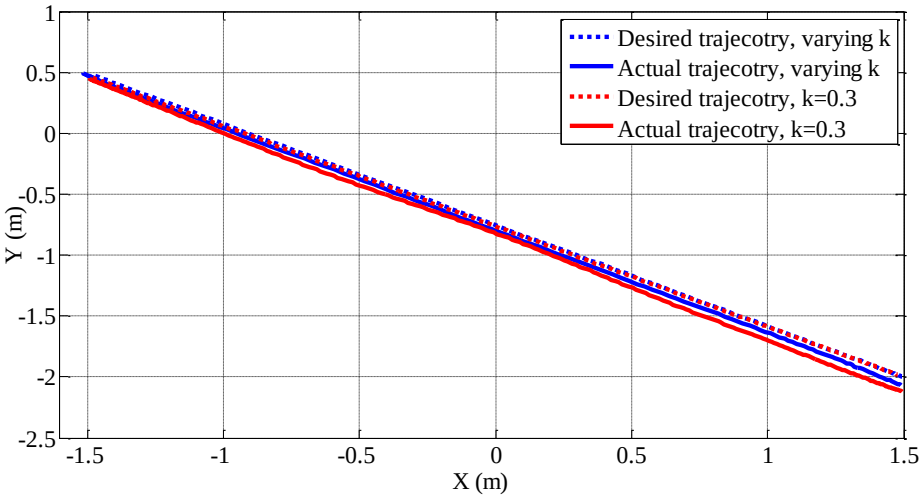

Figure 4.10 Desired (dotted curves) and actual flight trajectories (solid curves) under intrinsic tau-coupling guidance with varying (blue) and constant (red) k

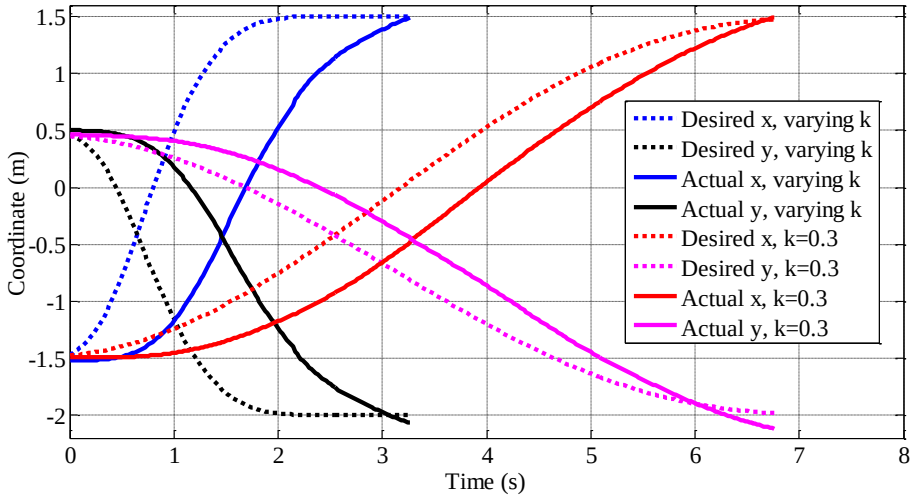

Figure 4.11 Desired and actual Coordinates of the UAV with varying and constant intrinsic coupling coefficients. Dotted curves represent the desired coordinates, and solid curves denote the actual values.

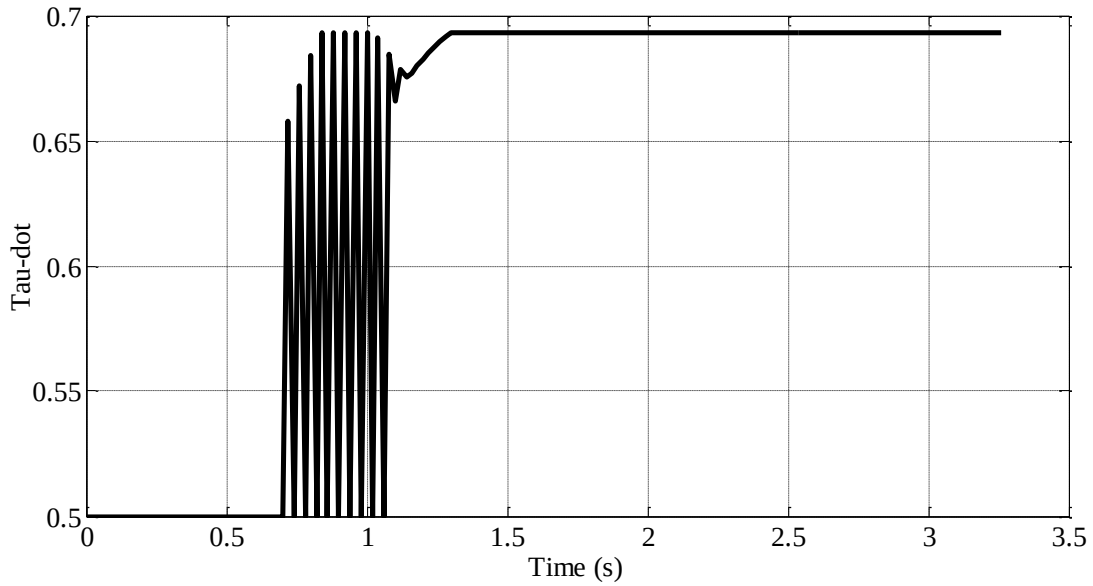

Figure 4.12 Varying intrinsic coupling coefficient generated by the fuzzy logic

Figure 4.11 shows the details of motion in x and y directions separately. Larger differences between desired and actual positions are observed for varying coefficient than for constant coefficient. It should be noted, however, that the desired positions in x and y directions reach the target positions in less than 2s for varying coefficient while it takes about 7s for constant coefficient. It thus makes sense that the significant delay could be mainly because the challenging demands on the reaction of the quadrotor is beyond its dynamics. One beneficial consequence of the fast tuning of the desired positions due to varying coefficient is apparently that the duration of the motion is shortened dramatically (3s compared to 7s). Another interesting thing observed is that motion gap in y direction is closed slightly earlier than in x direction for both varying and constant coefficient. This is consistent with the small offsets of the trajectories at the stop point in Figure 4.10. It is probably because the initial motion gap in y direction is smaller than that in x direction, although theoretically they should still be closed simultaneously, as shown by the desired position curves (dotted ones). The varying coefficient generated by the fuzzy logic based on motion in x direction is shown in Figure 4.12. It is always equal to or larger than 0.5 through the flight, meaning the logic is trying to close the motion gap in x direction faster. This is consistent with the large delay between the desired position and the actual one in x direction. Moreover, the energy consumption for the motion can be supposedly lowered, as indicated in Figure 4.9. The frequent oscillation around the

point of 1s shows the responsive tuning of the coefficient, and it is believed to be related to the prescribed conditions for motion in x direction. Consequently, it can be concluded that the proposed guidance strategy of varying tau-coupling coefficient for multiple dimensional motion is effective for pre-perching flights of UAVs.

4.6 Summary

In this chapter perching patterns of varying tau-dot from perching parrots are investigated first, showing good potentials of guiding UAVs for faster perching flight. Then a fuzzy logic tuning tau-dot in real time is designed based on one of the parrots' varying patterns and integrated into the control loop of our UAV testing system. Experiments of 1D pre-perching flights with both varying and constant tau-dot are conducted and the effectiveness of the fuzzy tau-dot logic is verified, which further validates the applicability of the varying tau-dot as a control strategy for UAV perching. To make the varying tau-dot strategy more applicable, it is extended to varying tau-coupling coefficient as the guidance strategy for multi-dimensional motion, based on the theoretical fundamentals of tau-coupling and intrinsic tau. Experiments of 2D pre-perching flights with both varying and constant intrinsic tau-coupling coefficient are carried out. Results show that the proposed strategy can guide the flight not only as effectively as the constant case but also more efficiently in terms of flight time and energy consumption.

Chapter 5 Visual Perception of Tau-dot during Pre-perching Flight of UAVs

Birds need to identify the target perch and estimate the distance to it and even approaching velocity before they initiate the perching procedure to make sure they can eventually perch successfully. The way birds achieve these tasks is acquiring the visual information of the potential perches by their eyes and processing the data by their brain. For UAVs to achieve automatic perching, they also need their own eyes and brain, that is, sensors and controller. As proposed for the guidance methodology of approaching flight in previous chapter, the autopilot based on *Tau Theory* requires feedback of approaching velocity and distance to the perch, or tau directly. In previous experiments, such feedback is realized through an indoor motion capture system. For more general cases like outdoor environments, appropriate navigation methodology that relies merely on onboard sensors to obtain desired information and accomplish automatic perching still needs to be addressed.

5.1 Advantages of Visual Guidance of UAVs

There are multiple methods of sensing the distance and velocity relative to the target for UAVs. Laser range finders, for example, have been utilized to detect the distance to the objects or obstacles, if any, around the UAV platform. This method is mostly employed for applications of simultaneous localization and mapping (SLAM) which generally don’t require identification of the target object and only need obstacle avoidance. Moreover, the laser range finders currently available in the market are mainly for 2D applications, which means they can only detect obstacles in a certain plane. This therefore limits its applicability to perching flight guidance for UAVs significantly. Ultrasonic sensors can also detect the distance, but their range is limited to only a few meters. GPS sensors are capable of providing global positions, because of which range will no longer be a problem, but they lack the ability of sensing the surrounding environment along the flight path. Combination of these sensors cannot resolve the problem, because one critical feature for automatic perching is still missing in them. It is the ability of target identification which distinguishes visual guidance from other methods.

Visual guidance has been applied to UAVs for a long time. Information that can be extracted from vision sensors is comprehensive. Image processing methods such as segmentation, registration and correlation can be utilized to identify and extract a target perch with or without a template. Such information can be further processed for tracking and odometry. Visual odometry techniques are capable of estimating the distance, and even the relative pose of the UAVs, to the target object [78][79][80][81][82][83][84][85][86][87][88]. Thus visual guidance possesses intrinsic advantages in terms of biomimetics over other methods because the visual guidance strategy used by birds and insects can be readily adopted for UAVs [89][90][91][92][93][94][95][96]. Moreover, tau-dot, as the navigation parameter utilized in this research, is found directly related to the rate of expansion of the visual image [97][98]. It means the feedback of the tau-dot can be easily achieved by identifying the scale of a certain object in the image and calculating its rate of change, without the troublesome labor of directly calculating the spatial distance. This could significantly alleviate the heavy computation usually associated with visual guidance methods, which makes them even more suitable for applications with UAVs.

In summary, visual guidance is definitely advantageous for perching flight of UAVs. The strategy of visual guidance proposed in this chapter consists of two aspects, namely perch identification and tau-dot estimation. Perch identification is meant for direction alignment for the perching flight and also for measurement of image expansion rate. Tau-dot estimation is based on its relation with the image expansion rate which is systematically evaluated.

5.2 Template-based Perch Identification Using LabVIEW

Generally speaking, object identification without a template requires more advanced techniques, higher computation capability and longer computation time than template-based one. On the other hand, the autopilot systems of UAVs are generally of lower computation capability due to lower payload capacity and limited form factors of UAVs compared to ground and underwater unmanned systems. Moreover, UAVs require real-time control for the purpose of system safety. This makes the

computation of non-template object identification with UAV autopilot system really time-consuming, and therefore intolerable. To handle this problem, a high level control system independent of the autopilot system should be integrated into the UAVs. It should be more capable of heavy computation of vision algorithms, and of compact form factor to fit into the UAV platforms.

5.2.1 LabVIEW-based Control System for Vision Algorithms

LabVIEW has been applied to develop control systems with UAVs in many literatures as programming language and control environment. Its graphic programming interface makes implementation of the control really easy, and the abundant function library facilitates the programming significantly. Moreover, LabVIEW has a unique advantage over other engineering programming software, for example, Matlab. It is the seamless integration with embedded control hardware systems. National Instruments has produced various real-time hardware systems for applications of embedded control. For vision-based control systems, such advantage still applies. Controllers such as Single-Board RIOs and myRIO have compact form factors that fit for applications with UAVs while not compromising the capability of powerful real-time computation which vision algorithms require. On the contrary, other software and libraries mainly used to develop vision algorithms in the field of computer vision and machine learning, such as Matlab, C++, Python, Java and OpenCV, either only run on a computer system or have limited choices of powerful embedded controller board. This qualifies LabVIEW as the control environment of vision algorithms for applications with UAVs. It should be noted that because of the fast development of the Single-Board Computers recently it provides another competent solution to vision-based embedded control.

In this section LabVIEW-based vision algorithms of object identification, tracking and measurement are developed to provide feedback for the fuzzy tau-pilot controller designed in previous chapter. In LabVIEW, there are generally three methods of object identification, namely geometric matching, pattern matching and object tracking [99][100][101]. They are all template-based methods, which means they require a pre-defined template for identification. As the focus of this chapter is on the

relation between visual clues and tau-pilot guidance, the target perch for development is prescribed and assumed as known. Therefore a template photo of the perch is available for the algorithms designed. The three identification methods are evaluated.

5.2.2 Geometric Matching

There are two types of geometric matching method in LabVIEW, edge-based method and feature-based method. The edge-based geometric matching calculates the gradient at each pixel of the edges and the matching is carried out based on the information of the gradient and position of the pixels. On the other hand, the feature-based geometric matching utilizes geometric features of curves in the image to match with those in the template [102]. Due to the simplicity of the edge-based algorithm, it's less demanding on the computation resources and can obtain better matching results under general circumstances. Moreover, the edge features of the target perch used in this research is fortified with black and yellow strips. Therefore, the edge-based geometric matching is implemented, as shown in Figure 5.1.

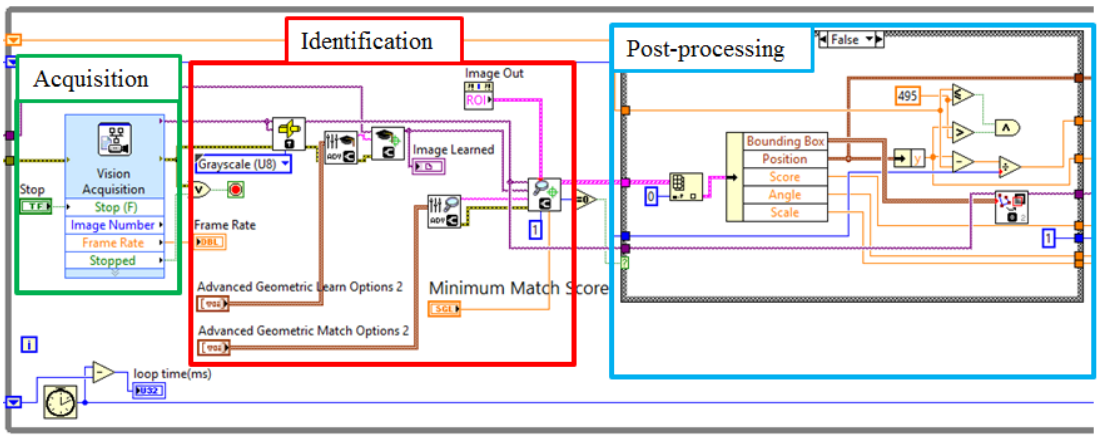

Figure 5.1 Edge-based geometric matching algorithms implemented in LabVIEW

Basically, the algorithm consists of three parts, namely image acquisition (green rectangle), template learning and match finding (red rectangle), and post-processing of the matching results (blue rectangle). The image acquisition part obtains images from the camera in the continuous mode. The edge features of the template image is extracted and then is passed to the matching module which looks for the same edge features in each acquired image. If any match is found, the matching results such as

matching score, scale and pixel position of the match will be displayed and recorded, and the identified target will be overlaid in the image for illustration.

5.2.3 Pattern Matching

There are also two methods for pattern matching in LabVIEW, pyramidal matching and image understanding. Both of the methods are based on normalized cross-correlation which is the most common method for template matching. However, cross-correlation requires heavy computation and therefore is time consuming. This is why pyramidal matching is applied. It reduces the size of the template and acquired image to a scale of powers of ½, so the computation can be dramatically alleviated depending on the chosen pyramidal level. The image understanding method uses intelligent sampling technique to extract features in a non-uniform manner [103]. In this research the pyramidal matching is employed because of its better flexibility of range configuration of scale and angle. See Figure 5.2.

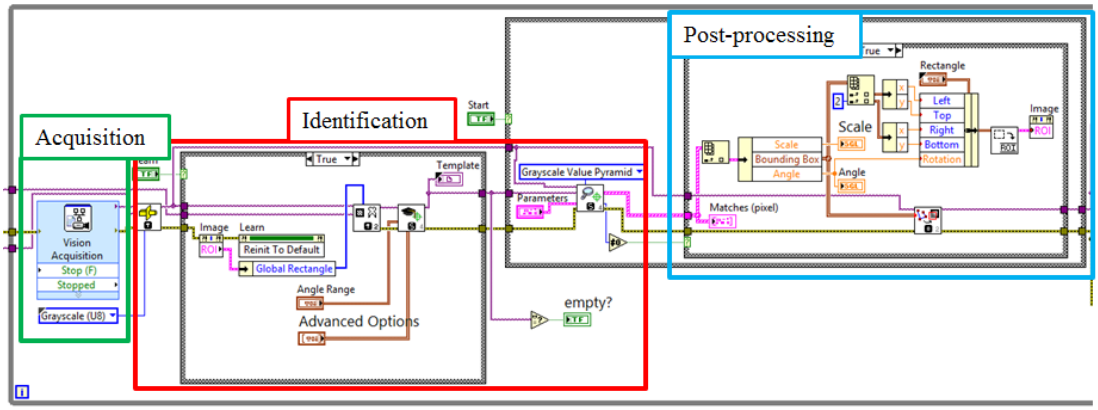

Figure 5.2 Pyramidal pattern matching algorithms implemented in LabVIEW

The structure of the pattern matching algorithm is similarly comprised by three parts. It is programmed in such a way that the template is confirmed to be learned before the pattern matching is performed.

5.2.4 Object Tracking

The object tracking method in LabVIEW also has two types of algorithm. One is mean shift and the other is shape adapted mean shift. The former one is the simple process of histogram extraction, weight computation and derivation of new location of the tracked object, while the latter one also tracks the shape, for instance, scale, of the object [104]. Object tracking method still requires an object template for tracking,

but it has the capability of tracking colored object which is the bigger difference from the other two matching methods. To increase the detectability of the method and to obtain the scale information of the object, the algorithm of shape adapted mean shift is utilized, as illustrated in Figure 5.3.

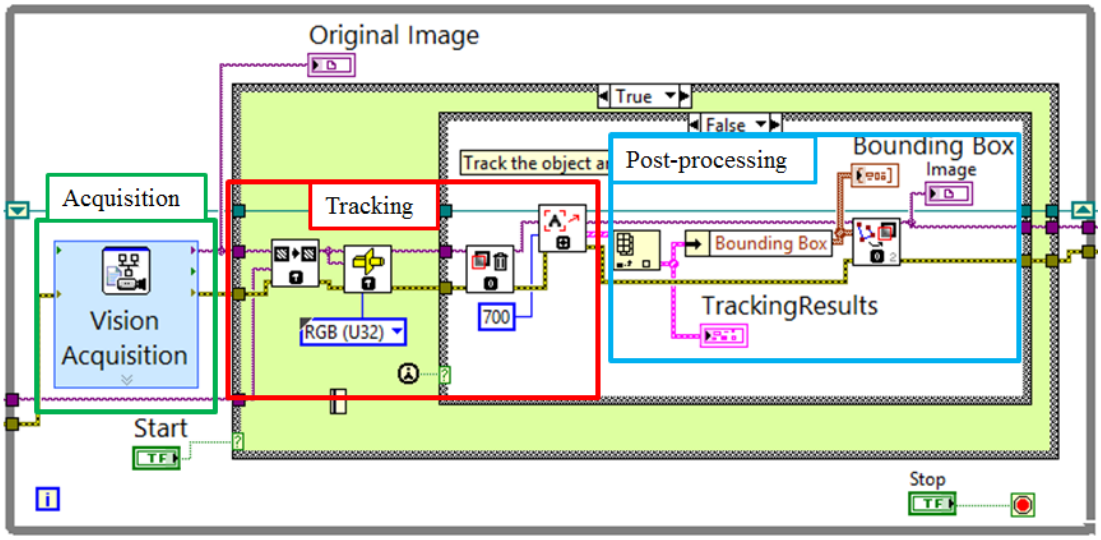

Figure 5.3 Object tracking algorithm implemented in LabVIEW

The algorithm is comprised by acquisition, tracking and post-processing. The initialization of the tracking algorithm is first conducted partially outside the while loop, and it is finished in tracking part by adding the object to be tracked as the template when running the corresponding code for the very first time. The scale of the tracked object is extracted and shown in the post-process part.

5.3 Experiments of Template-based Perch Identification

Experiments on the effectiveness of the three methods of object identification are introduced in this section. The experimental setup is presented in detail, and the experimental scenarios are also explicitly explained. The results are shown and analyzed accordingly to demonstrate the applicability of the identification methods.

5.3.1 Experimental Methods

The experiment setup is also based on the VICON motion capture system. A 10-inch quadrotor is utilized as the UAV platform that a Logitech C920 webcam is mounted to. The webcam is calibrated before operation. The calibration method is presented in

detail in Appendix A. The quadrotor is controlled via Simulink from the same workstation that runs the VICON system to follow certain flight paths designed for object identification. The target perch is modified from the previous version used for other gripping and perching experiments. Paper tapes are pasted to the rubber surface of the perch to form a grid which increases the contrast of the perch for identification. A myRIO controller from NI is attached to the quadrotor to run the object identification code onboard, and the camera is connected to it via the USB port. Meanwhile, to monitor the identification process, the myRIO controller is connected to the workstation via wireless LAN connection and the program front panel is used as the interface. The video frames overlapped with the identification results are streamed to the workstation. Besides, the matching score of up to 1000 for each successful match is recorded by the myRIO controller for post-processing and analysis.

To evaluate the applicability and reliability of the three identification methods, three scenarios namely straight approach, bypass flight and circle flight are taken into account, as depicted in Figure 5.4. In scenario 1 of straight approach the quadrotor flies directly towards and then away from the target perch. In scenario 2 of bypass flight the quadrotor flies along the longitudinal axis of the perch at a lateral offset of 2 meters to the perch. The yaw angle of the quadrotor is tuned accordingly to keep the camera pointing at the perch during the flight. In scenario 3 of circle flight the quadrotor circles 1.2m above the perch with a diameter of 2.4m. The height and the diameter are determined so as to make a decent distance for imaging the target perch. The camera looks downward at the perch while the yaw angle of the quadrotor is tuned in a similar way to scenario 2. The key difference between the three scenarios is that in scenario 1 basically only the scale of the perch in the image is changing, in scenario 3 mainly the planar angle of the perch is altering, while in scenario 2 both the scale and the planar angle of the perch are varying. In such a way, the effects of changes in scale and angle on identification result can be examined systematically.

In each scenario 10 flights are carried out for each identification method. Since a zero will be logged into the score result file when no match is found in a frame, the

score results are a mix of original score values and zeroes. The magnitude of the score values and the percentage of the non-zero score are analyzed to assess the reliability and applicable range of the identification methods. Besides, the scale of the identified perch is also logged to further verify the identification methods.

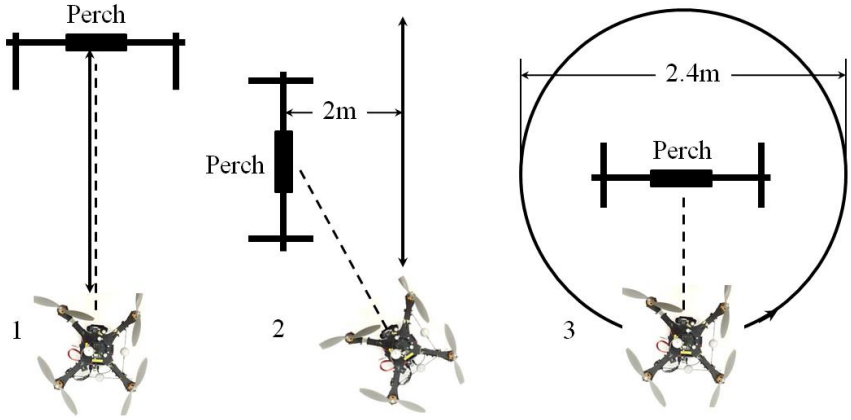

Figure 5.4 Three scenarios of the experiments on object identification. 1: Straight approach; 2: Bypass flight; 3: Circle flight. The solid lines with arrows show the flight paths, while the dashed lines demonstrate the view orientation of the camera.

5.3.2 Results and Discussion

The mean non-zero matching scores, the corresponding standard deviations and the mean percentages of the successful identifications out of the overall identification results including zeroes are calculated from the 10 flights for each scenario and compared among the three identification methods, as shown in Figure 5.5 and Figure 5.6, respectively. The detailed data of the identification results can be found in [105].

It should be noted that only three of the ten trials in scenario 1 have yielded presentable results for both pattern matching and object tracking. It can be seen that in scenario 1 geometric matching and object tracking almost have the same high average matching score around 960, while pattern tracking obtains an average score a little lower around 858. The biggest difference, however, lies in the identification percentage. Geometric matching shows an excellent identification percentage of 92.3%, while on the other hand pattern matching and object tracking only lead to an average identification percentage of 48.0% and 33.2%, respectively. This means geometric matching is more capable of achieving successful and reliable identification of the perch in scenario 1 than the other two methods. In scenario 2 all

three identification methods obtain good matching scores of above 920, with geometric matching getting the highest one of 992. Furthermore, difference in identification percentage is not as big as in scenario 1. Geometric matching, once again, has the highest identification percentage of 97.4%, which means it rarely fails to identify the perch in any frame. Object tracking also demonstrates a good percentage of 86.4%. However, identification percentage of pattern matching remains around 50%. Moreover, the standard deviations of the scores and the percentages by geometric matching are the smallest, verifying its excellent identification consistency. In scenario 3 both geometric matching and object tracking are able to detect the perch with good matching scores of above 920, while pattern matching only renders scores of 839. Besides, geometric matching has the smallest standard deviation of 6.6. Thus geometric matching can identify the target perch with the highest confidence and the most accurate result. However, in terms of identification percentage, object tracking outperforms the other two methods with an overwhelming 96.3%, compared to 55.1% by geometric matching and 63.7% by pattern matching. Note that geometric matching also yields the largest standard deviation for identification percentage. Therefore geometric matching will meet some difficulties in identifying objects of big rotation angle from the template.

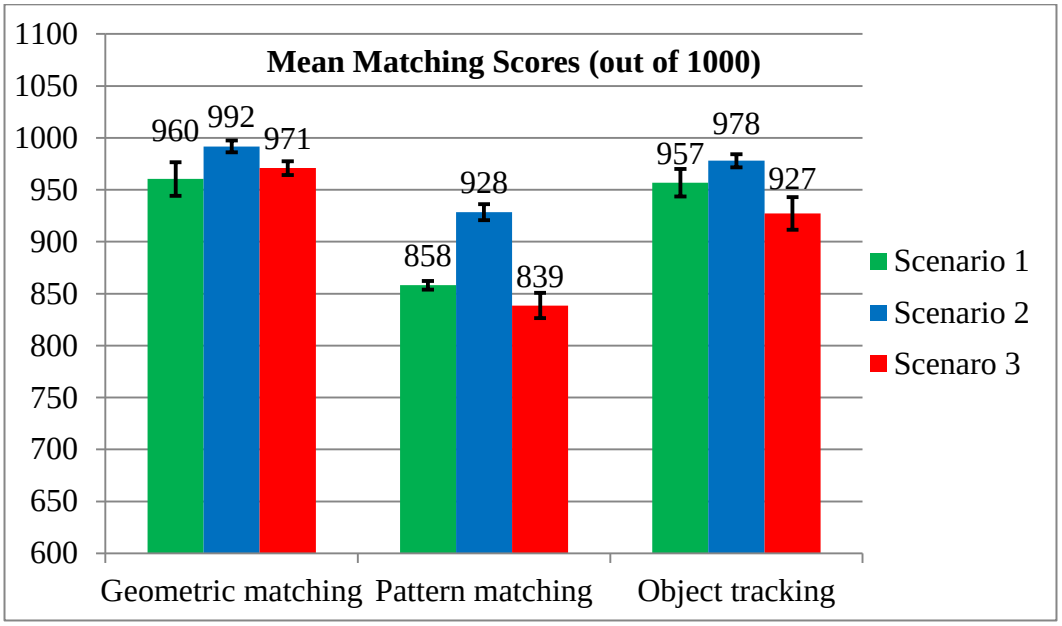

Figure 5.5 Mean matching scores of the three methods in three scenarios

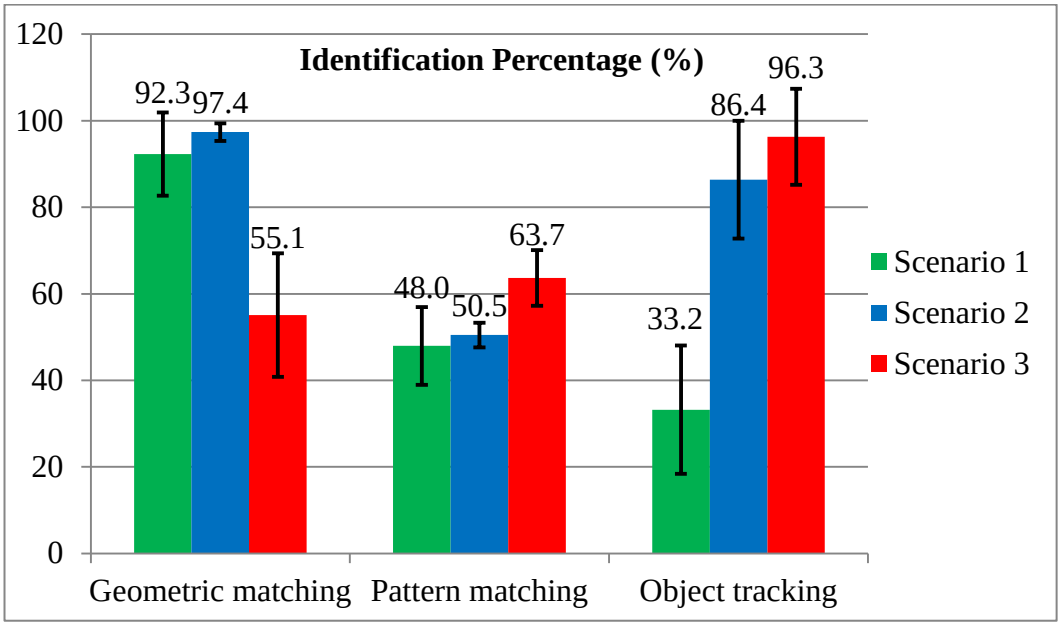

Figure 5.6 Identification percentage of the three methods in three scenarios

To further analyze the effectiveness of the three methods, their identification performances are qualitatively summarized into different effectiveness regions along the flight path, as shown in Figure 5.7, Figure 5.8 and Figure 5.9. Green represents good detectability, yellow denotes moderate detectability and red means non-detectability.

It is rather obvious that in scenario 1 geometric matching shows good detectability throughout the flight while the other two methods only have good detectability close to the start point. Pattern matching basically has non-detectability when it is further away from the start point. On the other hand, object tracking shows inconsistent performance for different flight directions. It gets moderate detectability when approaching to the perch at a further distance from the start point and when departing from the perch at the region close to the start point. It can be concluded that geometric matching outperforms pattern matching and object tracking significantly when only scale of the object varies. In scenario 2 it shows that again good detectability is obtained throughout the flight path by geometric matching. For object tracking moderate detectability is achieved for the first half of the flight path and good detectability for the other. Pattern matching succeeds in identifying the perch for the first half of the flight path, but totally fails for the second half. It can be

concluded that geometric matching shows the best detectability under the circumstances where both scale and angle of the object in the image change. In scenario 3 geometric matching and pattern matching have similar effectiveness regions around the start point and at the opposite position about the perch. This is because the perch appears in the image with almost the same scale to the template and also its relative angle to the template is either close to zero or close to 180°. On contrary, when the quadrotor flies to the positions exactly or almost in line with the longitudinal axis of the perch successful identification can hardly be achieved by these two methods. In these positions the identified angle of the perch is supposed to be close to ±90°, which will lead to the biggest dissimilarity between the template and the image. Object tracking, surprisingly, can detect the perch from all angles all the way along the flight. No specific region in which it encounters difficulty in identifying the perch is observed. However, incorrect identification with obvious position offset or wrong identified angle exists. This further shows that the effectiveness regions are only for qualitative evaluation of the three methods.

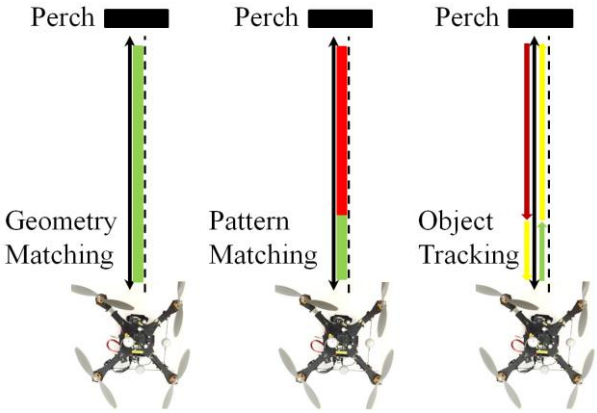

Figure 5.7 Effectiveness regions of the three methods in scenario 1

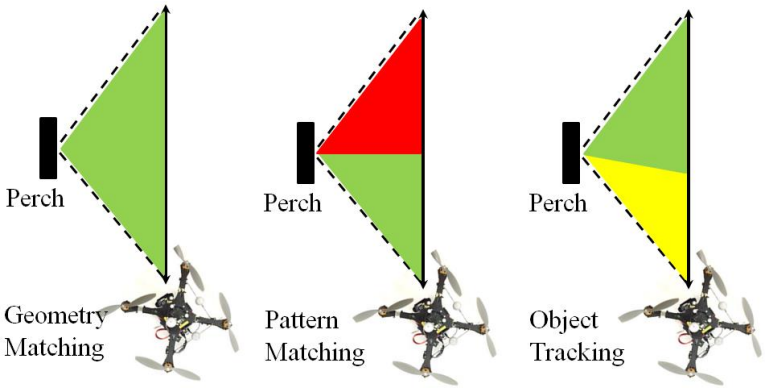

Figure 5.8 Effectiveness regions of the three methods in scenario 2

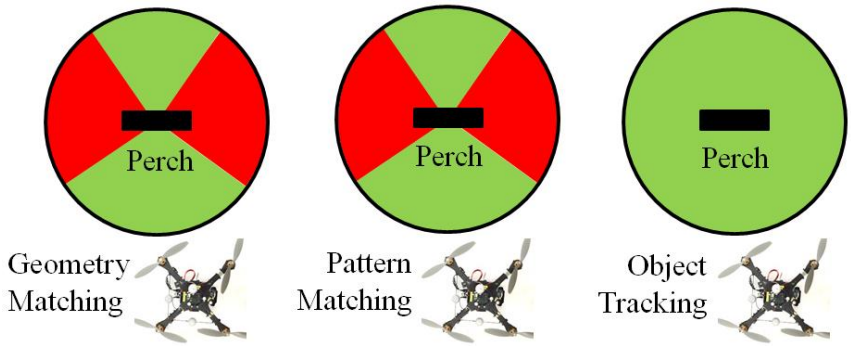

Figure 5.9 Effectiveness regions of the three methods in scenario 3

5.3.3 Summary

It can be concluded from the results above that geometric matching shows the most excellent and the most consistent overall detectability under prescribed circumstances that the scale and/or the rotation angle of the target object vary along the flight. Therefore, geometric matching is chosen as the identification method for further investigation on visual guidance.

5.4 Tau-dot Estimation based on Scale Variation

5.4.1 Scale-dependent Expansion Model (SEM) of Tau-dot Estimation

After the best identification method has been resolved, the relation between the visual cues and the tau information for guidance need to be addressed. The classic model of relative retinal expansion velocity (RREV) yields

$$\mathrm{RREV} = \frac{1}{a}\frac{\mathrm{d}a}{\mathrm{d}t} - 2\frac{1}{x}\frac{\mathrm{d}x}{\mathrm{d}t} = \tau^{-1} \tag{5.1}$$

under the assumption that the distance x to the target is so larger than the physical size r (for example, radius) of the target that the retinal size of the target $a \approx \pi r^2/x^2$ [98]. Without the approximation from the assumption above, the model of retinal size-dependent expansion threshold (RSDET), which is essentially identical to RREV, leads to

$$\tau = \frac{\alpha}{\Omega} = \frac{-2\sin\frac{\alpha}{2}}{\Omega\sqrt{1-\sin^2(\frac{\alpha}{2})}} \tag{5.2}$$

where α is the retinal size of the target and Ω is the retinal expansion velocity [98]. Obviously, the ratio of the angular size of the object in image to its angular rate of

expansion is deemed as the τ defined by D. Lee. As geometric matching is utilized to identify the target perch, its scale in the dimensions such as length and width of the object, instead of the retinal size, to the template, are directly obtained during the matching. Thus, a scale-dependent expansion model that describes the relation between the linear dimensions of the target in the camera view and the tau information and takes the camera model into account is rather necessary.

Consider the simple scenario that the camera approaches the target object with its optical axis always towards the object, as illustrated in Figure 5.10. For simplicity, a circular object of radius *R* is assumed. The focal length of the camera is *f*. *r* denotes the object radius in the image plane and *Z* is the distance between the optical center of the camera and the object. According to the pinhole camera model, it can be derived that

$$\frac{r}{R} = \frac{f}{Z}. \tag{5.3}$$

Therefore, with the initial conditions of r_0 and Z_0, the relation between the distance to the object and the object dimension in image plane can be obtained that

$$Z = \frac{r_0 Z_0}{r} = \frac{C}{r}. \tag{5.4}$$

Then the time to contact τ can be expressed as

$$\tau = \frac{Z}{V} = \frac{Z}{\dot{Z}} = \frac{C/r}{-C\dot{r}/r^2} = -\frac{r}{\dot{r}} \tag{5.5}$$

where *V* is the approaching velocity and *C* is the constant of initial conditions. It shows that the conclusion that time to contact *Tau* is the ratio of image size to the rate of expansion still holds for geometric dimensions in image plane. Actually the scale-dependent model is also essentially identical to RREV and RSDET. However, no assumption that $Z \gg r$ is made, which significantly extends the applicability of the model proposed. Note that Eqn. (5.5) is in a continuous analytical form. In reality, a discrete form is necessary for implementation, and it is further analyzed.

In discrete domain τ at instance *i*=1,2,3,… can be derived as

$$\tau_i = \frac{Z_i}{V_i} = \frac{Z_i}{(Z_i - Z_{i-1})/\Delta t_i} = \frac{\Delta t_i}{1 - \frac{Z_{i-1}}{Z_i}} = \frac{\Delta t_i}{1 - \frac{r_i}{r_{i-1}}} = \frac{\Delta t_i}{1 - S_i} \tag{5.6}$$

where Δt_i is the time interval between two image samples of *i-1* and *i*, and it is not necessarily a constant. S_i represents the scale between two consecutive identified images, as

$$S_i = \frac{r_i}{r_{i-1}}. \tag{5.7}$$

Generally S_i is not supposed to be 0 because the camera should keep approaching the target. However, it is still possible that S_i is so close to 1 that τ_i exceeds the reasonable range. To resolve this issue, saturation can be applied to make sure τ_i stays in acceptable range. The scale can be readily obtained from the geometric matching algorithm. As stated in [64], information of tau doesn't solely define the control strategy of the perching flight, and it only specifies the moment of landing initiation. Therefore, tau-dot is of more interest than tau in this research. The expression of discrete tau-dot is further derived as

$$\dot{\tau}_i = \frac{\tau_i - \tau_{i-1}}{\Delta t_i} = \frac{1}{1 - S_i} - \frac{\Delta t_{i-1}/\Delta t_i}{1 - S_{i-1}}, i = 2,3,4, \ldots \tag{5.8}$$

It can be seen that to calculate discrete tau-dot it requires only two consecutive scales and two consecutive time intervals, all of which can be easily obtained by the vision algorithm.

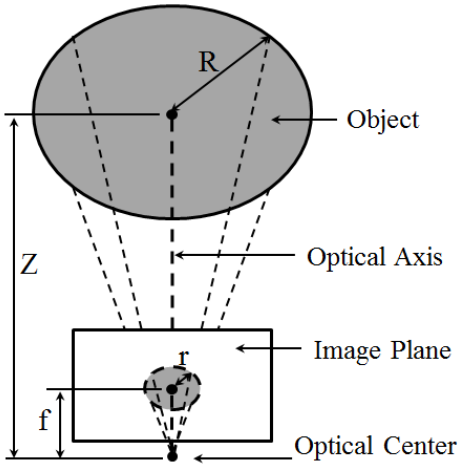

Figure 5.10 The scale-dependent expansion model with integration of the pinhole camera model

5.4.2 Experimental Evaluation of the SEM

The SEM established in previous section provides direct connection between the scale of the object in image and the tau-dot information. Although the theoretical derivation is substantial, experimental evaluation of its effectiveness is still needed.

The evaluation methods are as follows. The NI myRIO controller to which the Logitech C920 webcam is connected via the USB port is mounted to the quadrotor, and runs the vision algorithm programmed based on the SEM. The calibration process is also performed here to obtain the calibrated focal length of *f*. The quadrotor will fly automatically towards the perch under the guidance of the VICON system, and eventually stops at a position about 0.5m from the perch. The distance and velocity data from VICON system are taken to calculate the tau-dots which further serve as the ground truth for the vision algorithms. During the flight, the overall scales of the successful identified matches to the original template are logged, together with the time at which these matches are identified. The estimated discrete tau-dots are further obtained during post-processing. The flight is performed 10 times. It should be noted that the vision algorithm is only acquiring data of scales and time for validation of the SEM, and it is not integrated into the flight control loop of the quadrotor. The logged scales are plotted verse the corresponding time in Figure 5.11, with the time of first successful identification as time zero. Also, the tau and tau-dot estimated from the experiment data using the SEM are compared with the corresponding ground truth values calculated from the VICON data as shown in Figure 5.12 and Figure 5.13.

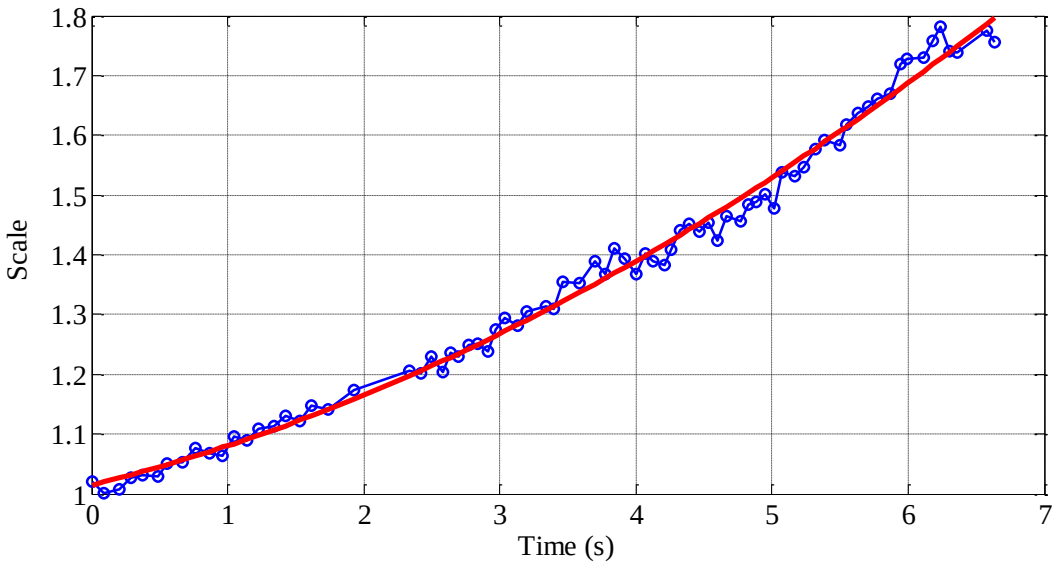

Figure 5.11 Overall scale of the perch in the image to the template during one flight. Blue curve with circles represents the experiment data while the red curve shows the values fitted with a second order polynomial.

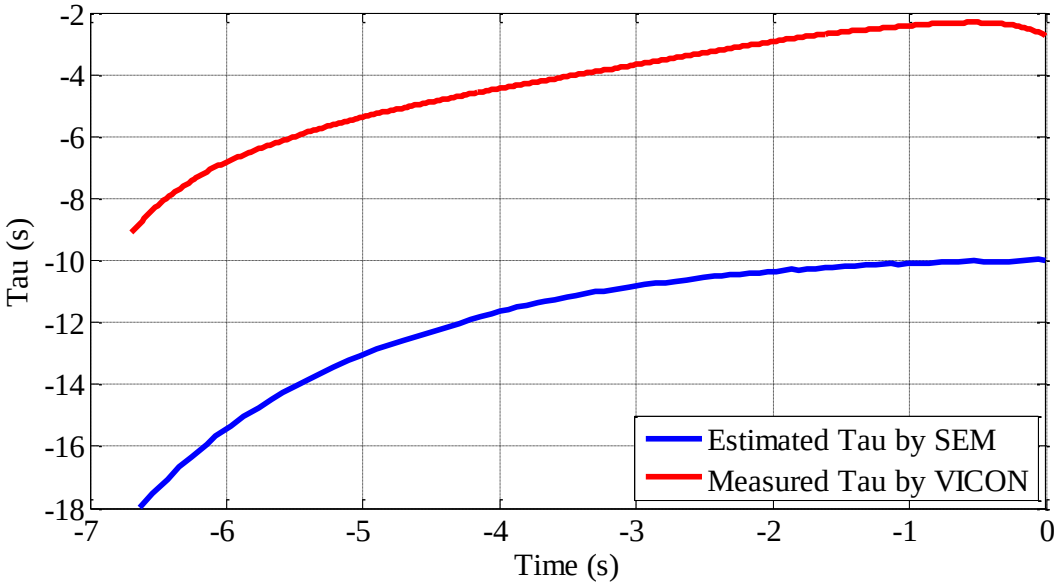

Figure 5.12 Comparison between tau estimated by SEM (blue) and corresponding ground truth tau from VICON system (red)

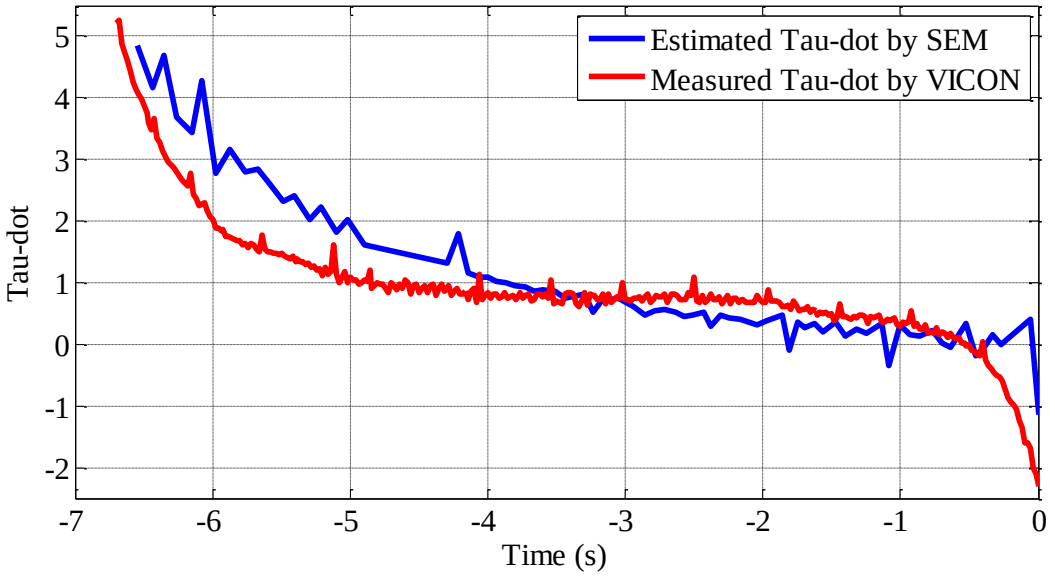

Figure 5.13 Comparison between tau-dot estimated using SEM (blue) and corresponding ground truth tau-dots from VICON system (red)

From Figure 5.11 a smooth increasing trend of the scale can be observed clearly as the quadrotor approaches the perch, and it can be fitted with a second order polynomial. Small fluctuations of the scale do exist along the course, but the scale overall follows the fitted trend very closely. Generally the trend does not necessarily have to fit a second order polynomial. It totally depends upon the flight kinematics of

the quadrotor. As differential division needs to be performed to obtain the scale interval between two consecutive matches, the fitted values of the scales are employed to improve the calculation results of the estimated tau and tau-dot.

On the other hand, for calculation of the ground truth values from VICON system, the approaching velocity of the quadrotor is fitted with a fourth order polynomial to filter the noise from environments, the VICON system and the differentiation process. The distance values adopted for calculation are original, so some fluctuations can still be observed in the red curve in Figure 5.13. Generally speaking, the estimated tau-dots agree with the ground truth rather decently. Discrepancies mainly exist in the beginning and at the end where the tau-dots from VICON system decrease dramatically. It is probably because the quadrotor accelerates in the beginning of the flight and brakes to stop far before it reaches the target perch at the end of the flight. From the second to the fourth second the actual tau-dot is maintained almost constant between 0 and 1, while the estimated tau-dots from the SEM gradually decrease to below 1 at a slight slope. Instead of dropping quickly to negative values at the end of the flight as the ground truth tau-dots, the estimated tau-dots remain almost constant at a value slightly above 0. This indicates the effectiveness of the estimated tau-dots may not hold under velocities close to 0. However, more investigations into this problem are required before an explicit conclusion can be drawn. Without loss of generality, the estimated tau-dot can still be deemed as effective for visual guidance of UAVs.

5.5 Summary

In this chapter the advantages of visual guidance for perching flight is discussed first and the link between the proposed tau-theory-based guidance method and visual cues is also covered. As the first step towards visually-guided perching, three template-based perch identification methods using LabVIEW vision development module are programmed and examined systematically through experiments with different perching circumstances. Results show geometric matching method has the best overall performance for perch identification, and it is thus chosen as the identification method for visual guidance. Furthermore, taking the available visual

cues in account, a scale-dependent expansion model (SEM) is proposed for tau-dot estimation. Theoretical derivation is presented and the relationship between the tau/tau-dot and the identified scale of the perch is obtained. Experimental validation of the proposed SEM is conducted and results show rather good agreement with the model. With the SEM model, the visual feedback of tau/tau-dot to the fuzzy guidance controller for perching flight is achieved.

Chapter 6 Dynamics Modeling of On-perching Process and Development of the Perching Mechanism System for UAVs

Reliable attachment to the perch is eventually the key point for successful perching. Birds have the most suitable body structures like legs, feet and claws and also the best control strategy optimized through the long evolution history for the task. To achieve the same task with a UAV, a dynamics model of the balancing process after touchdown with the dynamics of the UAV taken into account should be established to provide profound insights into the process. With the balancing process thoroughly understood, a perching mechanism of desired characteristics can then be designed and implemented with the UAV. Control laws of the perching mechanism also need to be developed to accomplish effective and reliable perching and to get incorporated into the visual guidance control for automatic perching. These problems are addressed in this chapter.

6.1 Modeling of On-perching Dynamics of UAVs

A perching model covering the dynamic interactions between the perching mechanism, the UAV platform and the perch is definitely necessary for perching methodology development. Although investigations on aerodynamic control of UAV platforms during contact with or manipulation of objects, generally called control of tethered UAVs, can be found in many literatures [106][107][108][109], the perching modeling that is based on the bio-inspirations from birds and specifically addresses the interaction between a landing UAV and environments has been studied only in a few literatures [110][111]. Therefore such a bio-inspired dynamics perching model for UAVs is studied in this section.

6.1.1 Two-dimensional Dynamics Perching Model with a Quadrotor

Several conditions are prescribed as follows. Firstly, quadrotors are taken as the UAV platform since they not only are more agile in terms of aerial manipulation but also can carry larger payloads compared to fixed-wing UAVs and ornithopters of

similar size. Secondly, the configuration of the perching mechanism is supposed to be symmetric about longitudinal and lateral planes as a quadrotor is. Thirdly, a gripping mechanism mimicking birds' foot is chosen as the end effector for securing the connection between the UAV and the perch, while the posture manipulation is performed by the UAV. Certainly a gripper cannot suit all potential perching circumstances, for instance vertical surfaces, but it works with most common perch in nature such as tree branches, roofs and ground. Similar concept is also used in [15][16][111][112]. This is also why a cylindrical pole fixed to ground reference frame, approximating tree branches, is adopted as the target perch in this investigation. Furthermore, for simplicity, the target perch is assumed to be horizontal so that the lateral roll angle of the UAV remains 0 degree. Consequently, the conditions above lead to a simplified two-dimensional dynamic perching model in the longitudinal plane, as shown in Figure 6.1.

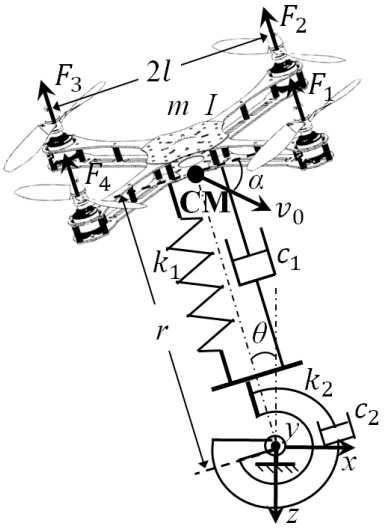

Figure 6.1 Two-dimensional dynamic model for perching with a quadrotor. Dynamic properties, namely the stiffness and damping coefficients, are associated with the 2 DOFs, as a typical mass-spring system. Lifting forces from the quadrotor are taken as the external inputs of the system and the radial coordinate r and angular coordinate θ are taken as the outputs.

The distance between two rotors of the quadrotor is denoted as $2l$. m is the mass of the quadrotor while I is its moment of inertia about the axis that goes through its center of mass and parallel to Y axis. The center of mass is depicted as the black dot. r represents the distance from the center of mass of the quadrotor to the rotation

center of the system about the perch. The angle θ between the vertical axis of the quadrotor and the vertical axis of the global frame as shown in Figure 6.1 is defined as the perching angle. It's equal to the pitch angle of the quadrotor. The global frame is defined in the same way as it is in the field of quadrotor control. The velocity of the quadrotor at touchdown is denoted as initial velocity vector v_0, and the angle between the velocity vector v_0 and the quadrotor plane is defined as the attack angle α. k_1 and k_2 are the stiffness coefficients of the perching mechanism in the 2 degree-of-freedom respectively, while c_1 and c_2 are the corresponding damping coefficients. F_i, i=1,2,3,4, are the lift generated by the four rotors respectively. A dynamic perching model of quadrotor platforms can therefore be derived using Lagrange's equation as follows.

The kinetic energy of the system can be expressed as

$$\mathrm{U} = \frac{1}{2}m\dot{r}^2 + \frac{1}{2}m(\dot{\theta}r)^2 + \frac{1}{2}I\dot{\theta}^2. \tag{6.1}$$

The potential energy of the system can be written as

$$\mathrm{V} = \mathrm{mgr}\cos\theta + \frac{1}{2}k_1(r - r_0)^2 + \frac{1}{2}k_2(\theta - \theta_0)^2 \tag{6.2}$$

where r_0 is the original length of the spring and θ_0 is the initial perching angle.

For generalization of the model, damping is taken into account in both of the two degrees of freedom. Therefore the dissipative term in Lagrange's equation can be represented as

$$\mathrm{D} = \frac{1}{2}c_1\dot{r}^2 + \frac{1}{2}c_2\dot{\theta}^2 \tag{6.3}$$

where c_1 and c_2 are the damping coefficients for the translational and rotational motion respectively. The Lagrange's equation can therefore be expressed as

$$\frac{\mathrm{d}}{\mathrm{dt}}\left(\frac{\partial L}{\partial \dot{q}_i}\right) - \frac{\partial L}{\partial q_i} + \frac{\partial D}{\partial \dot{q}_i} = f_i, \mathrm{i} = 1,2 \tag{6.4}$$

where L=U-V, and $\mathrm{q} = [r \quad \theta]^T$ denotes the generalized coordinates. f_i represents the non-dissipative external forces which mainly are the aerodynamic forces applied to the UAV, such as lift, thrust and torque. In the case of an X-type quadrotor,

$$\mathrm{f} = \begin{bmatrix} F \\ T \end{bmatrix} = \begin{bmatrix} 1 & 1 & 1 & 1 \\ -l & -l & l & l \end{bmatrix} \begin{bmatrix} F_1 \\ F_2 \\ F_3 \\ F_4 \end{bmatrix} \tag{6.5}$$

where F denote the resultant lift of the four rotors, and T is the resultant torque contributing to the pitch angle control. It should be noted that for other UAV platforms like a fixed-wing airplane, the external forces can also be expressed in a similar form.

Substituting the equations above into Lagrange's equation yields

$$\begin{cases} m\ddot{r} - mr\dot{\theta}^2 + mg\cos\theta + k_1(r - r_0) + c_1\dot{r} = F \\ (mr^2 + I)\ddot{\theta} + 2m\dot{\theta}\dot{r}r - mgr\sin\theta + k_2(\theta - \theta_0) + c_2\dot{\theta} = T. \end{cases} \tag{6.6}$$

It is obvious that the equations of motion of the perching system are coupled and nonlinear, which makes it difficult for dynamic analysis and control. The assumption of small oscillations around the equilibrium position is therefore adopted to linearize the equations. For the final steady state, equilibrium equations can be obtained as

$$\begin{cases} mg\cos\theta_e = k_1(r_0 - r_e) \\ mgr_e\sin\theta_e = k_2(\theta_e - \theta_0). \end{cases} \tag{6.7}$$

Then the equations of motion above can be rewritten by substituting the equilibrium equations into them as

$$\begin{cases} m\ddot{r} - mr\dot{\theta}^2 + mg(\cos\theta - \cos\theta_e) + k_1(r - r_e) + c_1\dot{r} = F \\ (mr^2 + I)\ddot{\theta} + 2m\dot{\theta}\dot{r}r + mg(r_e\sin\theta_e - r\sin\theta) + k_2(\theta - \theta_0) + c_2\dot{\theta} = T. \end{cases} \tag{6.8}$$

Define the displacements of radial translation and rotational perching angle from their final equilibrium positions respectively as,

$$\Delta r = r - r_e, \text{ and } \Delta\theta = \theta - \theta_e. \tag{6.9}$$

Based on the assumption of small oscillations, approximations below can be derived.

$$\begin{cases} \sin\Delta\theta = \Delta\theta \\ \cos\Delta\theta = 1 \\ \left(\frac{d}{dt}\right)^2 = 0. \end{cases} \tag{6.10}$$

Thus, by expanding r and θ and using the approximations, the linear form of the equations of motion can be obtained as

$$\begin{cases} m\ddot{\Delta r} + c_1\dot{\Delta r} + k_1\Delta r - mg\Delta\theta\sin\theta_e = F \\ I_m\ddot{\Delta\theta} + c_2\dot{\Delta\theta} + k_2\Delta\theta - mg(r_e\Delta\theta\cos\theta_e + \Delta r\sin\theta_e) = T. \end{cases} \tag{6.11}$$

where I_m is the angular momentum at equilibrium state and assumed constant to decouple the two degrees of freedom. Define the state variable as $\mathbf{X} = \left[\Delta r \;\; \dot{\Delta r} \;\; \Delta\theta \;\; \dot{\Delta\theta}\right]^T$ and the output as $\mathbf{Y} = [\Delta r \;\; \Delta\theta]^T$. The equations of motion in state-space can therefore be expressed as

$$\begin{cases} \dot{\mathbf{X}} = \mathbf{AX} + \mathbf{Bu} \\ \mathbf{Y} = \mathbf{CX} \end{cases} \tag{6.12}$$

where $\mathbf{u} = [F_1 \;\; F_2 \;\; F_3 \;\; F_4]^T$ is the control input of the perching system,

$$\mathbf{A} = \begin{bmatrix} 0 & 1 & 0 & 0 \\ -k_1/m & -c_1/m & g\sin\theta_e & 0 \\ 0 & 0 & 0 & 1 \\ mg\sin\theta_e/I_m & 0 & (mgr_e\cos\theta_e - k_2)/I_m & -c_2/I_m \end{bmatrix},$$

$$\mathbf{B} = \begin{bmatrix} 0 & 0 & 0 & 0 \\ 1/m & 1/m & 1/m & 1/m \\ 0 & 0 & 0 & 0 \\ -l/I_m & -l/I_m & -l/I_m & -l/I_m \end{bmatrix}, \text{ and } \mathbf{C} = \begin{bmatrix} 1 & 0 & 0 & 0 \\ 0 & 0 & 1 & 0 \end{bmatrix}.$$

6.1.2 Numeric Simulation for Model Validation

Numeric simulation of the free responses of the perching model is conducted to validate its applicability to describing the perching maneuvers of birds. The parameters in Table 6.1 are prescribed for simulation according to the physical characteristics of bird 3. For birds, $\theta_e = 0$, so it leads to $k_2 = 0$ from Eqn. (6.7). However, this makes the model unstable. Instead, it is assumed that the perching mechanism could be pre-loaded in the angular dimension so that the upright equilibrium state can be achieved with a small non-zero k_2 even without active control efforts. Dynamics parameters are thus prescribed as in Table 6.2 to make the model exponentially stable, observable and controllable. Besides, the initial conditions of the model, such as displacements, velocities and perching angle, are set to the values of the experiment data. The comparison between the absolute radial and angular responses of the perching model and the corresponding experimental data of bird 3 is depicted in Figure 6.2. It should be noted that the direct outputs of the model are relative displacements to the equilibrium position, as shown in Eq. (6.12). The absolute displacements can be obtained by using Eq. (6.9). The Cartesian trajectory response can also be derived using Eq. (3.4). It is further compared with the mean perching trajectory of bird 3 in Figure 6.3.

Table 6.1 Prescribed parameters of quadrotor

m (g)	I_m (kg.m^2)	l (m)
63	5.6×10^{-5}	0.0443

Table 6.2 Parameters tuned to duplicate the perching maneuvers of bird 3

k_1 (N/m)	c_1 (N·s/m)	k_2 (N/m)	c_2 (N·s/m)
100	3	0.05	0.0022

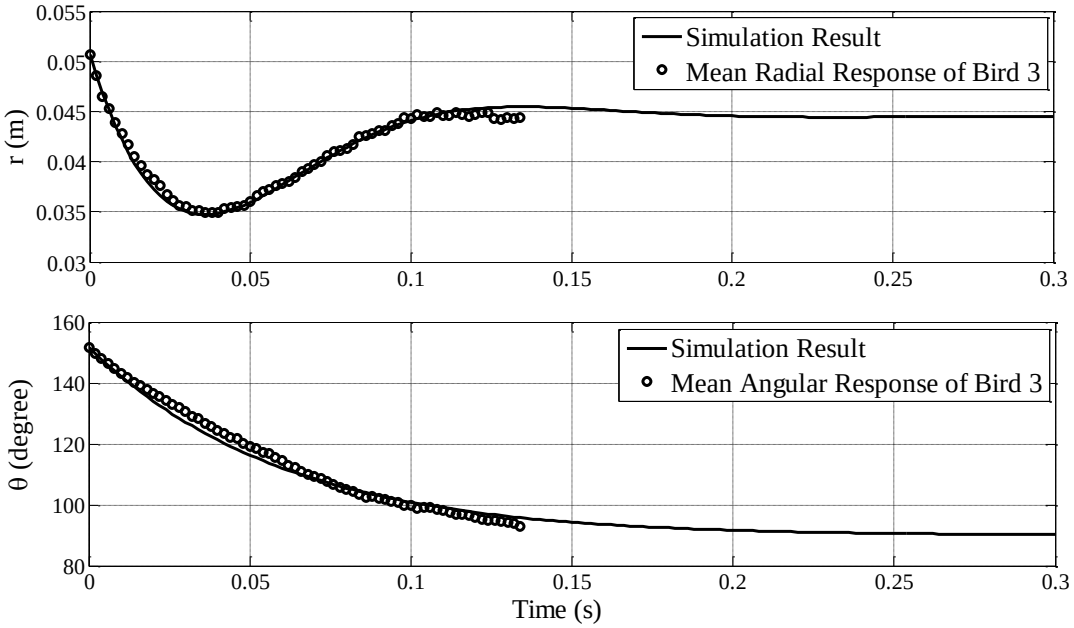

Figure 6.2 Comparison between the simulation results (solid curves) of the absolute radial and angular responses and the corresponding experiment data (circle points) of bird 3.

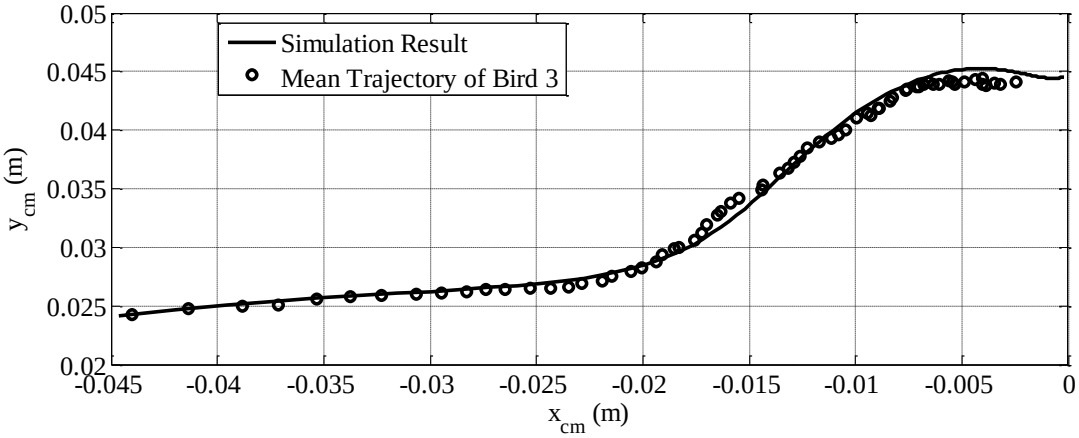

Figure 6.3 Comparison between the simulation result (solid line) of the Cartesian trajectory response and the mean perching trajectory of bird 3 (dashed line).

Obviously the simulation results agree very well with the experiment data in both radial and angular displacements in Figure 6.2, with only slight difference existing between them. The undulation of the radial displacement and the decaying of the angular displacement of the CM of bird 3 are successfully duplicated with the proposed dynamic perching model. The simulation results show longer responses because experiment data are limited to the shortest perching trial for the purpose of averaging. Similar agreement between the model response and the experimental data should hold for bird 1 because it employs similar maneuvers to bird 3's, as shown in Figure 3.16. Also, only trivial discrepancy exists between the Cartesian trajectory response of the perching model and the mean perching trajectory of bird 3, as shown in Figure 6.3. Basically they are overlapping each other and converging to a common balanced position directly above the perch. In summary good agreement between the simulation results and the experiment data validates the applicability of the model to describing the dynamic characteristics of the bird's on-perching maneuvers. Moreover, the dynamic parameters in Table 6.2 are the key characteristics associated with individual bird, since the difference in the perching maneuvers of different birds can generally be covered by tuning these parameters. Such a model makes the design of a controller for dynamic perching with quadrotors possible, because the interface to quadrotor dynamics has already been taken into account, and the state space model is generally observable and controllable with proper dynamic parameters. With active inputs from the quadrotor, the response of the perching model could be further regulated. The optimization of the perching controller can thus be accomplished by identifying the characteristic parameters and adjusting the control efforts.

6.2 Gripping Mechanism Design for Perching

With the perching model and design reference obtained, a perching mechanism for reliable perching with a quadrotor is designed. As predicted in the perching model, the UAV will oscillate before it's balanced and stopped. Although control effort from the UAV will assist in balancing, the primary balancing effort should come from the constraints between the perching mechanism and the perch. Therefore, the perching mechanism should be capable of generating the constraining forces and torques under working conditions of perching. Since grasping concept is utilized in the

dynamic perching model, the grasping forces perpendicular to the contact surface and the friction forces parallel to the contact surface will be the source of constraints, and their maximum values should envelop the reaction forces and torques required under potential perching circumstances. As the friction forces are dependent upon the grasping forces, the only critical parameter is thus the grasping forces. Given that the maximum actuation force from the motor remains the same, feature of force amplification is greatly desired for the perching mechanism to generate as large grasping forces as possible.

6.2.1 Force Amplification

A force amplifier can be defined as a mechanism that generates output forces larger than input actuation forces. If a force transfer ratio is further defined as

$$\lambda = \frac{F_{out}}{F_{in}} \tag{6.13}$$

a force amplifier can therefore be characterized with $\lambda > 1$. To design a perching mechanism featuring force amplification, a concept in Figure 6.4 is applied.

If a rhombic four-bar linkage is in equilibrium under two pairs of balancing forces, F_a and F_g, which are applied to its four joints symmetrically as depicted in Figure 6.4, the transfer ratio from F_a to F_g can be expressed as

$$\lambda_0 = \frac{F_g}{F_a} = tan\frac{\alpha}{2} \tag{6.14}$$

where α is the angle of input joint.

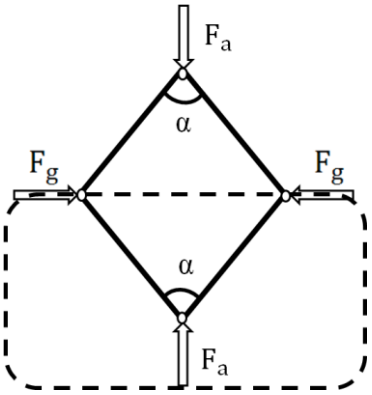

Figure 6.4 The force amplifier concept

Thus $\lambda_0 \geq 1$ for $90^o \leq \alpha \leq 180^o$, satisfying the force amplification requirement for perching mechanism design. Moreover, as α increases to 180^o, λ_0 tends to become infinite. This characteristic will benefit the design significantly. To simplify the mechanism, only the lower half of the rhombic linkage (the part enclosed by dashed lines in Figure 6.4) is utilized. Note that such a simplification has no effect on λ_0 because F_a will be balanced by vertical reaction forces at the output joints.

6.2.2 Kinematic Optimization

Taking into account the force amplification concept, a gripping mechanism is designed as in Figure 6.5. The actuation force is transmitted to the gripping digits via the shaft constrained to vertical linear motion and the transmission links which in pairs form a force amplifier, as shown in the red dashed region. Kinematic optimization is performed to maximize the force transfer ratio of the design.

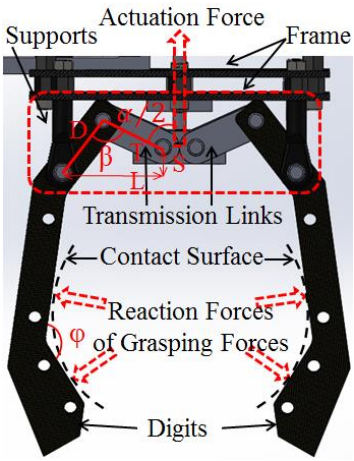

Figure 6.5 The gripping mechanism with force amplification

Obviously, the gripping mechanism is based on four-bar linkages which consist of actuation shaft, transmission link, digit and the frame. Therefore a kinematic diagram is drawn in Figure 6.6 for analysis. The zero point of the reference frame is set to the fixed joint. The slider is constrained to vertical linear motion, serving as the input link, and its coordinate is (L, S) where L is constant and S is variable. The lengths of the output link which is the digit and the coupler link which is the transmission arm are represented with D and T respectively. The angle $\alpha/2$ between the transmission arm and vertical axis is defined as the input angle, the angle β between the digit and the transmission arm denotes the coupling angle, and the angle γ between the digit

and x axis is defined as the output angle. The input actuation force is denoted by $\frac{F_i}{2}$, while the output force transmitted to the digit is represented by F_o. As the digit can only rotate, the effective output force, F_e, can be expressed as

$$F_e = F_o\, sin(\pi - \beta) = F_o\, sin\,\beta = \frac{F_i sin\beta}{2cos\frac{\alpha}{2}}. \tag{6.15}$$

Therefore the force transfer ratio is derived as

$$\lambda = \frac{F_e}{F_i/_2} = \frac{sin\beta}{cos\frac{\alpha}{2}}. \tag{6.16}$$

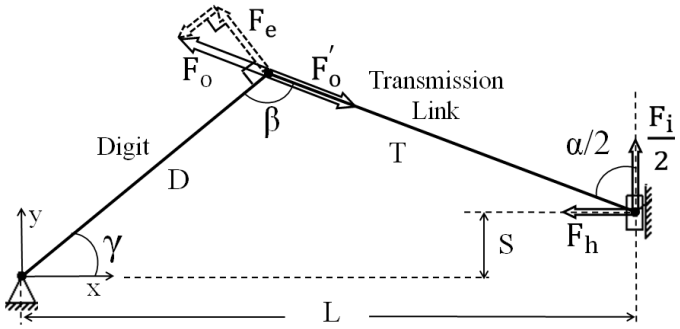

Figure 6.6 Kinematic diagram of the gripping mechanism

Based on the geometry of the mechanism in x and y directions, the equations below can be obtained.

$$\begin{cases} Dsin\left(\beta - \frac{\alpha}{2}\right) + Tsin\frac{\alpha}{2} = L \\ Dcos\left(\beta - \frac{\alpha}{2}\right) - Tcos\frac{\alpha}{2} = S. \end{cases} \tag{6.17}$$

Eliminating α and β separately yields the equations below.

$$cos\beta = \frac{D^2 + T^2 - S^2 - L^2}{2DT} \tag{6.18}$$

$$\cos(\frac{\alpha}{2} - \phi) = \frac{D^2 - T^2 - S^2 - L^2}{2T\sqrt{S^2 + L^2}} \tag{6.19}$$

where ϕ satisfies $\tan\phi = \frac{L}{S}$.

Taking the dimensions of the quadrotor utilized into account, L and D are prescribed to be 35mm and 20mm respectively. Moreover, the range of input S is limited to [-7, 12] mm which is the applicable workspace for the actuation shaft. Hence, λ is

reduced to be a function of S and T, and only T needs to be determined. Since the optimization objective is to maximize the effectiveness of force amplification of the design over the workspace, an accumulated force transfer ratio λ_a is further defined.

$$\lambda_a(T) = \int_{S_{min}}^{S_{max}} \lambda(S,T)\, dS. \tag{6.20}$$

Given a constant actuation force F_i, λ_a reflects the overall effectiveness of force amplification in the workspace with different T. To identify the constraints imposed on T, the range of $\cos\beta$ is considered. Obviously, $-1 < \cos\beta < 1$. It can thus be obtained from Eqn. 6.18 that

$$\sqrt{|S|_{max}^2 + L^2} - D < T < \sqrt{|S|_{min}^2 + L^2} + D. \tag{6.21}$$

Furthermore, two cases of singularity, in which α reaches 180° before S reaches the maximum position or β reaches 180° when S is maximum, and one extreme case, in which γ reaches 90° when S is maximum, are considered, as illustrated in Figure 6.7.

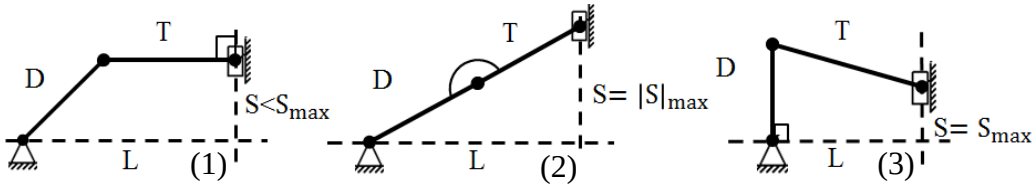

Figure 6.7 Three extreme cases for constraints of T. Left: singularity of α; Middle: singularity of β; Right: maximum γ.

The corresponding constraints on T can therefore be derived as below.

For α: $$L - \sqrt{D^2 - S_{max}^2} < T < L + \sqrt{D^2 - S_{max}^2} \tag{6.22}$$

For β and γ: $$\sqrt{L^2 + S_{max}^2} - D < T < \sqrt{(D - S_{max})^2 + L^2}. \tag{6.23}$$

Consequently, the optimization problem can be expressed as

Objective: Maximize $\lambda_a(T)$,

Subject to: $S \in [S_{min}, S_{max}]$, Inequalities 6.21, 6.22 and 6.23.

The optimization problem defined above is investigated numerically using Matlab. S and T are discretized first within their constraint ranges, and values of λ_a with different values of T_i are then calculated and illustrated in Figure 6.8. It's obvious that the maximum of λ_a corresponds to $T_1 = 0.020$m. The force transfer ratio λ in

this case with respect to *S* is further calculated and shown in Figure 6.9. It shows that the force transfer ratio is already larger than 1 at the initial position and it increases gradually to almost 12 at the maximum input position. Such a characteristic is consistent with the fact that the smaller the diameter of the target is, the larger the grasping force is needed to generate the balancing moment for the quadrotor, and will therefore greatly benefit the grasping performance of the perching mechanism. The initial force transfer ratio of 1.3 is still acceptable since the impact at the beginning of perching will facilitate the grasping, resulting in less actuation force required from the motor. The maximum force transfer ratio of 12 is rather promising, with combination of a powerful motor.

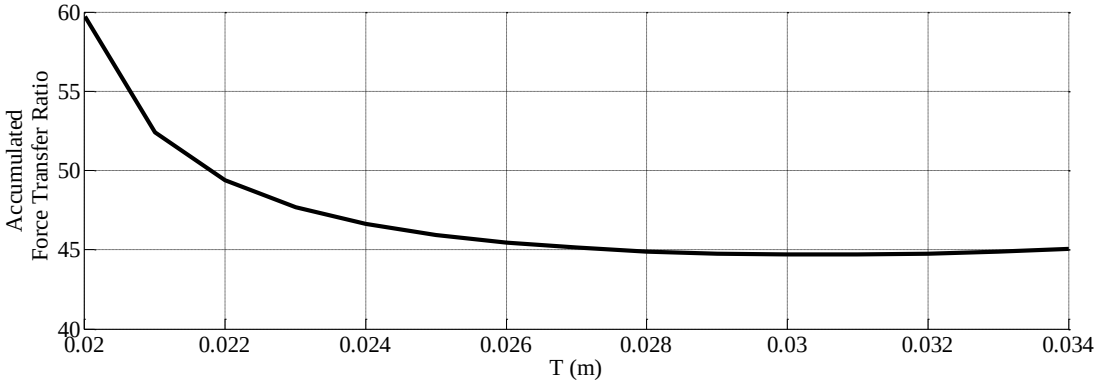

Figure 6.8 Accumulated force transfer ratio λ_a under different lengths of *T*

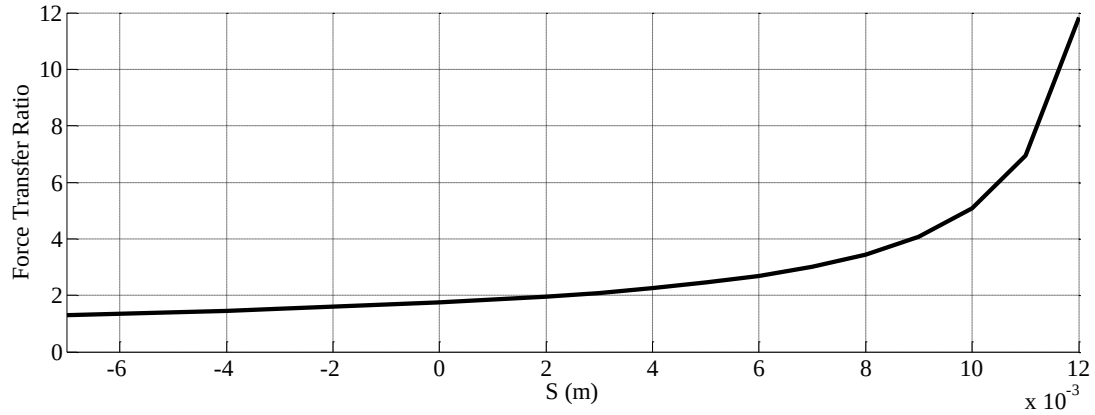

Figure 6.9 Force transfer ratio λ under the optimal $T_i = 0.020$m

As the digit is a solid link that works as a lever about its pivot joint, it introduces a constant force transfer ratio *K* into the force transmission loop. *K* can be determined according to the workspace required for various applications. The overall force transfer ratio λ_{tot} for the perching mechanism can further be written as

$$\lambda_{tot} = K\lambda = K\frac{sin\beta}{cos\frac{\alpha}{2}}. \tag{6.24}$$

To feature envelop grasping as inspired by birds, the digit is designed to have a curvature angle as suggested in Figure 6.5. Since friction forces are utilized to secure the balance of the UAV and avoid slippage, the coefficient of static friction between the materials of contact is rather critical. The coefficients of static friction between wood and some common materials range from 0.2 to 0.8, while those between rubber and common materials are mostly larger than 0.4 [113]. As rubber is supposedly to be applied to the digits, a conservative value of 0.4 is estimated for the coefficient of static friction, μ.

As impact happens during perching, the perching mechanism is supposed to be strong enough to withstand it. Another critical issue of perching with UAVs is the weight of the mechanism, or payload capacity of the UAVs. In the case of perching, the less the perching mechanism weighs, the more agility in manipulation it will give the UAV, which will significantly benefit the whole perching system. Therefore, carbon fiber sheets are utilized for the mechanism frame and the digits to increase the strength of the whole structure and also reduce its weight. Nylon spacers are employed to support the frames, and Delrin shafts are designed for all the revolute joints. As a result, the mechanism, including the servo, weighs only about 330g which is far within the payload capacity of the quadrotor used. Figure 6.10 shows one version of the perching mechanism that is designed and fabricated. Two pairs of the gripping mechanism are employed such that effective grasp is guaranteed and lateral stability of the quadrotor is secured.

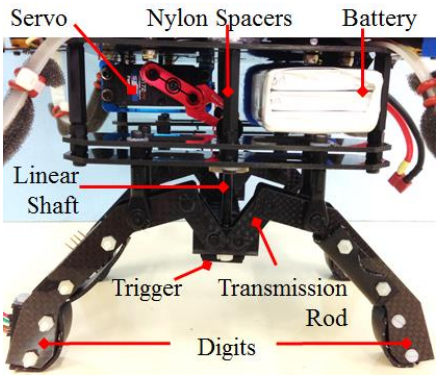

Figure 6.10 Final version of the perching mechanism

6.2.3 Force Sensing Mechanism

Contact with the perch is the critical factor during perching. During approaching flight to the perch it means the proper instance to activate the perching mechanism; it reflects the intensity of the grasp during balancing the UAV. The forces resulted from the contact during perching are therefore monitored by a trigger mechanism and a grasping force feedback mechanism respectively, to provide valuable information for automatic and adaptive perching.

Force sensing resistors (FSRs) are applied to such mechanism designs because of their excellent linearity in the relationship between input force and output voltage, convenience for integration into the control circuits, and their compact size. For the trigger, a simple switch function is sufficient. Besides, the larger the triggering area is, the more reliably the trigger mechanism functions. Therefore, force sensors of a long form factor that can detect impact along a long distance serve the goal better. On the other hand, force sensors of small contact area are employed to measure the grasping forces on the digits because only discrete contact forces need to be monitored. Two versions of the force sensing mechanism designed are illustrated in Figure 6.11.

The trigger is attached to the junction blocks of the digits so that its neutral position not only is within the grasp range of the perching mechanism but also gives sufficient reaction time to the grasping mechanism. The grasping force feedback mechanisms are integrated into the digit of the gripper, with two sensors for the two digit sections respectively. The protruding probes of version 1 or the sensor's back plate of version 2 will be pushed against the perch surface and will therefore squeeze the sensor due to reaction forces. The force sensors are calibrated before integrated into the control loop, which is introduced in detail in Appendix A.

The perching mechanism is assembled after the gripping mechanism, the trigger and the force feedback mechanism are finalized. It is further mounted to a quadrotor and integrated into its control loop. Two versions are developed along the progress, with different quadrotors and improved perching mechanisms, as shown in Figure 6.12.

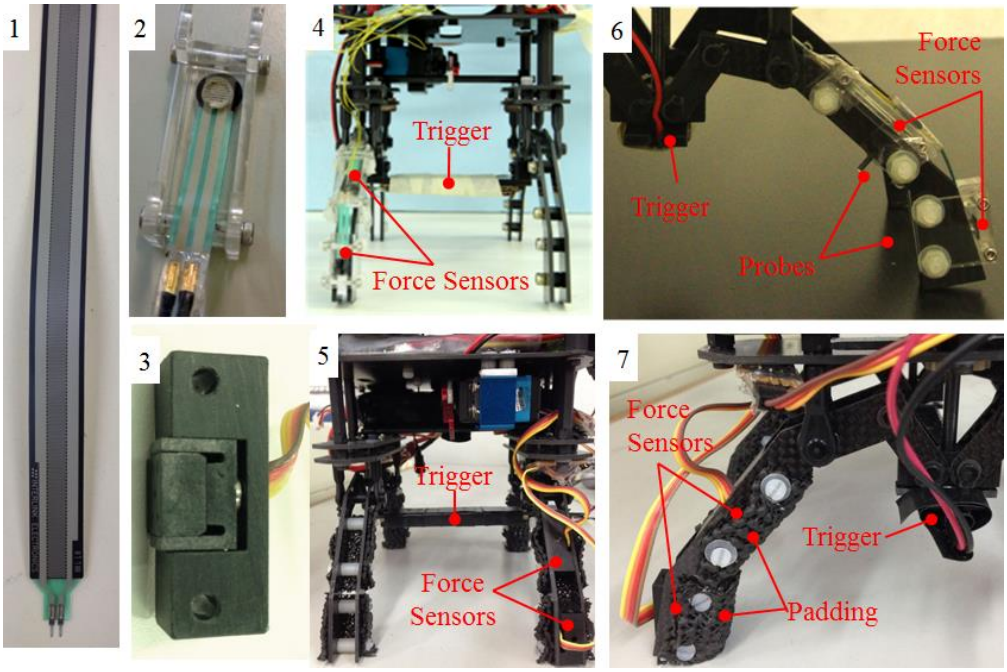

Figure 6.11 Force sensing mechanism design. 1: Trigger sensor. 2 and 3: Force sensors. 4-7: Grasping force feedback mechanisms.

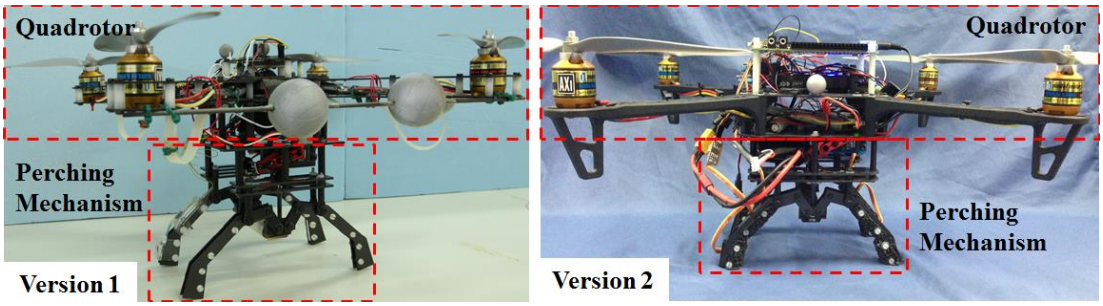

Figure 6.12 Two versions of the perching mechanism integrated into different quadrotors

The differences between the two versions mainly include new quadrotor equipped with advanced high level controller board and revised perching mechanism with more reliable force sensor installation and more compact battery installation. The advanced high level controller allows for more challenging tasks such as fuzzy control and image process. The revised perching mechanism can measure the grasping force reliably with larger contact area. Moreover, it lowers the center of gravity by integrating the battery into the same layer of the servo, and increases the polygon of balance in lateral direction by widening the lateral span of the two digit pairs. Consequently balance of the quadrotor system can be obtained more readily.

Some parameters of the integrated system are as follows. The mass of the perching system including the perching mechanism is 1.65kg, and the equivalent distance from the center of mass to the grasping center is approximately 0.15m. The digit curvature angle is 140^{o}, and the equivalent length of the servo horn is 3cm.

6.3 Experiments on the Effectiveness of the Perching Mechanism

Throughout the development of the perching mechanism a series of experiments are performed to assess its effectiveness qualitatively in different scenarios. Firstly, indoor dynamic perching experiments with a remote-controlled quadrotor are performed. Secondly, the remote-controlled dynamic perching with a quadrotor is also conducted in outdoor environment. In these two experiments the perching mechanism is controlled manually. Finally, with only the open loop control of the perching mechanism, indoor automatic perching experiments with a quadrotor are carried out with position control based on the VICON motion capture system. Note that a PVC tube enclosed with a piece of foam which later is changed to natural rubber to increase the friction coefficient is utilized as the target perch in the experiments. Also, complementary experiments of static grasp and dynamic object-picking-up are presented in Appendix B.

6.3.1 Indoor Remotely Controlled Dynamic Perching with a Quadrotor

Three experiments of dynamic perching under remote control were conducted in indoor environment, the first one being taking off from ground and perching to the target pole, the second one taking off from the perch and perching again, and the third one taking off from the perch and perching again with a misalignment angle. The experiment procedures and results are illustrated in Figure 6.13.

In perching experiment 1, the UAV system successfully perched to the pole with the first trial, although only digit tips contacted the pole. It shows that even an incomplete grasp can secure the perching. In perching experiment 2, the quadrotor stumbled a bit when re-launching, but it managed to release from the pole and take off. Moreover, the perching later was properly performed in terms of alignment with

the pole, and a complete grasp was formed. In perching experiment 3, the quadrotor succeeded in launching again and it happened to misalign with the pole during perching, leading to a misaligned but complete grasp. The misalignment angle is within the range that the gripper can withstand, so the perching is still reliable.

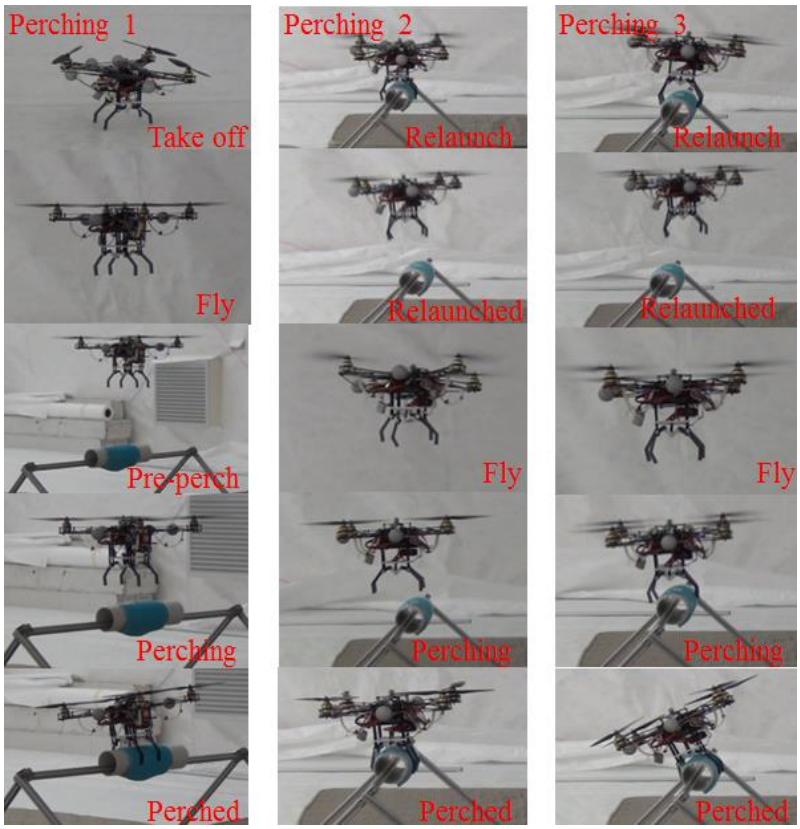

Figure 6.13 Dynamic perching experiments with the quadrotor under remote control(left to right: three experiments; top to bottom: procedures of each perching)

6.3.2 Outdoor Remotely Controlled Dynamic Perching with a Quadrotor

Although the grasping ability and reliability of the perching mechanism have been validated in lab environment, experiments in outdoor environment are also deemed necessary to make the validation thorough since the mechanism ultimately aims at applications in natural circumstances. Therefore, experiment of remote-controlled perching of a quadrotor to a tree branch is conducted.

In this perching experiment, the quadrotor will take off from ground and perch to a tree branch with sufficient clearance and moderate diameter for the quadrotor to approach and grasp. Figure 6.14 illustrates the perching procedure. It can be seen that misalignment between the gripper and the tree branch exists and the final perching

state is a little off balance in lateral direction. This is because of the error in remote control of the quadrotor and the breeze blowing during the experiment. However, the whole perching procedure was still very smooth and the perching was deemed as reliable since no oscillation of the quadrotor was observed during post-perching.

Figure 6.14 Perching to a tree branch (1: Hovering; 2: Descending; 3: Grasping; 4: Perched)

6.3.3 Indoor Automatic Perching with a Quadrotor

It should be noted that the gripper was remotely, instead of automatically, controlled in all the experiments above. Therefore, automatic perching is necessary for validation of the perching effectiveness of the mechanism designed. As gripping force feedback control laws haven't been developed yet, automatic perching is performed with only the trigger feedback and open loop control of the perching mechanism in VICON system. The quadrotor is modelled with infrared-reflective markers and localized via VICON system. With simple position control implemented in Simulink, the quadrotor, with the perching mechanism attached to it, is commanded to follow the perching trajectory. When the trigger is activated by contact with the perch, the low level onboard controller will rotate the servo shaft to a certain position which is prescribed according to the perch dimensions. The experimental setup for indoor automatic perching is shown in Figure 6.15.

In this experiment the quadrotor first automatically takes off and fly to the prescribed location above the perch. Then it descends vertically toward the target perch while maintaining its position in the horizontal plane. The perching mechanism stands by from the beginning of the quadrotor's descending. Once the onboard controller detects the contact with the perch from the trigger it automatically actuates the gripper to grasp the perch. When reliable perching is achieved the quadrotor then stops the rotors. To take off, the quadrotor powers up the rotors first to generate

sufficient thrust. As the thrust increases, the orientation of the quadrotor may be gradually adjusted to an optimal vertical direction if an initial misalignment angle exists during perching. The gripper is commanded to release when thrust is large enough to disengage the trigger. One successful automatic perching and take-off sequence is shown in Figure 6.16. The same procedure was duplicated for several times, revealing the reliability of the automatic perching system.

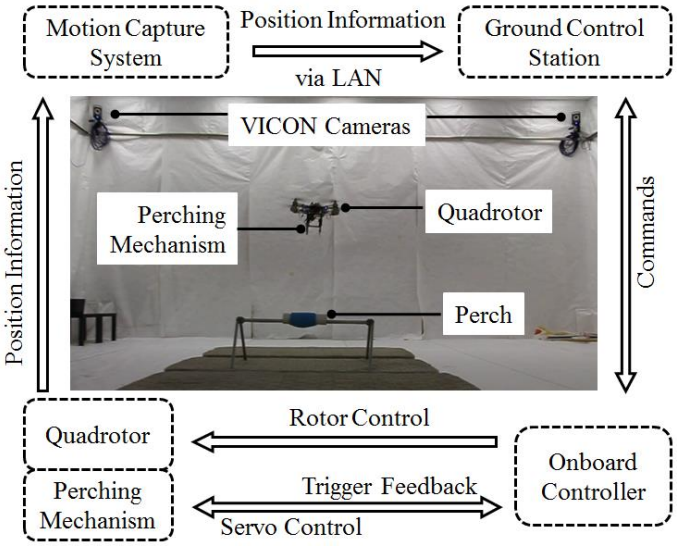

Figure 6.15 Experimental Setup for Indoor Automatic Perching with a Quadrotor

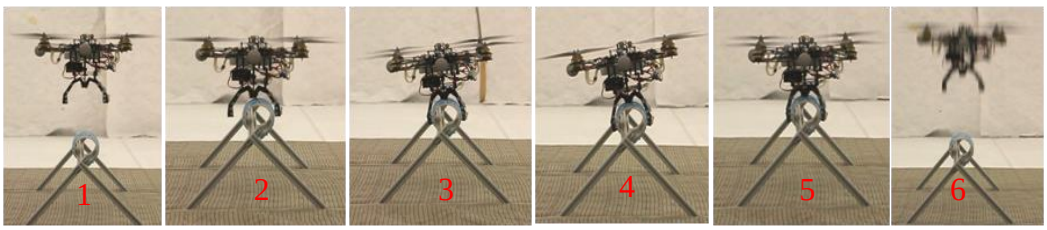

Figure 6.16 Indoor automatic perching (1: Declining, 2: Triggered and 3: Perched) and take-off (4: Powering up, 5: Self-adjusting and 6: Released)

6.4 Control Laws of the Perching Mechanism

6.4.1 Control Flow Design

The onboard controller board of the quadrotor is where all the control algorithms of the perching mechanism will be centralized at. Therefore, the control flow designed for the actuation of the perching mechanism starts with a command from the onboard controller which is either to perch or to take off. The generalized perching procedure is taken into account in the control flow, as demonstrated in Figure 6.17.

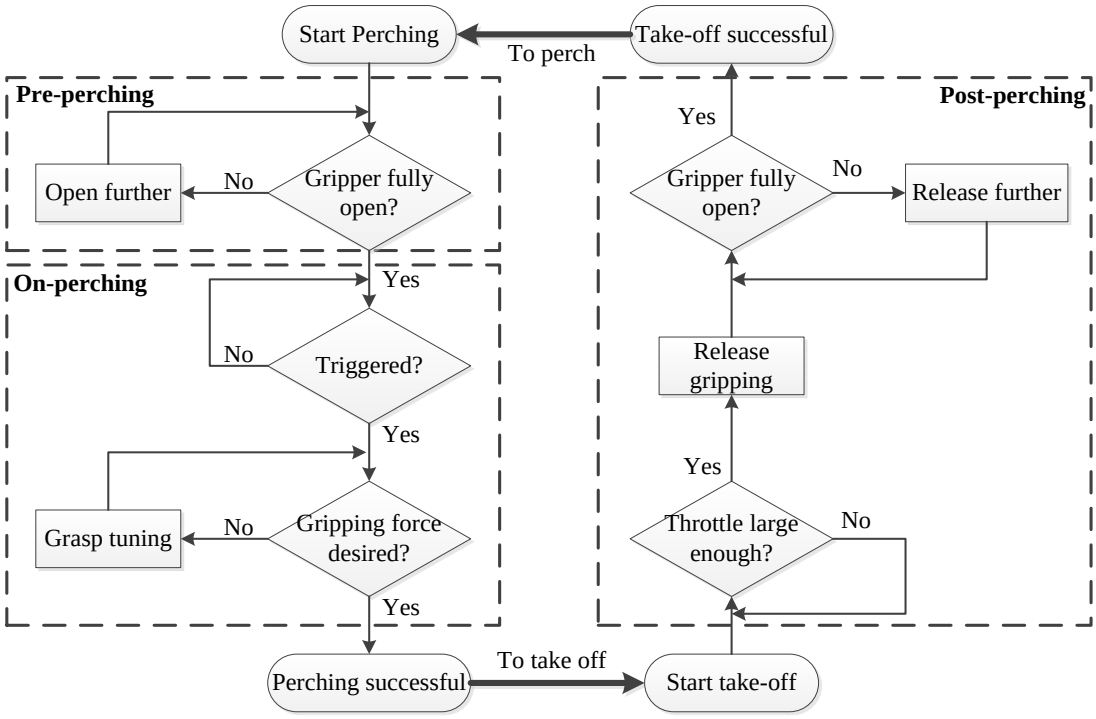

Figure 6.17 Control flow of the perching mechanism based on the generalized perching procedure

In pre-perching, when the onboard controller commands to perch, the gripper controller checks whether the current state of the gripper is fully open. Then the gripper controller rolls into the perching stage, and starts monitoring the triggering event. Once triggered, it activates the gripper immediately to establish the firm grasp to the perch. Meanwhile, the grasping forces are fed back to the gripper controller to secure the effectiveness and reliability of the grasp. When taking off, it is necessary for the quadrotor to initialize the throttle to the hovering level so that the safety of the UAV can be guaranteed even if the release of the gripper fails. The gripper controller then releases the gripper from the perch and resets it to the standby state for next perching. Once totally disengaged with the perch, a ready-to-go signal will be sent to the autopilot controller which further switches the quadrotor into flight mode.

6.4.2 Conventional Control Law

Based on the dynamic perching model that has been established and the control flow above, a conventional control scheme for automatic perching is proposed as in Figure 6.18. At the instance the perching system is triggered, the desired grasping force F_o is

calculated based on the perching dynamics model. Taking into account the threshold value of grasping force F_t and the actual grasping force F_g exerted by the gripper on the target as well, the controller will output the step value accordingly to adjust the duty cycle D_c of the servo so that the gripper will be actuated to desired position and generate desired grasping force to secure the perching.

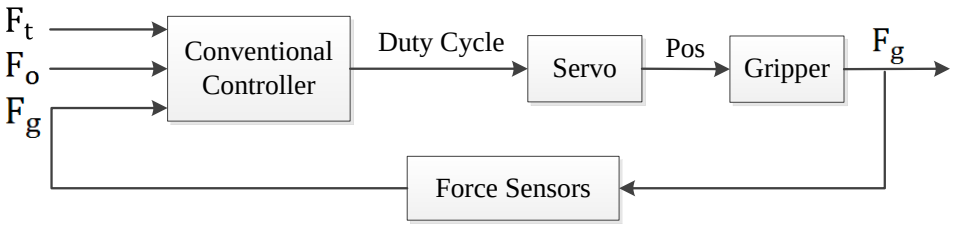

Figure 6.18 Conventional control for automatic perching

The only parameter of the servo motor that can be directly controlled is the angular position of the servo shaft, while the output torque is automatically controlled by its onboard controller based on the position error of the rotation. As long as position error exists and the required output torque is within its capability, the actual output torque will be increased automatically. Therefore a threshold F_t of the force feedback from the force sensors can be set as a Boolean indicator of the gripper status. It means the gripper contacts the target and starts grasping it when force feedback exceeds the threshold F_t. The duty cycle D_c should be tuned at the optimal step which makes the servo actuate at the fastest speed when no contact happens; otherwise the step itself should be varied according to the actual grasping force such that grasping under loading can be finished as quick as possible while avoiding damaging the servo. Consequently, the controller can be expressed as

$$D_c(k+1) = D_c(k) + D_{step} \tag{6.25}$$

$$D_{step} = \begin{cases} D_{max}, & F_g < F_t \\ c_1 \cdot D_{max} - c_2 \cdot \Delta D, & F_t \le F_g \le F_o \\ 0, & F_g > F_o \end{cases} \tag{6.26}$$

where $D_c(k)$ is discrete duty cycle value, D_{step} is the step value for tuning the duty cycle, D_{max} is the maximum step value that the servo can follow without rotation error at certain control loop rate, ΔD is the resolution of duty cycle for the specific servo, and c_1 and c_2 are coefficients that adjust the step value. Besides, $c_1 \in \mathbb{R}, (0,1]$

and $c_2 \in \mathbb{Z}, [0, n]$, where $n = \left\lfloor \frac{c_1 \cdot D_{max}}{\Delta D} \right\rfloor - 1$. The formula for calculation of c_2 can be expressed as $c_2 = \max(0, \min(n, \left\lfloor \frac{F_o - F_t}{F_o - F_g} \right\rfloor - 1))$. That is, c_2 is equal to the floor integer of $\left\lfloor \frac{F_o - F_t}{F_o - F_g} \right\rfloor - 1$ saturated to $[0, n]$. To determine the parameters in the controller design, the characteristics of the servo and the force sensors need to be evaluated. Readers are advised to refer to appendix A for details. Also, the specifications of the control system of the quadrotor need to be taken into account. The finalized parameter values are listed in Table 6.3.

Table 6.3 Parameters of the conventional controller designed

D_{max} (μs)	ΔD (μs)	F_t (N)	c_1
120	10	4	0.5

6.4.3 Fuzzy Control Logic

The onboard controller of the servo unknown to users makes direct control of the output torque impossible. Since only desired position is taken as the input variable of the servo, the fuzzy controller to be designed for the perching mechanism is supposed to be able to handle the unknown transfer function of the servo and generate desired gripping force via position control. Moreover, the actuation design of the perching mechanism introduces nonlinearity into the force transmission loop from the servo to the digit tips, which makes linear model of the perching mechanism even more unobtainable. Besides, fuzzy logic has been successfully utilized in many applications of gripping mechanism control [114][115][116][117][118][119][120], which shows its good applicability in the perching case. Therefore, fuzzy logic based on empirical knowledge of the system to be controlled is applied.

The inputs and outputs of the fuzzy controller are determined first. As the servo takes desired rotation position as input, the fuzzy controller should output such kind of information. To adopt similar strategy of the conventional controller design, a step value of the rotation is taken as the direct output of the fuzzy logic. However, the same step value will lead to different travel distances of the digit tips of the perching mechanism with different current rotation position of the servo. Thus, the current rotation position of the servo needs to be taken as an input. Besides, sufficient

gripping force is required to guarantee safe perching in the perching methodology proposed, so the gripping force should be monitored and serve as feedback for actuation adjustment. On the other hand, the dynamic perching model estimates the reference gripping force based on the current status such as perching angle and velocity of the UAV. As a result, the error between the gripping force and the reference one is input to the fuzzy controller for actuation adjustment. Consequently the diagram of the fuzzy control is shown in Figure 6.19. Note that the resultant duty cycle is mapped to the rotation position as a feedback.

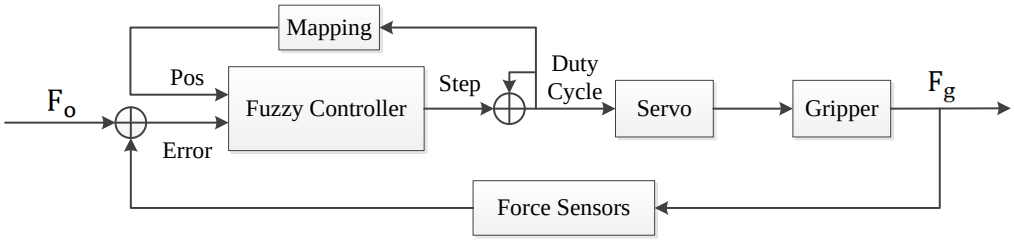

Figure 6.19 Fuzzy control for automatic perching

The membership functions of the input and output variables are depicted in Figure 6.20, Figure 6.21 and Figure 6.22, respectively. The position is divided into small (S), medium (M), and big (B). The range [-7mm, 12mm] is determined by the mechanical design of the perching mechanism. -7mm corresponds to the fully open state, while 12mm the fully grasping state. Apparently, the range is not symmetric. The classification is therefore skewed towards positive values. For the gripping force error, however, it is distributed symmetrically about zero. To improve the force adjustment performance, the force error is classified into five functions, including negative big (NB), negative small (NS), zero (Z), positive small (PS), and positive big (PB). Negative represents over-grasping and positive means insufficient grasp.

The output range of the step value is from -90μs to 90μs in which negative means the duty cycle is decreased and positive increased. It is also divided into five classes to enhance the tuning resolution of the duty cycle of the servo. They are negative big (NB), negative small (NS), zero (Z), positive small (PS), and positive big (PB). Also, they are symmetrically distributed about zero. Note that the membership function of Z is of singleton type, which is to eliminate the oscillation of the output step value introduced when de-fuzzifying for zero (Z) case.

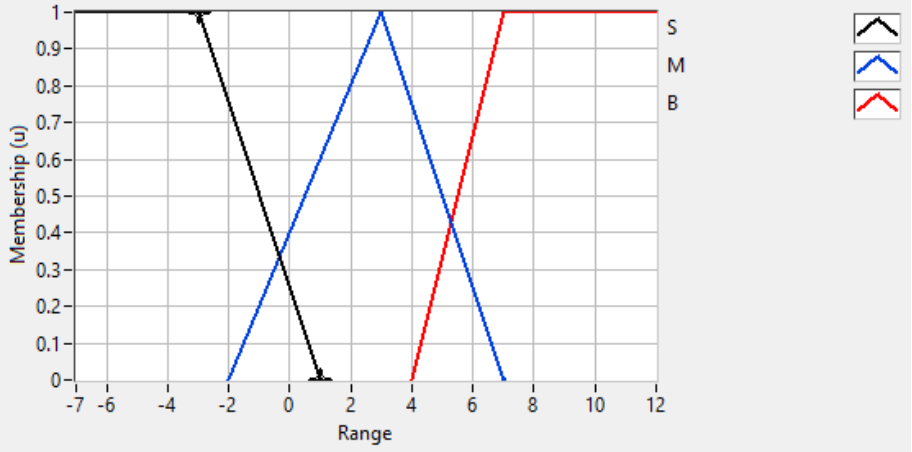

Figure 6.20 Membership functions of the input variable of position. The range of the position is from -7mm to 12mm.

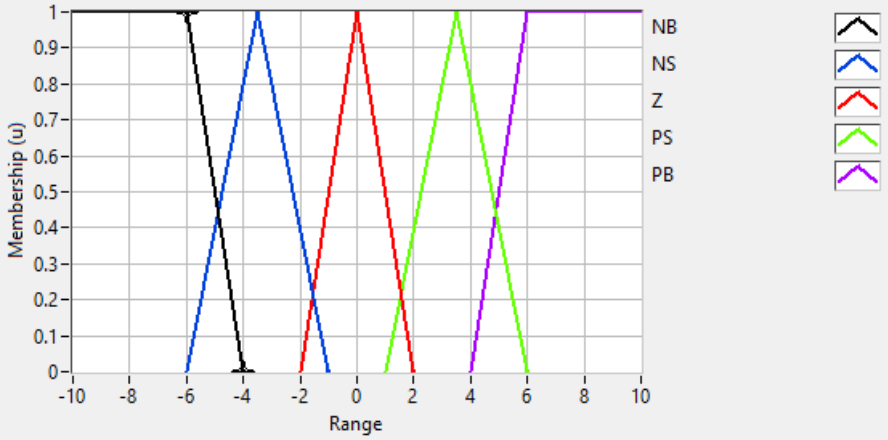

Figure 6.21 Membership functions of the input variable of force error. The force error ranges from -10N to 10N.

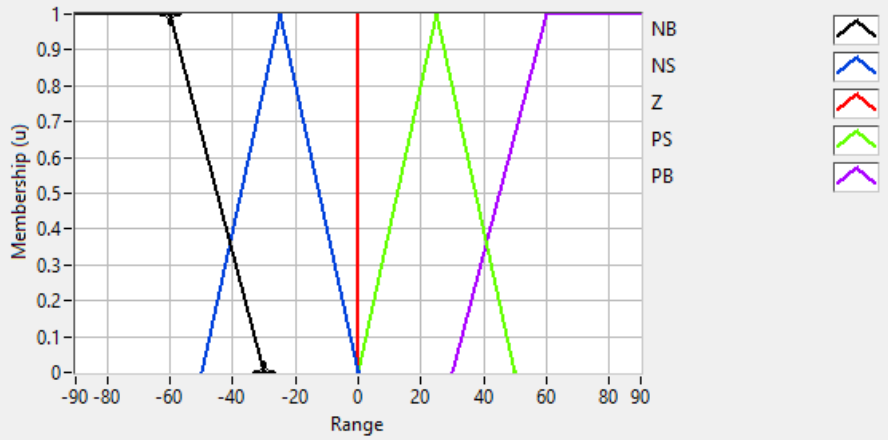

Figure 6.22 Membership functions of the output variable of step value. The step value range from -90μs to 90μs.

The fuzzy inference rules based on the empirical knowledge of the perching mechanism are listed in Table 6.4. Generally, the step value corresponds to the gripping force errors when the gripping perching mechanism is in middle way (M) or full grasp (B). If the gripper is in or close to fully open state (S), small or zero step value applies to non-positive force errors. Furthermore, the step value will be close to zero for trivial gripping force errors (Z). Basically, it requires more rotation and larger torque for the servo to generate the same travel distance and grasping force on the digit tips when the rotation position is small or large than when medium. However, to avoid damaging the perching mechanism or the servo due to rotation position exceeding its limits (S or B), the step value in the cases of over-grasping at small rotation position and insufficient grasp at big rotation position is limited to small value (NS and PS respectively), instead of big value. It can be seen that the rules are designed exactly based on the characteristics of the perching mechanism. To demonstrate the controller performance, the 3D surface of the rules is plotted in Figure 6.23. The defuzzification method used is center of sums, which takes every factor that affects the output into account.

Table 6.4 Fuzzy inference rules of the gripping controller

		Gripping Force Error				
		NB	NS	Z	PS	PB
Rotation Position	S	NS	Z	PS	PS	PB
	M	NB	NS	Z	PS	PB
	B	NS	Z	Z	PS	PS

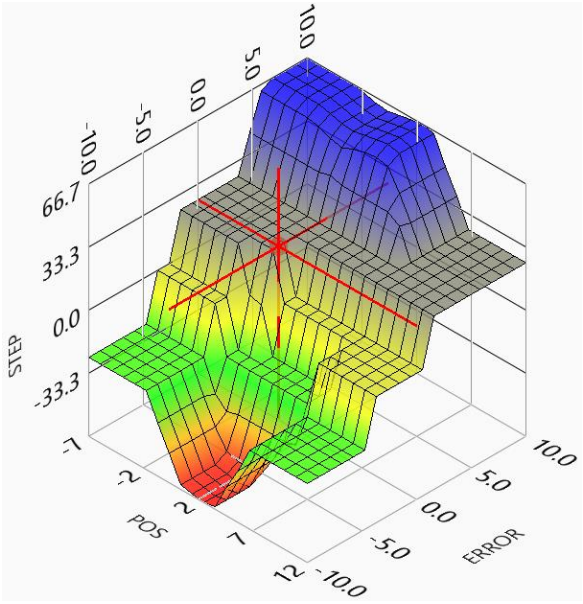

Figure 6.23 Surface plot of the fuzzy gripping controller

6.5 Experiments of the Control Laws for Perching Mechanism

The control laws including the control flow and two different controllers designed for the perching mechanism are further experimentally evaluated in this section.

6.5.1 Drop-and-Grasp with Conventional Control

In this experiment the quadrotor with the perching mechanism installed is first manually aligned with the perch. Then it is dropped and grasps the perch automatically under the proposed conventional controller when it's triggered. After successful perching is accomplished disturbances will be applied to the UAV to simulate random loading after perching, like gust. The experiment procedure is demonstrated in Figure 6.24. To evaluate the effectiveness of the trigger the sensor reading during the triggering stage from one experiment is illustrated in Figure 6.25.

The solid curve in Figure 6.25 represents the voltage reading of the trigger sensor, and the dashed line denotes the threshold value of 3.3v for triggering the perching mechanism. It can be seen that the sensor voltage reading stays about 4.2v after initialization of the perching mechanism, and it drops significantly when engaged with the perch. The switching feature of the trigger is so effective that the threshold can be readily set. Also, the voltage drop happens within three samples, leading to a

really short response time of 6ms with 500Hz sampling rate of the trigger sensor. It means the perching mechanism can be almost instantly activated once contacting the perch. Therefore, the trigger of the perching mechanism can work effectively.

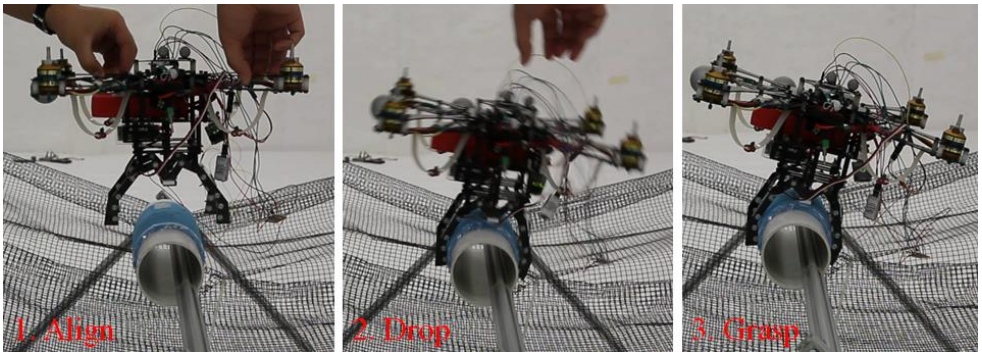

Figure 6.24 Drop-and-Grasp (1: Align the quadrotor with the target manually; 2: Drop the quadrotor; 3: The perching mechanism gets triggered upon impact and grasps automatically)

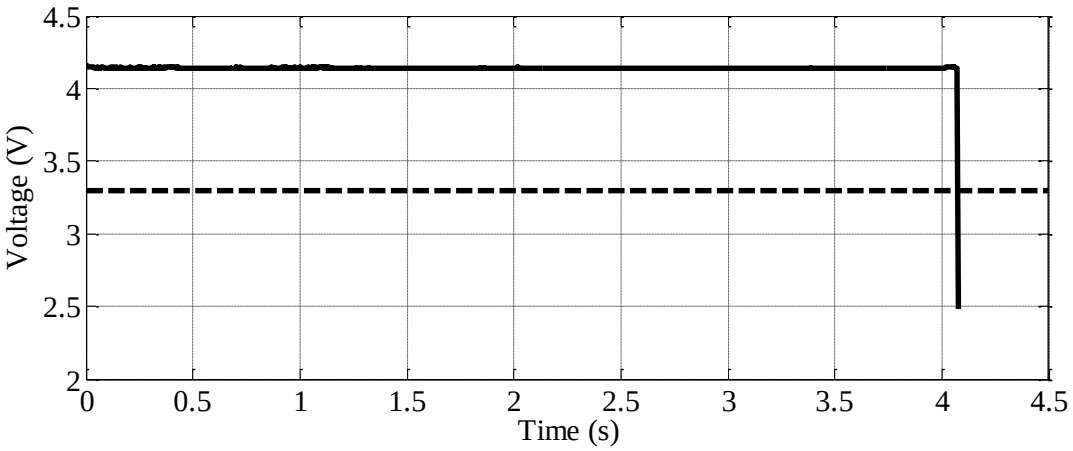

Figure 6.25 Trigger sensor reading during triggering stage

The perching mechanism is then put into the drop-and-grasp tests to verify its effectiveness. The resultant gripping force from the four force sensors installed in the digits of the perching mechanism and the corresponding duty cycle calculated for actuation from one experiment are plotted in Figure 6.26. The vertical axis on the left (blue) is for the resultant gripping force, while the one on the right (red) is for the duty cycle. The intensification process in the beginning is magnified for details. The disturbances applied are emphasized with black circles.

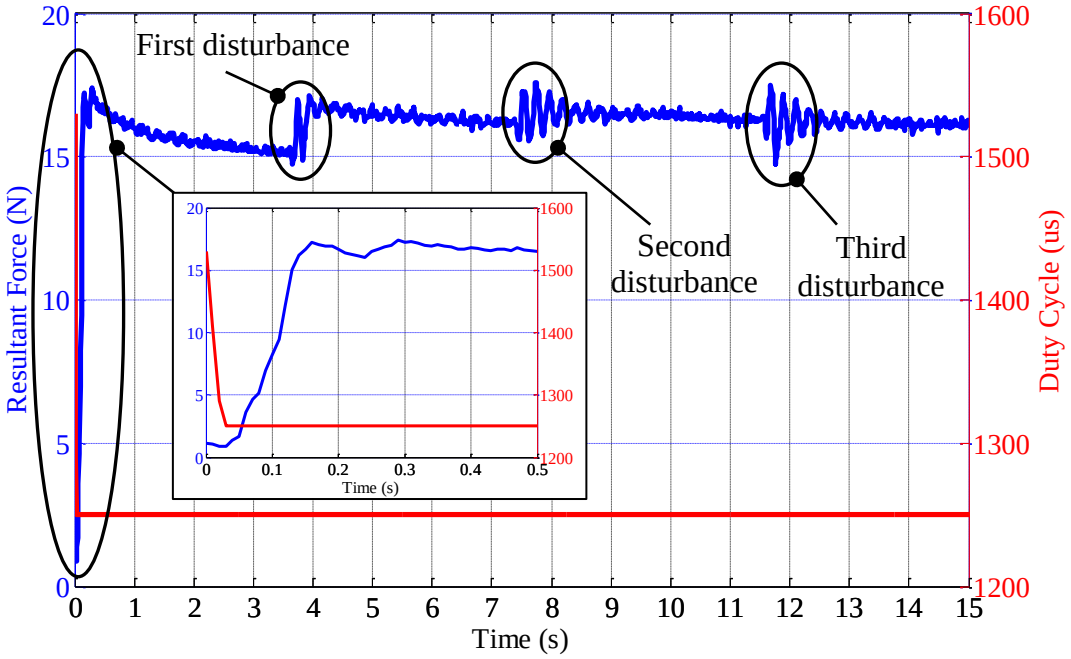

Figure 6.26 Resultant gripping force (blue) and duty cycle tuning (red) with the proposed conventional control. The desired gripping force is set to 15N.

It is obvious that the conventional controller starts tuning the duty cycle immediately after the perching mechanism is triggered. The duty cycle is adjusted to the minimum value within 0.04s since the resultant gripping force hasn't reached the desired value. This delay in response of resultant gripping force is probably caused by factors such as inertial of the servo, time taken by the gripper digits to engage the perch and the slight hysteresis of the force sensor. It takes about 0.13s for the resultant gripping force to reach desired 15N, and it remains above 15N thereafter. The overshoot of the gripping force reflects the hysteresis of the force sensors because the conventional controller is designed only to fasten the grasp and no reverse tuning other than full release is taken into account to guarantee firm and reliable grasp. This can be further demonstrated when the disturbances are applied. The first disturbance increases the resultant gripping force instantly, but there is no releasing adjustment made by the controller to the perching mechanism. For the second and third disturbances the oscillation of the gripping force is rather apparent, but the duty cycle remains put. From the perspective of actual performance, the perching mechanism achieves reliable grasp over the perch in every trial and succeeds in maintaining the grasp without failure like slippage when disturbances are imposed to the UAV.

Result in Figure 6.24 shows a successful grasp with a certain misalignment angle between the UAV yaw axis and the vertical axis of the perch. It should be noted that the oscillation of the resultant gripping force is not because of insufficient damping of the perching mechanism. Instead, it is mainly because the connection between the tube serving as the perch and the supporting frame is not ideally fixed. In summary, the performances of the perching mechanism are rather effective, reliable and consistent. Thus the conventional controller works effectively for automatic perching with a quadrotor.

6.5.2 Drop-and-Grasp with Fuzzy Control

The method in this experiment is basically the same as in the experiment of drop-and-grasp with conventional control, as shown in Figure 6.27, except that the proposed fuzzy controller is employed for grasp tuning. Similarly, to evaluate the effectiveness and reliability of the fuzzy controller, disturbances are imposed after successful perching has been achieved. The resultant gripping force from the force sensors and the duty cycle of the servo actuation after being triggered from one of the experiments are shown in Figure 6.28. Due to the quickness of the intensification process, it is zoomed in to elaborate the force increase and duty cycle tuning. The instants when disturbance is applied are marked with black ellipses. Note that the *y* axis of the resultant gripping force is on the left side (blue), while that of the duty cycle on the right side (red).

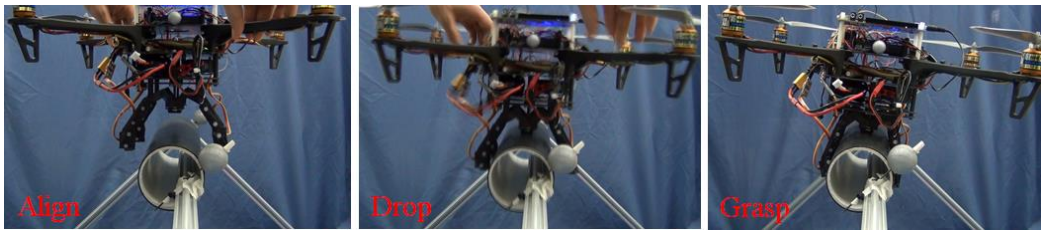

Figure 6.27 Experimental procedure of the drop-and-grasp testing

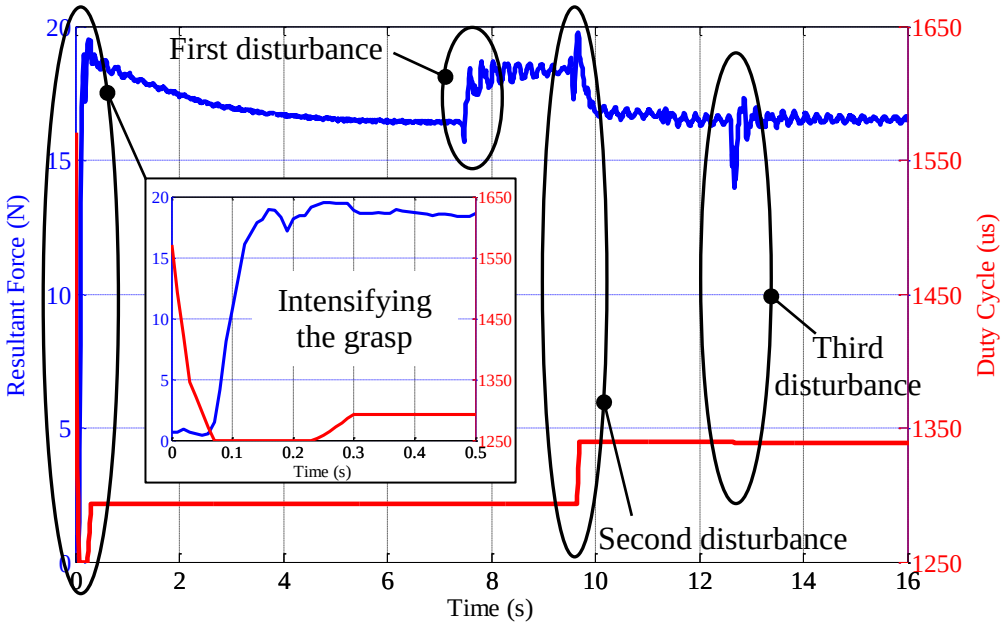

Figure 6.28 Resultant gripping force (blue curve) and duty cycle tuning (red curve) with the proposed fuzzy control. The desired gripping force is set to 15N.

Apparently tuning of the duty cycle starts immediately after the perching mechanism is triggered, and it is adjusted to the minimum value (1250μs, fully gripping) within 0.08s. The resultant gripping force remains trivial during this period, and increases dramatically from the instant of 0.08s. As a matter of fact, the perching mechanism contacts the perch far before the servo rotates to the position corresponding to the duty cycle of 1250μs. However, due to the inertial of its components the servo cannot execute as quick as the duty cycle signal. Therefore the gripping force doesn't increase before the instant of 0.08s. It takes 0.05s for the gripping force to increase from trivial value to the desired value of 15N. The overshoot of the gripping force is close to 5N, and the fuzzy controller adjusts the duty cycle accordingly to slightly release the perching mechanism. Hysteresis can be observed as the gripping force gradually converges to about 16.5N. This is probably resulted from the force sensors and the padding of gripper digits. The stable gripping force is larger than 15N because the fuzzy control law is biased on purpose toward over-gripping to secure the safety during perching. The first disturbance doesn't affect the duty cycle calculated by the fuzzy controller at all. The second one, however, leads to an increase of the duty cycle to further release the grasp as the instantaneous gripping force almost reaches 20N. The third disturbance causes the instantaneous gripping

force lower than 15N, which leads to a slight adjustment of the duty cycle. This demonstrates one advantage of the fuzzy controller over the conventional controller that the grasp of the perching mechanism can be tuned in two directions. As over-grasp of the perching mechanism will increase current consumption of the servo significantly, the fuzzy controller can mitigate the waste of the battery energy over maintaining the grasp for the UAV. From Figure 6.27 it can also be noted successful perching is achieved with existence of a misalignment angle of the quadrotor, which further validates the good reliability of the fuzzy controller. In summary, the fuzzy controller proposed has been verified to be effective and reliable for automatic perching with quadrotors.

6.6 Summary

In this chapter a two-dimensional dynamics perching model is first established for quadrotors. Then a perching mechanism with gripping concept is developed. Kinematics optimization is performed to maximize the force amplification, and force sensors are integrated for gripping force sensing. Its control strategy for automatic perching is further proposed, including a control flow and two gripping control laws. The perching mechanism and its control strategy are evaluated sophisticatedly via a series of experiments. Results show that the perching mechanism can generate sufficient grasping force to secure the attachment to the perch, and the control strategy is rather effective in tuning the perching mechanism for reliable perching.

Chapter 7 Conclusions and Future Works

7.1 Conclusions

Perching is a concept proposed to resolve the problem of very limited airborne endurance of MUAVs and MAVs. Due to its vast potential in both civil and military applications, it is now garnering more interest among researchers in fields of guidance, navigation and control of UAVs, biomimetic engineering, and development of UAVs with morphing structures. In this thesis a bio-inspired methodology of automatic perching for UAVs was presented.

In Chapter 1, the background of UAV development in history was briefly introduced and the limits of the UAVs of the targeted scale were identified. The motivation behind the solution of perching with UAVs was then emphasized. The objective and scope of the research were subsequently presented to draw a panorama of the thesis.

Literatures on the topics related to perching, be it of birds in nature or with UAVs in engineering applications, were reviewed comprehensively in Chapter 2. Such topics ranged from ornithological research on birds' anatomy structures that play an important role during perching and those on birds' strategies guiding their perching behaviors, to prototype development of perching mechanisms for various UAVs and the perching strategies for navigation and control of the UAVs, for example, *Tau Theory*. Bio-inspirations for perching with UAVs were concluded from the review.

In Chapter 3 an experimental study of birds' perching behaviors and strategies behind them were presented in detail. Based on the perching experiments of parrots, the locomotion of perching parrots was for the first time analyzed from a perspective of the complete perching procedure. Consequently the perching procedure was generalized into three stages, namely pre-perching, on-perching and post-perching, which serves as the reference for the following investigations. Tau-dot during the pre-perching flight was calculated, and, instead of being constant as assumed in *Tau Theory*, it was found varying with different patterns. It suggests an interesting topic

to further study. The dynamic regulation of the parameters such as trajectory and body angle after touchdown was also addressed, indicating the applicability of a dynamic model.

The features of varying tau-dot during the pre-perching flight were further researched in Chapter 4. The varying tau-dot was first interpreted as discrete constant tau-dot using the theoretical expressions of constant tau-dot, and validated by comparing with the experimental data of tau-dot. This extends the potential of the employment of varying tau-dot for guidance. Moreover, the superiority of varying tau-dot over constant tau-dot in shortening approaching flight time was demonstrated based on experimental data, which further justified the application of varying tau-dot to perching guidance for UAVs. To tackle the nonlinearity of the varying tau-dot, a fuzzy logic based on the decreasing pattern was designed. The effectiveness of the fuzzy logic was experimentally verified with the indoor VICON motion capture system, showing that varying tau-dot can be used as the fuzzy guidance strategy for efficient and safe perching. This introduces a novel topic, varying tau-dot, to the field of bio-inspired guidance and control.

To provide feedback of tau-dot for the fuzzy logic, visual perception of tau-dot during pre-perching flight was explored in Chapter 5. Necessity of visual guidance for automatic perching of UAVs was discussed first. As perch identification is the first step towards visual perception of tau-dot, three LabVIEW-based object identification methods were systematically evaluated and the one that showed the best overall performance was utilized for identification of the target perch. To cope with the tau-theory-based guidance strategy, the relation between the identified object scale with respect to the template and the tau-dot of the current flight motion was analytically modeled. The model, named SEM, was integrated with the classical pinhole camera model. The validity of tau-dot estimate obtained from the proposed SEM was then examined with the ground truth measurement from VICON system. Good agreement between these values means the SEM can complete the control loop of automatic pre-perching flight of UAVs. However, enhancement of the accuracy and reliability of the tau-dot estimated visually by SEM is definitely needed.

Based on the bio-inspirations concluded from the literature review in Chapter 2 and the experimental study in Chapter 3, a dynamic perching model describing the balancing process of UAVs during on-perching was proposed in Chapter 6. The equations of motion of the perching UAV were derived and linearized under some assumptions. Simulation showed the perching model could yield responses close to the experiment data of the parrots under the same initial conditions. Since a gripping end effector was adopted in the model, a gripping mechanism for reliable attachment to target perch was further developed. Kinematic optimization, with a combination of analytical derivation of the mechanical constraints as well as numerically evaluation, was conducted to achieve maximum amplification of the gripping force. Besides, force sensors were also integrated to monitor the triggering impulse and measure the gripping force. A series of experiments to determine the mechanical effectiveness of the perching mechanism were performed under various circumstances, ranging from indoor scenarios to outdoor environments, and from remotely piloted UAVs to automatically controlled UAVs. Results showed that the perching mechanism was capable of generating sufficient gripping force for the UAV to perch reliably.

Towards automatic perching, the control flow of the gripping mechanism through the whole perching procedure was further designed. Moreover, both a conventional controller and a fuzzy controller for automatic gripping were developed, with emphasis on the latter. The fuzzy controller took into account the mechanical constraints of the perching mechanism, the force feedback and the indeterminacy of the output torque of the servo, and was experimentally proven effective and reliable in handling the nonlinearity associated with these factors. With the control strategies for pre-perching, on-perching and post-perching (take-off) developed and implemented, the automatic perching methodology for UAVs was completed. Quadrotors generally can follow this methodology to achieve successful perching.

7.2 Future Works

Although a complete methodology for automatic perching with UAVs was proposed, it is still far away from practical applications in free natural environments. Many

aspects of the research topic, such as the subtle perching dynamics model of birds, 3D perching model of UAVs, features of effective suspension, differential gripping and locking of the perching mechanism, fully intelligent non-template target identification, 3D real-time visual odometry, and more advanced control strategy of UAVs for perching using more aggressive maneuvers, remain to be studied. The detailed discussion about possible future works is presented in sections below.

7.2.1 Perching Dynamics of Birds

With experimental results indicating the contribution of adaptive posture adjustment of bird to body balance during perching, the study of parrots' perching has laid promising groundwork for the dynamics modeling of perching in birds. The dynamics model of perching was developed and validated using the experimental data of birds in this thesis, but it can only be applied to quadrotors with an attached mechanical perching mechanism. Therefore more work can be done to experimentally study the principles of birds' perching maneuvers for dynamics modeling, and to expand the applicability of the model to UAVs of different form factors. Three aspects that can potentially be studied are shown as follows:

- Body posture. Stable perching is achieved by birds through manipulations of their center of gravity, body orientation and so on. Information regarding birds' body kinematics is probably advantageous in decoding their balancing maneuvers in perching.

- Adaptive legs. Legs are the locomotors that takes over the task of balancing the body during the perching step. The way they function, for instance, how they exert forces or torques to the perch, should be researched.

- External Environment. During perching birds interact with external environment. Factors such as the kinematics and dynamics of the perch, wind disturbance and accessibility to the perch need to be taken into account so that the perching dynamics model of birds and their control strategy can be more comprehensively studied.

Moreover, the classic model from the bipedal walking of humans, the inverted pendulum model, may have a connection with the dynamics model of perching. As perching is interpreted as the transition from winged locomotion to legged locomotion, the inverted pendulum model that applies to legged locomotion can potentially be applied to perching. Actually, the dynamics perching model established in this thesis has shown similarity to the inverted pendulum model for bipedal walking. Besides, the horizontal CM trajectories immediately after touchdown from the experimental data with parrots are also in favor of this hypothesis because the inverted pendulum model of walking assumes that the vertical position of the mass remains constant. Therefore, it seems to be a really interesting topic to look into when modeling the perching dynamics of birds.

7.2.2 Improvement of the Dynamic Perching Model and Perching Mechanism

As the dynamics perching model was developed based on several assumptions, its application is currently limited to quadrotor platforms and 2 DOF. To generalize the applicability of the model, effort should be made to look into the dynamics of different UAV platforms as well as the perching dynamics of birds. Eventually the model should be capable of predicting the perching performance of different UAVs under various circumstances.

Other than the dynamics model, the perching mechanism can also be further improved. Desired features such as differential actuation, suspension in corresponding DOFs and grasp locking need to be realized and integrated into the perching mechanism. The predictions from the dynamics perching model can serve as design references for improving the perching mechanism.

7.2.3 Fully Intelligent Visual Target Identification

The target identification methods evaluated in this thesis are all template-based, which means a template of the target perch is required before initiating the perching procedure. This significantly compromises the practicability of the perching methodology in natural environments, where the target perch is not known

beforehand. To achieve such kind of perching on a more autonomous level, methods of fully intelligent visual target identification need to be developed. Research in the fields of computer vision, artificial intelligence and machine learning has addressed similar topics broadly and profoundly. Application and further improvement of these methods can be looked into for UAV perching. Such visual target identification methods overcome the prerequisite of the template, and can facilitate UAVs to achieve the ultimate goal of fully intelligent and autonomous perching. However, such methods generally require even higher computation capability of the system than template-based methods, and it's thus more challenging to accomplish real-time operations.

7.2.4 3D Visual Odometry for Navigation of Perching Flight

Apart from the fully intelligent visual target identification, another primary aspect of future work lies in 3D visual odometry for navigation of pre-perching flight. In this thesis, trouble on direct information acquisition of the distance to the target perch was remedied by the proposed tau-theory-based method which requires only the scale of the object in image to calculate tau and tau-dot. Despite being an advantageous way to guide the approaching flight of UAVs, it led to an inevitable problem that when the distance to the target is close to zero, the size of the target in image will expand to infinity and exceed the field of view of the camera. Since the proposed method encounters ineffectiveness in close range to the target, alternatives that can guide the UAV when close to touchdown are required. Furthermore, the estimated tau-dot based on the scale of the object in image has a certain amount of error from the ground truth values. Possible sources of error include the proposed analytical model (SEM), scale identification, or other stages in the perceptional loop. A promising method to solve these problems is the monocular or binocular 3D visual odometry that obtains the depth (distance) information of the object directly [79][80][81][82][83][84][85][86][87][88]. With the depth information obtained, not only can tau and tau-dot be derived more straightforwardly, conventional guidance techniques can also be easily applied. Besides, data fusion can also be integrated into this solution to provide more comprehensive and useful information of both the locomotion of UAVs and the environments for the control strategy to perform better.

Furthermore, such a solution can also improve the compatibility of the UAV system with future upgrades and/or the integration of new features.

7.2.5 Improvement of the Fuzzy Logic/Controller

The fuzzy logic designed to tune the desired tau-dot and the fuzzy controller designed for automatic gripping can surely use some modifications to improve their performance. Firstly, the number of the membership functions defined for the inputs and the outputs was only 3 or 5. This leads to limited resolution in fuzzification and defuzzification, which further affects the smoothness of the surface plot of the fuzzy logic. Increasing all the number to 5 or even 7 should enhance the performance. It should be noted that the fuzzy inference rules will get more complex as well and it will have more flexibility in handling the nonlinearity or uncertainty of the system being controlled. Secondly, the type of the membership functions can be changed to alternatives like Gaussian function. Supposedly, the smoothness of the surface plot of the fuzzy logic can also be improved. Thirdly, the inputs of the fuzzy logic/controller can be replaced with other parameters, for instance, the error between desired and actual value of the control variable and its rate of change. This fits even more with the intrinsic characteristics of fuzzy logic. Consequently, the corresponding control strategies cooperating with the fuzzy logic/controller need be modified accordingly.

Appendix A. Servo Characterization and Sensor Calibrations

(1) Servo Characterization

The servo motor utilized in the design is Futaba BLS 157HV which, according to its datasheet, can rotate up to 180^o and speed up to 0.11 second per 60^o， i.e., 9.52 rad/s, at 7.4 voltages. However, its dynamic characteristics with both the rotation range and the speed taken into account should be evaluated. As the actuation speed is more critical during perching, the max speed is deemed to be optimal. Hence the transfer function between the output angle A and the input duty cycle D_c is established under the condition of max rotation speed of around 7.25 rad/s. The rotation range at this speed is 85^o (see Figure A.1), while the percentage of the duty cycle ranges from 3.9% to 10.9%.

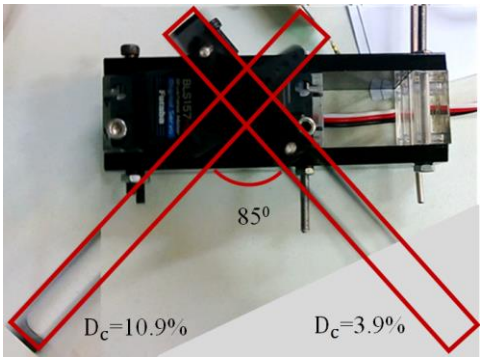

Figure A.1 Rotation range of the servo motor

In the specific configuration of the perching mechanism developed, the available rotation range of the servo is only 40^o, from -20^o to 20^o with the horizontal position defined as neutral position (see Figure 6.10). Accordingly the available duty cycle lies between 4.2% and 7.5%. Therefore the transfer function of the servo can be written as

$$A + 20^{\circ} = K_s(D_c - 4.2\%) \quad \text{A.1}$$

where K_s denotes the gain of the servo and is equal to 1212.1.

(2) Force Sensor Calibration

Force sensors serve as the feedback block in the control loop to gauge the generated grasping forces on the digits. Calibration is required to determine their feedback gains. The calibration circuit utilized is a typical voltage divider circuit with the force sensor connected to the voltage supply which is 5V, as shown in Figure A.2.1. Forces are imposed to the sensor with a force gauge mounted to a linear motion platform. The output voltage is then picked up by an Arduino controller board and further passed to a laptop for data logging. See Figure A.2.2. During the development two kinds of force sensor are employed, namely A400 from Interlink Electronics (Figure A.2.3) and FSG15N1A from Honeywell (Figure A.2.4). For A400, the linearity of the sensor is evaluated with different voltage-dividing resistors to optimize the sensitivity of the force sensing mechanism. As FSG15N1A is based on differential voltage measurement and the raw output voltage difference is very small, an instrumentation amplifier is used to magnify and output the voltage difference. Thus, it also reduces the required number of analog acquisition port on the controller board.

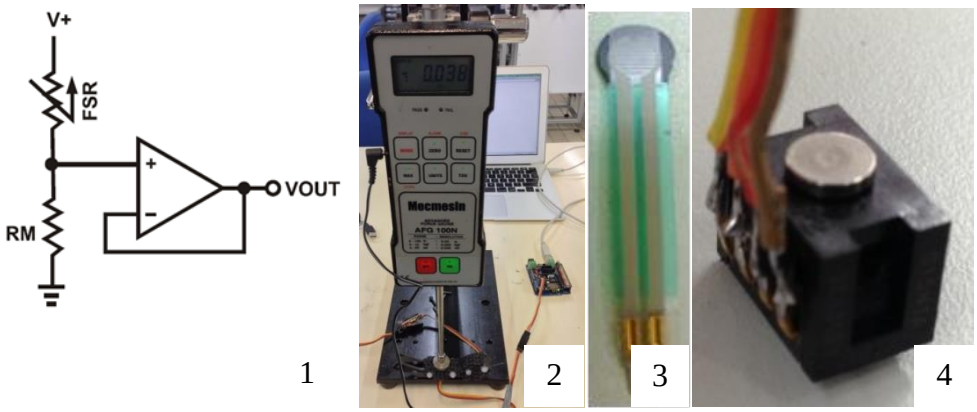

Figure A.2 Calibration setup. 1: Calibration circuit where FSR represents the force sensor, RM the voltage-dividing resistor, V+ the voltage supply and VOUT the output voltage [121]. 2: Force gauge mounted to a linear motion platform and applying force to the sensor. 3 and 4: Two types of force sensors utilized for gripping force sensing.

The output voltages of A400 with different resistors are plotted versus the force applied in Figure A.3. It can be seen that the force sensor shows better linearity with voltage-dividing resistors smaller than 30 KΩ. Besides, the output voltage ranges for

all the resistors are over 4V, which means no big difference in the sensitivity of the force sensing mechanism. To determine the optimal voltage-dividing resistance that leads to the best linearity of the force sensing mechanism, the linear fitting errors of the output voltages based on the least squares method with different resistors are calculated and shown in Figure A.4. It's obvious that with a 5.4 KΩ voltage-dividing resistor, the force sensor gets the best linearity. The corresponding linear fitting equation, which is also the characteristic formula of the A400 force sensor, is obtained as follows.

$$V = 0.04 \cdot F + 0.17, \text{where } 0 \leq F \leq 100\text{N}, \quad \text{A.2}$$

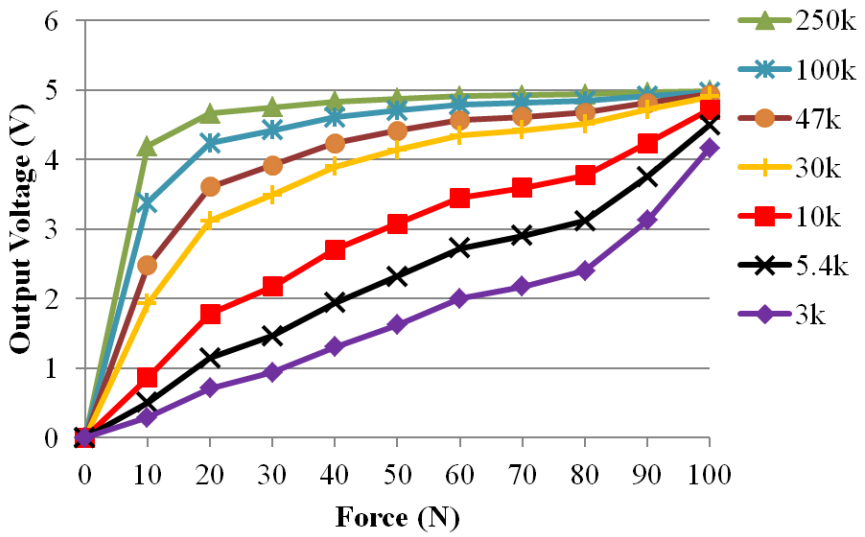

Figure A.3 Output voltage of A400 vs. force with different voltage-dividing resistors

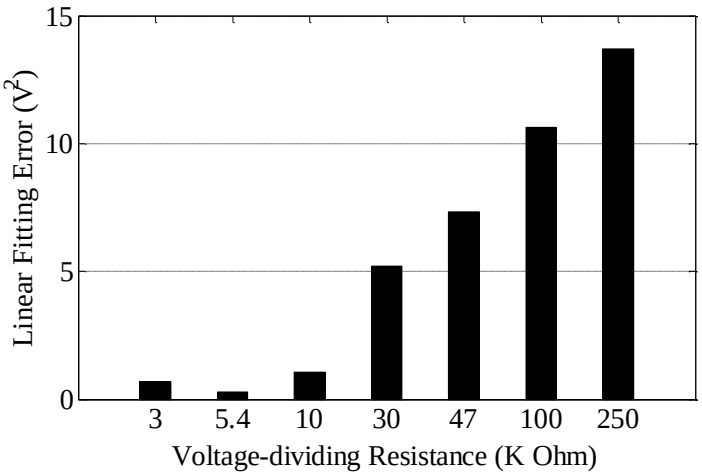

Figure A.4 Linearity fitting error vs. voltage-dividing resistance

The output voltages of FSG15N1A with integration of the instrumentation amplifier under different forces are depicted in Figure A.5. The output voltage range is about 4V, close to the range of A400. However, the applicable force range of FSG15N1A is far smaller than that of A400, which leads to better sensitivity of force sensing. Since multiple force sensors are used, the force sensing range of FSG15N1A is still sufficient according to the design. The linearity of the force sensor is also very good, even better than that of A400. The final characteristic formula is

$$V = 0.26 \cdot F + 0.05, \text{where } 0 \leq F \leq 15\text{N}. \quad \text{A.3}$$

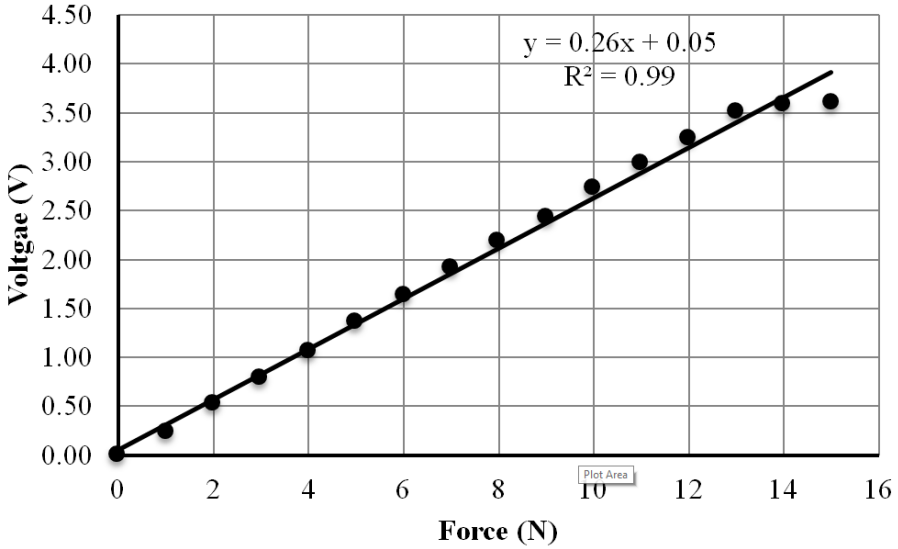

Figure A.5 Output voltage of FSG15N1A vs. force and its linear fitting

(3) Camera Calibration

The camera utilized for target identification and visual odometry needs to be calibrated before operation. This is because the pinhole camera model is taken into account in the SEM proposed, and the focal length of the camera is used for calculation of tau-dot. The focal length, and other parameters, of Cameras always deviate from the nominated values, which will certainly affect the accuracy of the calculation of tau-dot. Calibration can yield the actual values of these parameters, and minimize the errors introduced into the calculation. For target identification, it seems alright not to calibrate the camera as the template is taken by exactly the same camera. The truth is, however, the distortion at the corners of the camera sensor would definitely lower the matching score. Thus, calibration is rather necessary for accurate outputs of the camera.

The calibration algorithm is based on the example from LabVIEW and is customized to the author's needs, as depicted in Figure A.6. Basically, four calibrated parameters of the camera are obtained, namely the focal length in x axis of the camera, f_x, the focal length in y axis of the camera, f_y, x coordinate (in pixel) of the optical center of the camera, c_x, and y coordinate (in pixel) of the optical center of the camera, c_y.

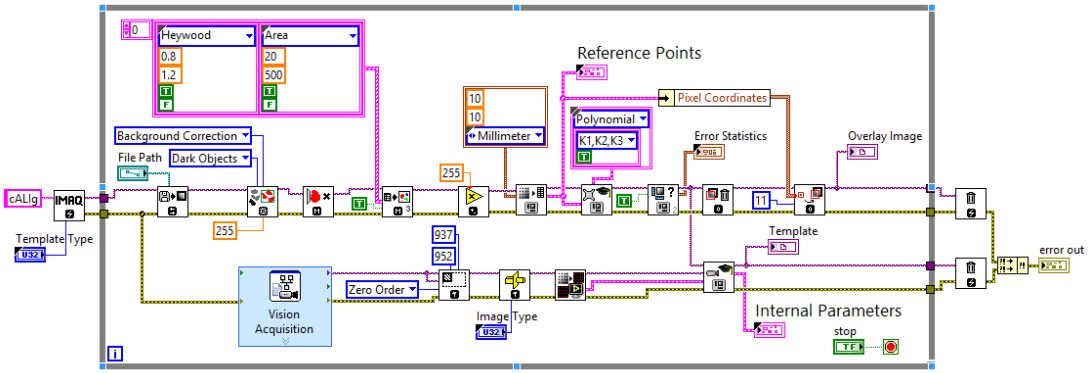

Figure A.6 The LabVIEW algorithm for camera calibration

The template image is provided by LabVIEW, as shown in Figure A.7, with its specifications known. The template is first processed and learned to obtain necessary information of the point grid, such as interval and distortion properties, as the reference. Meanwhile the point grid in the images captured by the camera is also extracted and compared with the reference information from the template. Finally the desired four parameters of the camera are derived. Results of one calibration process are demonstrated in Figure A.8 as an example.

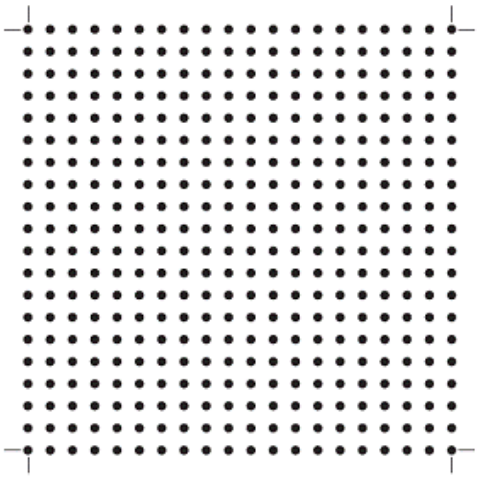

Figure A.7 Template image of point grid for calibration provided by LabVIEW

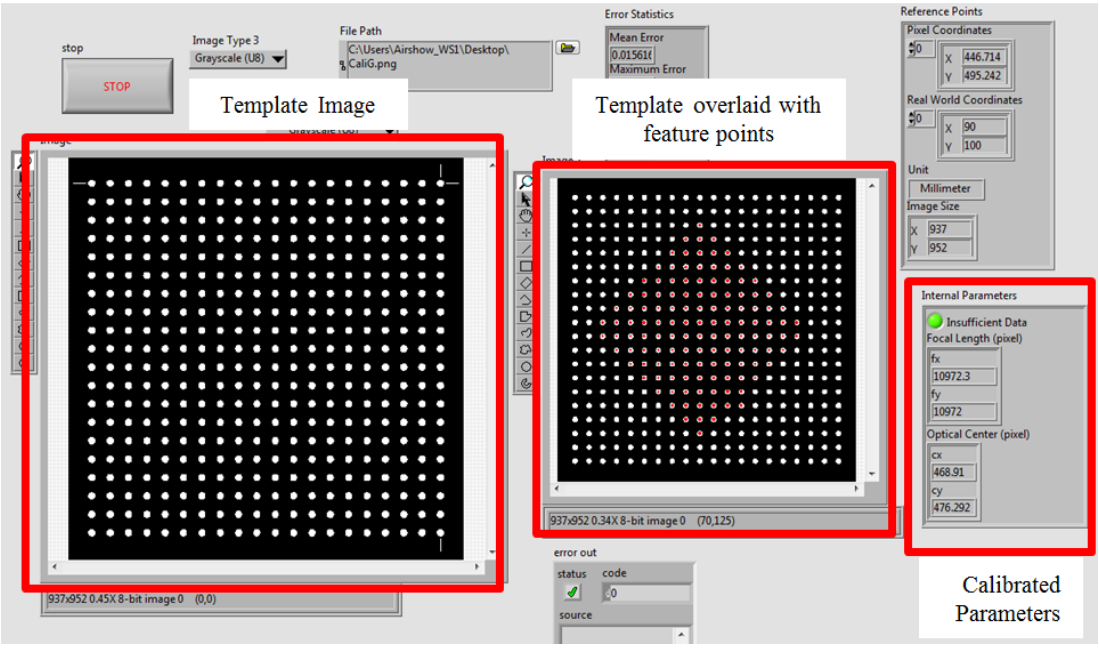

Figure A.8 An example of calibration results

Appendix B. Complementary Experiments of the Perching Mechanism

(1) Static Grasping without and with a Quadrotor

In the experiments of static grasping, a payload is first attached to the prototype of the gripping mechanism, simulating the weight of the quadrotor. Then the mechanism is aligned directly over the perch and actuated to completely grasp the perch. While the grasp is maintained, the perch is tilted gradually until the gripper slips off. Weights of 1kg and 2kg are utilized in first two experiments respectively, and the gripper is mounted to the quadrotor in the third one. Figure B.1 and Figure B.2 illustrate the max misalignment angles that the gripper can hold to in the experiments.

It can be seen that with 1kg payload, the gripper can hold up to 60^{o} of misalignment angle, while only up to 35^{o} with 2Kg payload. The quadrotor without battery weighs slightly above 1Kg, and the max misalignment angle with it reaches 50^{o}. The experiment results are consistent with the model prediction, and reveal that the gripper can readily secure the quadrotor in most common circumstances.

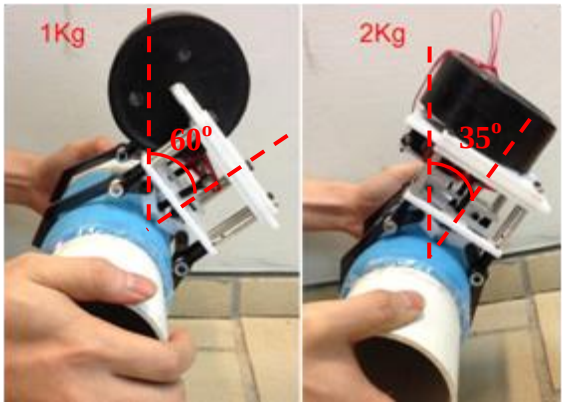

Figure B.1 Static grasp under misalignment and payload (Left: 1Kg; Right: 2Kg)

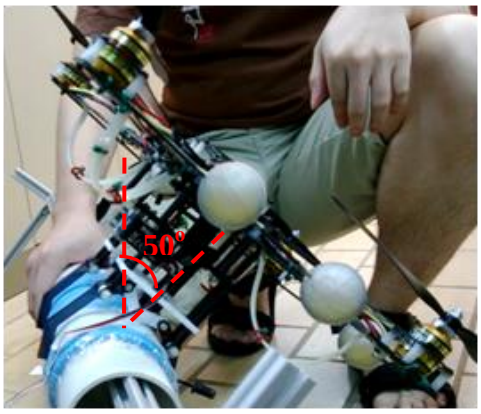

Figure B.2 Static grasp with the quadrotor

(2) Object-picking-up with a Remotely Controlled Quadrotor

In the experiment of objective-picking-up, a branch section is placed on the ground, and a quadrotor is remotely controlled to fly to it and pick it up using the perching mechanism designed. In the first trial the quadrotor successfully grasped and lifted the branch in the horizontal orientation, while in the second one the branch was grasped accidently by only two digits of the perching mechanism and lifted in the vertical orientation (see Figure B.3). The results show that the grasping ability of the perching mechanism is quite sufficient for natural circumstances like tree branches, and the gripper can even generate reliable grasping force in extreme cases such as the misaligned grasp.

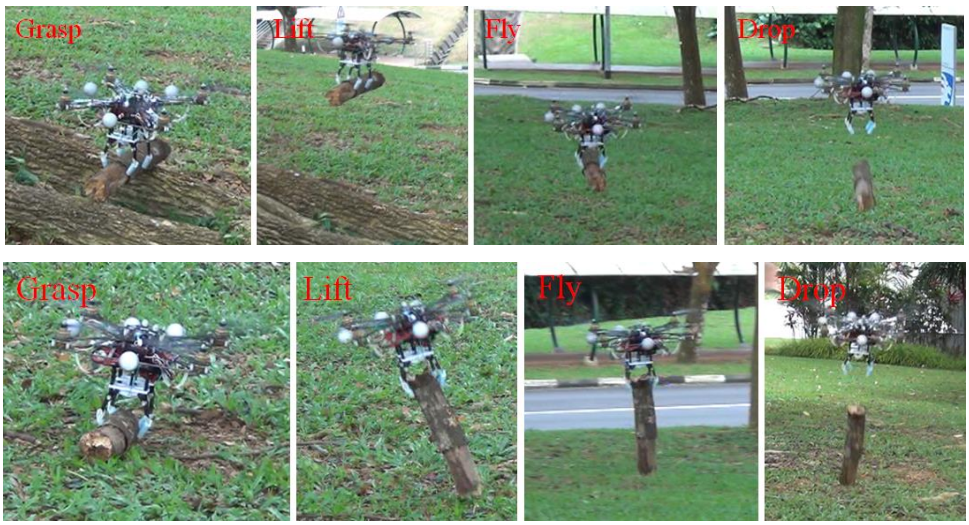

Figure B.3 Picking up a branch (top: horizontal grasp; bottom: vertical grasp)

List of Publications

Journal articles:

[1] W. Chi, K. H. Low, K. H. Hoon and J. Tang, "Design of Control Strategy for Autonomous Perching with a Quadrotor," *Applied Mechanics and Materials*, Vol. 461, pp. 506-512, 2013.

[2] W. Chi, K. H. Low, K. H. Hoon, J. Tang and T. H. Go, "A Bio-inspired Adaptive Perching Mechanism for Unmanned Aerial Vehicles," *Journal of Robotics and Mechatronics*, Vol. 24, No. 4, pp. 642-648, 2012.

[3] W. Chi and K. H. Low, "Review and fin Structure design for robotic manta ray (RoMan-IV)," *Journal of Robotics and Mechatronics*, Vol. 24, No. 4, pp. 620-628, 2012.

Conference articles:

[1] W. Chi, K. H. Low and K. H. Hoon, "Dynamic Modeling of Birds' Perching Maneuvers after Touchdown for Applications with Quadrotors," submitted to *2016 IEEE/RSJ International Conference on Intelligent Robots and Systems (IROS)* for review.

[2] W. Chi, K. H. Low and K. H. Hoon, "Visual Perception of Tau-dot for Guidance of Approaching Flights of Unmanned Aerial Vehicles," submitted to *The 5th International Conference of Bionic Engineering (ICBE2016)* for review.

[3] W. Chi, K. H. Low and K. H. Hoon, "Varying Tau-dot as a fuzzy control strategy for UAV perching," *AIAA Guidance, Navigation, and Control Conference*, San Diego, USA, 2016.

[4] W. Chi, K. H. Low, K. H. Hoon and J. Tang, "An optimized perching mechanism for autonomous perching with a quadrotor," *IEEE International Conference on Robotics and Automation (ICRA)*, Hong Kong, 2014.

[5] W. Chi, C. Wang, K. Tao, K. H. Low and S. H. Yeo, "Synthesis and kinematic analysis of a flapping wing mechanism," *Proc. Of the 8th International Conference on Intelligent Unmanned Systems*, Singapore, 2012.

References

[1] L. R. Newcome, *Unmanned Aviation: A Brief History of Unmanned Aerial Vehicles*, American Institute of Aeronautics and Astronautics, 2004.

[2] L. R. G. Carrillo, A. E. D. Lopez, R. Lozano, and C. Pegard, *Quad Rotorcraft Control: Vision-based Hovering and Navigation*, Springer, 2013.

[3] K. P. Valavanis, *Advances in Unmanned Aerial Vehicles: State of the Art and the Road to Autonomy*, Springer, 2004.

[4] DJI (2015). [Online]. Available: http://www.dji.com

[5] R. Dudley, *The Biomechanics of Insect Flight*, Princeton University Press, Princeton, NJ, 2000.

[6] R. Cory and R. Tedrake, "Experiments in Fixed-Wing UAV Perching," *AIAA Guidance, Navigation and Control Conference and Exhibit*, August 2008, Honolulu, USA.

[7] D. Mellinger, M. Shomin, and V. Kumar, "Control of Quadrotors for Robust Perching and Landing," *International Powered Lift Conference*, October 2010, Philadelphia, USA.

[8] A. Wickenheiser and E. Garcia, "Longitudinal Dynamics of a Perching Aircraft," *Journal of Aircraft*, vol. 43, No. 5, pp.1386-1392, 2006.

[9] A. Wickenheiser and E. Garcia, "Optimization of Perching maneuvers Through Vehicle Morphing," *Journal of Guidance, Control, and Dynamics*, vol. 31, No. 4, pp.815-823, 2008.

[10] J. Roberts, R. Cory, and R. Tedrake, "On the Controllability of Fixed-Wing Perching," *2009 American Control Conference*, June 2009, Hyatt Regency Riverfront, USA.

[11] M. Anderson, C. Perry, B. Hua, D. Olsen, J. Parcus, K. Pederson, and D. Jensen, "The Sticky-Pad Plane and other Innovative Concepts for Perching UAVs," *47th AIAA Aerospace Sciences Meeting Including The New Horizons Forum and Aerospace Exposition*, January 2009, Orlando, USA.

[12] M. Kovač, J. Germann, C. Hürzeler, R. Siegwart, and D. Floreano, "A Perching Mechanism for Micro Aerial Vehicles," *Journal of Micro-Nano Mechatronics*, vol. 5, No. 3, pp. 77, 2010.

[13] A. Desbiens and M. Cutkosky, "Landing and Perching on Vertical Surfaces with Microspines for Small Unmanned Air Vehicles," *Journal of Intelligent Robot System*, vol. 57, pp. 313-327, 2010.

[14] A. Desbiens, A. Asbeck, S. Dastoor, and M. Cutkosky, “Hybrid Aerial and Scansorial Robotics,” *2010 IEEE International Conference on Robotics and Automation*, pp. 1114-1115, 2010.

[15] C. Doyle, J. Bird, T. Isom, J. Johnson, J. Kallman, J. Simpson, R. King, J. Abbott, and M. Minor, “Avian-Inspired Passive Perching Mechanism for Robotic Rotorcraft,” *2011 IEEE/RSJ International Conference on Intelligent Robots and Systems*, September 2011, San Francisco, USA.

[16] C. Doyle, J. Bird, T. Isom, J. Kallman, D. Bareiss, D. Dunlop, R. King, J. Abbott, and M. Minor, “An Avian-Inspired Passive Mechanism for Quadrotor Perching,” *IEEE/ASME Transaction on Mechatronics*, vol. 18, no. 2, pp. 506-517, 2013.

[17] A. Nagendran, W. Crowther, and R. Richardson, “Biologically Inspired Legs for UAV Perched Landing,” *IEEE A&E Systems Magazine*, vol. 27, Issue 2, pp. 4-13, 2012.

[18] D. Mellinger, N. Michael, and V. Kumar, “Trajectory generation and control for precise aggressive maneuvers with quadrotors,” *The International Journal of Robotics Research*, vol. 31, No. 5, pp.664-674, 2012.

[19] D. II J. Pines and F. Bohorquez, “Challenges Facing Future Micro-Air-Vehicle Development”, *Journal of Aircraft*, vol. 43, No. 2, pp. 290-305, 2006.

[20] R. Owen, *On the anatomy of vertebrates. II. Birds and mammals*, Longman Green, London, 1866.

[21] M. Watson, “On the mechanisms of perching in birds,” *J. Anat.* vol. 3, pp. 379-384, 1869.

[22] J. L. Renaut, “Recherches sur las transformation vesiculeuse des elements cellulaires des tendons (Cellules tubulaires de Ranvier),” *Archs Physiol Norm Path*, vol. 4, pp. 271-191, 1872.

[23] I. Ranvier, “Sur les tendons des doigts chez les oiseaux. J Micrographie. Histologie humaine et comparee. Anatomie vegetale. Botanique. Zoologie. Bacteriologie,” *Applications diverses du Microscope*, vol. 13, pp. 167-171, 1889.

[24] T. H. Quinn and J. J. Baumel, “The digital tendon locking mechanism of the avian foot (Aves),” *Zoomorphology*, vol. 109, pp. 281-293, 1990.

[25] T. H. Quinn and J. J. Baumel, “Chiropteran Tendon Locking Mechanism,” *Journal of Morphology*, vol. 216, pp. 197-208, 1993.

[26] P. M. Galton and J. D. Shepherd, “Experimental analysis of perching in the European starling (Sturnus vulgaris: Passeriformes; passeres), and the automatic perching mechanism of birds,” *Journal of Experimental Zoology*, vol. 317, pp. 205-215, 2012.

[27] W. MacGillivray, *A History of British Birds, Indigenous and Migratory: Rasores, scrapers, or gallinaceous birds; Gemitores, cooers, or pigeons; Deglubitores, huskers, or conirostral birds; Vagatores, wanderers, or crows and allied genera*, Scott, Webster, and Geary, London, 1837.

[28] C. M. Perrins, D. Attenborough, and N. Arlott, *New generation guide to the birds of Britain and Europe*, Austin: University of Texas Press, 1987.

[29] H. Fisher, "The landing forces of domestic pigeons," *The Auk*, vol. 73, No. 1, pp. 85-105, 1956.

[30] H. Fisher, "Apparatus to measure forces involved in the landing and taking off of birds," *The American Midland Naturalist*, vol. 55, pp. 334-342, 1956.

[31] B. Wilson, *Birds: Readings From Scientific American*, San Francisco: W. H. Freeman, 1980.

[32] N. S. Proctor and P. J. Lynch, *Manual of Ornithology: Avian Structure and Function*, Yale University Press, New Haven, 1993.

[33] R. A. Norberg, "Why foraging birds in trees should climb and hop upwards rather than downwards," *Ibis*, vol. 123, pp. 281-288, 1981.

[34] A. V. L. Pike and D. P. Maitland, "Scaling of bird claws," *Journal of Zoology*, vol. 262, No. 1, pp. 73-81, 2004.

[35] D. W. Fowler, E. A. Freedman, and J. B. Scannella, "Predatory Functional Morphology in Raptors: Interdigital Variation in Talon Size Is Related to Prey Restraint and Immobilisation Technique," *PLoS ONE*, vol. 4, No. 11, pp. 1-9, 2009.

[36] F. Heppner and J. Anderson, "Leg thrust important in flight take-off in the pigeon," *The Journal of Experimental Biology*, vol. 114, pp. 285-288, 1985.

[37] R. Bonser and J. Rayner, "Measuring leg thrust forces in the common starling," *The Journal of Experimental Biology*, vol. 199, pp. 435-439, 1996.

[38] P. Green and P. Cheng, "Variation in kinematics and dynamics of the landing flight of pigeons on a novel perch," *The Journal of Experimental Biology*, vol. 201, pp. 3309-3316, 1998.

[39] D. N. Lee, "A theory of visual control of braking based on information about time-to-collision," *Perception*, vol. 5, no. 4, pp. 437-459, 1976.

[40] H. Hecht and G. Savelsbergh, *Time-to-Contact*, Eds. Elsevier, 2004.

[41] D. N. Lee, M. Davis, P. R. Green, and F. R. Van Del Well, "Visual Control of Velocity of Approach by Pigeons When Landing," *The Journal of Experimental Biology*, vol. 180, no. 1, pp. 85-104, 1993.

[42] D. N. Lee, “Guiding movement by coupling Taus,” *Ecological Psychology*, vol. 10, pp. 221-250, 1998.

[43] D. N. Lee, C. M. Craig, and M. A. Grealy, “Sensory and intrinsic coordination of movement,” *Proceedings of the Royal Society B: Biological Sciences*, Vol. 266, No. 1432, pp. 2029-2035, 1999.

[44] D. N. Lee, “General Tau Theory: evolution to date,” *Perception*, vol.38, no. 6, pp. 837-850, 2009.

[45] E. Yilmaz and W. Warren Jr., “Visual control of braking: a test of the tau-dot hypothesis,” *Journal of Experimental Psychology: Human Perception and Performance*, vol. 21, no. 5, pp. 996-1014, 1995.

[46] D. N. Lee, A. P. Georgopoulos, M. J. Clark, C. M. Craig, and N. Port, “Guiding contact by coupling the taus of gaps,” *Experimental Brain Research*, Vol. 139, No. 2, pp. 151-159, 2001.

[47] B. Hopkins, A. Churchill, S. Vogt, and L. Ronnqvist, “Braking Reaching Movements: A Test of the Constant Tau-Dot Strategy under Different Viewing Conditions,” *Journal of Motor Behavior*, vol. 36, no. 1, pp. 3-13, 2004.

[48] P. Rock, M. Harris, and T. Yates, “A test of the tau-dot hypothesis of braking control in the real world,” *Journal of Experimental Psychology: Human Perception and Performance*, vol. 32, no. 6, pp. 1479-1484, 2006.

[49] P. B. Rock and M. G. Harris, “Tau as a potential control variable for visually guided braking,” *Journal of Experimental Psychology: Human Perception and Performance*, vol. 32, no. 2, pp. 251-267, 2006.

[50] M. Jump and G. D. Padfield, “Progress in the development of guidance strategies for the landing flare manoeuvre using tau-based parameters,” *Aircraft Engineering and Aerospace Technology*, vol. 78, no. 1, pp. 4-12, 2006.

[51] D. Coombs, M. Herman, TH. Hong, and M. Nashman, “Realtime obstacle avoidance using central flow divergence, and peripheral flow,” *IEEE Transactions on Robotics and Automation*, vol. 14, pp. 49–59, 1998.

[52] J. Smith, M. Grealy, and G. J. Pepping, “Extrinsic tau-coupling and the regulation of interceptive reaching under varying task constraints,” *Motor Control*, Vol. 18, No. 4, pp. 347-367, 2014.

[53] Y. Kaneta, Y. Hagisaka, and K. Ito, “Determination of time to contact and application to timing control of mobile robot,” *IEEE International conference on robotics and biomimetics (ROBIO)*, Tianjin, China, 2010, pp. 161–166.

[54] F. Kendoul and B. Ahmed, “Bio-Inspired TauPilot for Automated Aerial 4D Docking and Landing of Unmanned Aircraft Systems,” *IEEE/RSJ International Conference on Intelligent Robots and Systems*, Vilamoura, Portugal, 2012, pp. 480-487.

[55] P. Xie, O. Ma, and Z. Zhang, "A Bio-inspired Approach for UAV Landing and Perching," *AIAA Guidance, Navigation, and Control (GNC) Conference*, Boston, MA, 2013.

[56] Z. Zhang, P. Xie, and O. Ma, "Bio-inspired Trajectory Generation for UAV Perching," *2013 IEEE/ASME International Conference on Advanced Intelligent Mechatronics (AIM)*, Wollongong, Australia, 2013.

[57] Z. Zhang, S. Zhang, P. Xie, and O. Ma, "Bioinspired 4D Trajectory Generation for a UAS Rapid Point-to-Point Movement," *Journal of Bionic Engineering*, vol. 11, no. 1, pp. 72-81, 2014.

[58] Z. Zhang, P. Xie, and O. Ma, "Bio-inspired Trajectory Generation for UAV Perching Movement Based on Tau Theory," *International Journal of Advanced Robotic Systems*, vol. 11, no. 141, 2014.

[59] F. Kendoul, "Four-dimensional guidance and control of movement using time-to-contact: Application to automated docking and landing of unmanned rotorcraft systems," *International Journal of Robotics Research*, vol. 33, no. 2, pp. 237-267, 2014.

[60] M. Davies and P. Green, "Optic Flow-Field Variables Trigger Landing in Hawk but not in Pigeons," *Naturwissenschaften*, vol. 77, pp. 142-144, 1990.

[61] D. Lee, M. Davies, P. Green, and F. R. Van Der Weel, "Visual Control of Velocity of Approach by Pigeons when Landing," *The Journal of Experimental Biology*, vol. 180, pp. 85-104, 1993.

[62] P. Green, M. Davies, and P. H. Thorpe, "Head-bobbing and head orientation during landing flgihts of pigeons," *Journal of Comparative Physiology A*, vol. 174, pp. 249-256, 1994.

[63] C. Evangelista, P. Kraft, M. Dacke, J. Reinhard, and M. Srinivasan, "The moment before touchdown: landing manoeuvres of the honeybee Apis mellifera," *The Journal of Experimental Biology*, vol. 213, pp. 262-270, 2010.

[64] E. Baird, N. Boeddeker, M. Ibbotson, and M. Srinivasan, "A universal strategy for visually guided landing," *PNAS*, vol. 110, no. 46, pp. 18686-18691, 2013.

[65] M. Srinivasan, S. Zhang, and J. Chahl, "Landing strategies in honeybees, and possible applications to autonomous airborne vehicles," *The Biological Bulletin*, Vol. 200, No. 2, pp. 216-221, 2001.

[66] C. V. D. Berg and J. Rayner, "The moment of inertia of bird wings and the inertial power requirement for flapping flight," *The Journal of Experimental Biology*, Vol. 198, pp. 1655-1664, 1995.

[67] A. Berg and A. Biewener, "Kinematics and power requirements of ascending and descending flight in the pigeon (Columba livia)," *The Journal of Experimental Biology*, vol. 211, pp. 1120-1130, 2008.

[68] A. Berg and A. Biewener, “Wing and body kinematics of takeoff and landing flight in the pigeon (Columba livia),” *The Journal of Experimental Biology*, vol. 213, pp. 1651-1658, 2010.

[69] T. Hedrick, “Damping in flapping flight and its implications for manoeuvring, scaling and evolution,” *The Journal of Experimental Biology*, Vol. 214, pp. 4073-4081, 2011.

[70] Tracker—Video Analysis and Modeling Tool, Software Package, Ver. 4.85, URL: www.cabrillo.edu/~dbrown/tracker/, 2014.

[71] M. Fujita, “Head bobbing and the movement of the centre of gravity in walking pigeons (Columba livia),” *Journal of Zoology*, London, vol. 257, pp. 373-379, 2002.

[72] J. A. Nyakatura, E. Andrada, N. Grimm, H. Weise, and M. S. Fischer, “Kinematics and center of mass mechanics during terrestrial locomotion in northern lapwings (*Vanellus vanellus*, Charadriiformes),” *Journal of Experimental Zoology Part A: Ecological Genetics and Physiology*, Vol. 317, pp. 580-594, 2012.

[73] P. Provini, B. Tobalske, K. Crandell, and A. Abourachid, “Transition from leg to wing forces during take-off in birds,” *The Journal of Experimental Biology*, Vol. 215, pp. 4115-4124, 2012.

[74] P. Provini, B. Tobalske, K. Crandell, and A. Abourachid, “Transition from wing to leg forces during landing in birds,” *The Journal of Experimental Biology*, Vol. 217, pp. 2659-2666, 2014.

[75] A. Robertson and A. Biewener, “Muscle function during takeoff and landing flight in the pigeon (*Columba livia*),” Vol. 215, pp. 4104-4114, 2012.

[76] R. Lock, S. Burgess, and R. Vaidyanathan, “Multi-modal locomotion: from animal to application,” *Bioinspiration & Biomimetics*, Vol. 9, pp. 11001-11018, 2013.

[77] W. Chi, K. H. Low, K. H. Hoon, and J. Tang, “An Optimized Perching Mechanism for Autonomous Perching with a Quadrotor,” *IEEE International Conference on Robotics and Automation (ICRA)*, Hong Kong, 2014, pp. 3109-3115.

[78] M. Achtelik, S. Weiss, and R. Siegwart, “Onboard IMU and monocular vision based control for MAVs in unknown in- and outdoor environments,” *IEEE International Conference on Robotics and Automation (ICRA),* Shanghai, China, 2011, pp. 3056-3063.

[79] J. Engel, J. Sturm, and D. Cremers, “Camera-based navigation of a low-cost quadrocopter,” *IEEE/RSJ International Conference on Intelligent Robots and Systems (IROS)*, Algarve, Portugal, 2012.

[80] J. Engel, J. Sturm, and D. Cremers, "Scale-aware navigation of a low-cost quadrocopter with a monocular camera," *Robotics and Autonomous Systems*, vol. 62, No. 11, pp. 1646-1656, 2014.

[81] C. Kerl, J. Sturm, and D. Cremers, "Robust odometry estimation for RGB-D cameras," *IEEE International Conference on Robotics and Automation (ICRA)*, Karlsruhe, Germany, 2013.

[82] J. Engel, T. Schops, and D. Cremers, "LSD-SLAM: Large-Scale Direct Monocular SLAM," *Computer Vision-ECCV 2014*, pp. 834-849, 2014.

[83] A. Wendel, M. Maurer, G. Graber, T. Pock, and H. Bischof, "Dense reconstruction on-the-fly," *IEEE Conference on Computer Vision and Pattern Recognition (CVPR)*, pp. 1450-1457, Rhode Island, USA, 2012.

[84] C. Kerl, J. Sturm, and D. Cremers, "Dense visual SLAM for RGB-D cameras," *IEEE/RSJ International Conference on Intelligent Robots and Systems (IROS)*, pp. 2100-2106, Tokyo, Japan, 2013.

[85] R. Newcombe, S. Lovegrove, and A. Davison, "DTAM: Dense tracking and mapping in real-time," *IEEE International Conference on Computer Vision, (ICCV)*, pp. 2320-2327, Barcelona, Spain, 2011.

[86] T. Whelan, H. Johannsson, M. Kaess, J. Leonard, and J. McDonald, "Robust real-time visual odometry for dense RGB-D mapping," *IEEE International Conference on Robotics and Automation (ICRA)*, Karlsruhe, Germany, 2013.

[87] L. Matthies, R. Szeliski, and T. Kanade, "Incremental estimation of dense depth maps from image sequences," *IEEE Conference on Computer Vision and Pattern Recognition (CVPR)*, pp. 366-374, Michigan, USA, 1988.

[88] Y. Ma, S. Soatto, J. Kosecka, and S. Sastry, *An invitation to 3-D vision from images to geometric models*, New York: Springer Science+Business Media, 2004.

[89] E. Baird, M. V. Srinivasan, S. W. Zhang, and A. Cowling, "Visual control of flight speed in honeybees," *The Journal of Experimental Biology*, Vol. 208, pp. 3895-3905, 2005.

[90] M. V. Srinivasan, S. W. Zhang, M. Lehrer, and T. S. Collett, "Honeybee navigation en route to the goal: visual flight control and odometry," *The Journal of Experimental Biology*, Vol. 199, pp. 237-244, 1996.

[91] W. H. Kirchner and M. V. Srinivasan, "Freely flying honeybees use image motion to estimate object distance," Naturwissenschaften, Vol. 76, No. 6, pp. 281-282, 1989.

[92] P. S. Bhagavatula, C. Claudianos, M. R. Ibbotson, and M. V. Srinivasan, "Optic flow cues guide flight in birds," *Current Biology*, Vol. 21, pp. 1794-1799, 2011.

[93] H. Chao, Y. Gu, and M. Napolitano, "A survey of optical flow techniques for robotics navigation applications," *Journal of Intelligent and Robotic Systems*, Vol. 73, pp. 361-372, 2014.

[94] H. Romero, S. Salazar, and R. Lozano, "Real-time stabilization of an eight-rotor UAV using optical flow," *IEEE Transactions on Robotics*, Vol. 25, No. 4, pp. 809-817, 2009.

[95] J. E. Gomez-Balderas, S. Salazar, J. A. Guerrero, and R. Lozano, "Vision-based autonomous hovering for a miniature quad-rotor," *Robotica*, Vol. 32, No. 1, pp. 43-61, 2013.

[96] F. Kendoul, "Survey of advances in guidance, navigation, and control of unmanned rotorcraft systems," *Journal of Field Robotics*, Vol. 29, No. 2, pp. 315-378, 2012.

[97] H. Wagner, "Flow-field variables trigger landing in flies," *Nature*, Vol. 297, No. 5862, pp. 147-148, 1982.

[98] F. Van Breugel and M. Dickinson, "The visual control of landing and obstacle avoidance in the fruit fly Drosophila melanogaster," *The Journal of Experimental Biology*, Vol. 215, No. 11, pp. 1783-1798, 2012.

[99] G. Sharma, S. Sood, G. S. Gaba, and N. Gupta, "Image Recognition System using Geometric Matching and Contour Detection," *International Journal of Computer Applications*, Vol. 51, No. 17, pp. 48-53, 2012.

[100] T. Klinger, *Image Processing with LabVIEW and IMAQ Vision*, Prentice Hall, 2003.

[101] K. S. Kwon and S. Ready, *Practical Guide to Machine Vision Software: An Introduction with LabVIEW*, Wiley-VCH Verlag GmbH & Co. KGaA, 2014.

[102] Geometric Matching Technique, NI Vision Concepts Help [Online]. Available: http://zone.ni.com/reference/en-XX/help/372916L-01/nivisionconcepts/geometric_matching_technique/

[103] Pattern Matching Technique, NI Vision Concepts Help [Online]. Available: http://zone.ni.com/reference/en-XX/help/372916P-01/nivisionconcepts/pattern_matching_techniques/

[104] Object Tracking technique, NI Vision Concepts Help [Online]. Available: http://zone.ni.com/reference/en-XX/help/372916P-01/nivisionconcepts/object_tracking_techniques/

[105] K. C. Shi, "Visual-guided perching of quadrotors," Nanyang Technological University Final Year Project (FYP), 2015.

[106] L. Kaufman and E. Schultz, "The Stability and Control of Tethered Helicopters," *Journal of the American Helicopter Society*, vol. 7, No. 4, 1962.

[107] P. Pounds and A. Dollar, "Hovering Stability of Helicopters with Elastic Tethers," *In Proc. ASME Dynamic Systems and Control Conference*, 2010.

[108] P. Pounds and A. Dollar, "UAV Rotorcraft in Compliant Contact: Stability Analysis and Simulation," *IEEE/RSJ International Conference on Intelligent Robots and Systems (IROS)*, San Francisco, USA, 2011.

[109] S. Oh, K. Pathak, S. K. Agrawal, H. R. Pota, and M. Garratt, "Approaches for a Tether-Guided Landing of an Autonomous Helicopter," *IEEE Transactions on Robotics*, vol. 22, No. 3, pp. 536-544, 2006.

[110] A. Alvers, S. Trautmann, T. Howard, A. N. Trong, M. Frietsch, and C. Sauter, "Semi-autonomous flying robot for physical interaction with environment," *IEEE Conference on Robotics Automation and Mechatronics (RAM)*, pp. 441-446, Singapore, 2010.

[111] H. Jiang, M. Pope, E. Hawkes, D. Christensen, M. Estrada, A. Parlier, R. Tran, and M. Cutkosky, "Modeling the dynamics of perching with opposed-grip mechanisms," *IEEE International Conference on Robotics and Automation (ICRA)*, pp. 3102-3108, Hong Kong, 2014.

[112] V. Ghadiok, J. Goldin, and W. Ren, "Autonomous indoor aerial gripping using a quadrotor," *IEEE/RSJ International Conference on Intelligent Robots and Systems (IROS)*, San Francisco, USA, 2011.

[113] Engineer's Handbook (2013), Reference Tables [Online]. Available: http://www.engineershandbook.com/Tables/frictioncoefficients.htm

[114] D. Petkovic, M. Issa, N. Pavlovic, L. Zentner, and Z. Cojbasic, "Adaptive neuro fuzzy controller for adaptive compliant robotic gripper," *Expert Systems with Applications*, Vol. 39, pp. 13295-13304, 2012.

[115] D. Petkovic, N. D. Pavlovic, Z. Cojbasic, and N. T. Pavlovic, "Adaptive neuro fuzzy estimation of underactuated robotic gripper contact forces," *Expert Systems with Applications*, Vol. 40, pp. 281-286, 2013.

[116] K. Lee and Y Qian, "A vision-guided fuzzy logic control system for dynamic pursuit of a moving target," *Microprocessors and Microsystems*, Vol. 21, pp. 571-580, 1998.

[117] C. Treesatayapun, "Adaptive control based on IF-THEN rules for grasping force regulation with unknown contact mechanism," *Robotics and Computer-Integrated Manufacturing*, Vol. 30, pp. 11-18, 2014.

[118] T. Dorsam, S. Fatikow, and I. Streit, "Fuzzy-based grasp-force-adaptation for multifingered robot hands," *Fuzzy Systems, 1994. IEEE World Congress on Computational Intelligence, Proceedings of the Third IEEE Conference on*, Vol. 3, pp. 26-29, 1994.

[119] N. I. Glossas and N. A. Aspragathos, "Fuzzy logic grasp control using tactile sensors," *Mechatronics*, Vol. 11, pp. 899-920, 2001.

[120] Z. Kovacic and S. Bogdan, *Fuzzy Controller Design: Theory and Applications*, Florida: Taylor & Francis Group, 2006.

[121] Interlink Electronics, *Force sensing resistor integration guide and evaluation parts catalog*, 2010.